



Flood Hazard Mapping and Risk Assessment for Chindwin River Basin, Myanmar

CHIT MYO LWIN

A THESIS SUBMITTED IN PARTIAL FULFILLMENT OF
THE REQUIREMENTS FOR MASTER OF SCIENCE
IN GEOINFORMATICS
FACULTY OF GEOINFORMATICS
BURAPHA UNIVERSITY

2020

COPYRIGHT OF BURAPHA UNIVERSITY

Flood Hazard Mapping and Risk Assessment for Chindwin River Basin, Myanmar



CHIT MYO LWIN

วิทยานิพนธ์นี้เป็นส่วนหนึ่งของการศึกษาตามหลักสูตรวิทยาศาสตร
มหาบัณฑิต
สาขาวิชาภูมิสารสนเทศศาสตร์
คณะภูมิสารสนเทศศาสตร์ มหาวิทยาลัยบูรพา
2563
ลิขสิทธิ์เป็นของมหาวิทยาลัยบูรพา

Flood Hazard Mapping and Risk Assessment for Chindwin River Basin, Myanmar



CHIT MYO LWIN

A THESIS SUBMITTED IN PARTIAL FULFILLMENT OF
THE REQUIREMENTS FOR MASTER OF SCIENCE
IN GEOINFORMATICS
FACULTY OF GEOINFORMATICS
BURAPHA UNIVERSITY
2020
COPYRIGHT OF BURAPHA UNIVERSITY

The Thesis of Chit Myo Lwin has been approved by the examining committee to be partial fulfillment of the requirements for the Master of Science in Geoinformatics of Burapha University

Advisory Committee

Examining Committee

Principal advisor

(Jianzhong Lu)

----- Principal
examiner

(Timo Balz)

Co-advisor

(Pakorn Penparkkul)

----- Member

(Parin Lopittayakorn)

(Xiaoling Chen)

----- Dean of the Faculty of Geoinformatics
(Kitsanai Charoenjit)

This Thesis has been approved by Graduate School Burapha University to be partial fulfillment of the requirements for the Master of Science in Geoinformatics of Burapha University

----- Dean of Graduate School
(Associate Professor Dr. Nujjaree Chaimongkol)

61910095: MAJOR: GEOINFORMATICS; M.Sc. (GEOINFORMATICS)

KEYWORDS: Flood GIS Hydrologic model Hydraulic model Google Earth Engine
Flood inundation Flood risk Flood exposure Flood vulnerability
Flood hazard

CHIT MYO LWIN : FLOOD HAZARD MAPPING AND RISK

ASSESSMENT FOR CHINDWIN RIVER BASIN, MYANMAR . ADVISORY

COMMITTEE: JIANZHONG LU, , PAKORN PENPARKKUL XIAOLING CHEN
2020.

Myanmar is a country exposed to natural disasters such as floods, cyclones, earthquakes, forest fires, landslides, etc. Among them, the flood is one of the natural disasters and mainly occurred in the Ayeyarwaddy River basin and my study area, Chindwin River is the biggest tributary of it. Such a flood disaster is threatening to the exposures and vulnerabilities in the Chindwin River Basin, and this study aims to prevent and manage the flood risk for disaster management

In this study, the GIS-based modelling of the flood inundation maps was developed using the hydrologic model (HEC-HMS) and hydraulic model (HEC-RAS) for two flood events. Also, it estimated the different return periods (2, 5, 10, 50 & 100 years) floods in the river basin. Moreover, the flood extent and depth of the flood were validated with the flood map calculated from the remotely sensed techniques in the google earth engine (GEE) and the flood river bed, respectively. To prevent and manage the flood disaster, the flood risk assessment in the village tract level is carried out by exploring the factors of the flood hazard, flood exposures, and flood vulnerability.

Firstly, in the development of the hydrologic model, the land use/land cover map, soil layer, etc. were prepared in GIS platform as a pre-processing step. Moreover, the automatic delineation of stream network, watershed boundary and the terrain analysis was carried out using the 12.5 m spatial resolution of the Digital Elevation Model (ALOS/PALSAR) in the HEC-GeoHMS which is an extension of GIS program. All of the processing datasets were exported into HEC-HMS for the further hydrologic model by mainly using the precipitation and water discharge. The selected flood events (2015 and 2017) were utilized to estimate the rainfall-runoff simulation using the hydrologic model with calibrated and validated approaches. The

model performance of the coefficient of correlation (R), the coefficient of determination (R^2), and the Nash-Sutcliffe model efficiency (EFF) have resulted in a range of 0.93 – 0.98, 0.8649 – 0.9532, and 0.804 – 0.944 respectively. According to the results, the relationships of the 2015 and 2017 storm events indicated an appropriate and closed relationship between the computed and observed flows.

Moreover, in the development of the hydrodynamic model, the Triangulated Irregular Network (TIN) was generated with the 30 m contour intervals computed from the Digital Elevation Model (DEM) in the GIS environment. Besides, the geometric data such as cross-section, flow path, streamline and bank lines were generated in the HEC-Geo-RAS, which is a plug-in of the GIS software and then exported into HEC-RAS for the hydraulic modelling. The cross-sections are very important and which can be validated with the field observation data in the editing option. The required Manning number “ n ” values were calculated for each cross-section of both sides of the river. The hydraulic model was used to perform the unsteady-flow simulations of the predicted flood hydrographs. The observed water level data were used for the calibration and validation of the HEC-RAS model performance. Validation of the results for the 2015 and 2017 flood events was compared with the flood maps derived from the Sentinel 1 radar satellite data in Google Earth Engine (GEE). In the comparison of the flood inundation area of the simulated result and the flood area from remote sensing, the overlapping area is 71.5% and 72.1% for 2015 and 2017 flood events respectively. And it is a closed validated checking for the flood area. The total flood inundation area of the 2015 flood event is about 4133.9 km², with a 13.8-meter maximum depth of the flood and extended into low land terrain and flood plain areas especially, in the Homalin, Kalay, and Monywa townships due to the low land topography. The flow conditions of 2, 5, 10, 20, 50, and 100 year return periods were also produced in the hydrologic model, and the flood extent and the surface water level are gradually increasing in the river basin.

Finally, to manage and prepare the risk in the study area, the flood risk assessment was analyzed by accounting the three main factors, namely, flood hazard map, which was the 50 year return period developed by hydrologic and hydraulic

models. The conceptual equation of this risk assessment is $FR = FH \times FE \times FV$. The flood exposure was included the layers of the population, crop, schools, hospital and road network, and flood vulnerabilities calculated from the parameters of age composition (< 14 and > 65 years old), literacy, and urban area. According to the result, 23.64 % of village tracts in the total 1341 village tracts will be affected. Flood risk area was described as the low, medium, high, and very high magnitude with 11.3%, 3.9%, 5.1%, and 3.3% in the village tract level, respectively. The higher flood risk area has mainly occurred in Homalin, where are the junction of upstream Chindwin river and U Yu tributary, Kalay low terrain at Kalay tributary, and downstream area, Monywa township.

ACKNOWLEDGEMENTS

Firstly, I would like to deeply grateful to the double master program of the Sirindhorn Center for Geo-Information (SCGI), which is collaborating amongst Wuhan University: China, Burapha University: Thailand, and GISTDA (under Ministry of Science and Technology: Thailand) for the scholarship program through the studying in China and Thailand.

I would like to express my sincere thanks to my advisor, Assoc. Prof. Jianzhong Lu, who guided and encouraged me throughout the research. And I would also like to thank Prof. Xiaoling Chen for accepting to be my studies of her research team in LIESMARS.

I want to express thank to my co-supervisor Dr Pakorn Petchprayoon (GISTDA) who taught and instructed me in the research improvement.

I would like to thank the guidance of Dr Tanita Suepa, Dr Haoran Zhang, and lecturers from GISTD for their kindly discussion for the research development and lectures for knowledge improvement.

Besides, I would also like to extend to my gratitude to Dr Kitsanai Charoenijit, and lecturers from the Burapha University for their lectures and contributions.

This acknowledgement will not be completed without additional thanks to all of the professors and lecturers from Wuhan University, Burapha University, and GISTDA.

I would like very much to extend my gratitude to teachers who always had my back during the whole research program, making sure that everything is in place to ensure smooth research progress.

I also would like to thank the reviewers and defense committee for their proper comments to improve my thesis.

I am very thankful to LIEMARS's Human Resource Team: Mrs Wei Min, and all of the staffs who always helped me with guidance and sharing during studying in China.

I would also like to express all of the staff from GISTDA and Burapha University for their kind guidance and administration during studying in Thailand.

I would also like to show my gratitude to Ms Khaing Chan Myae Thu for sharing her knowledge through the research.

I would like to thank all of my friends from the first generation of the SCGI master program and my classmates from Wuhan University.

I would like to extend my special thanks to the in Charges of Sustainable Environment Myanmar Co., Ltd., and Geo Trend Co., Ltd., which are my working environment for their permission to study and long to stay in oversea.

My sincere apologies to those whose person's names are not mentioned in this acknowledgement, but their help and contribution will never be forgotten.

Finally, I am incredibly grateful to my parents and siblings for their love and caring. I am very much thankful to Ms Nyein Soe Thwal (ADPC) for her precious discussion and encouragement during my study abroad.

Chit myo Lwin

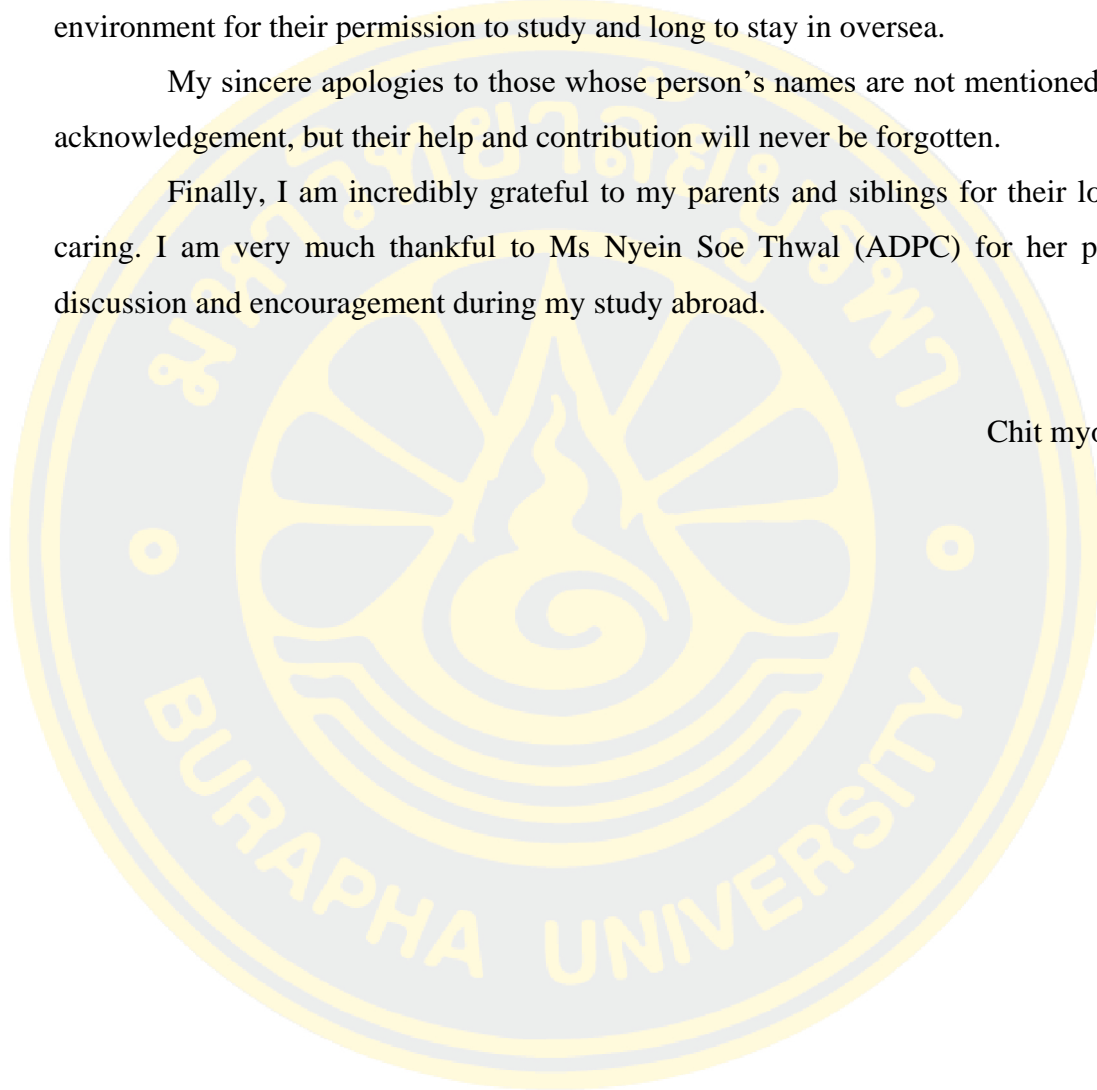


TABLE OF CONTENTS

	Page
ABSTRACT.....	D
ACKNOWLEDGEMENTS.....	G
TABLE OF CONTENTS.....	I
LIST OF TABLES.....	M
LIST OF FIGURES.....	N
1.1 Study Area	1
1.2 Problem statement	3
Research Objectives.....	3
Research questions.....	3
Scope of research.....	4
Thesis structure	4
CHAPTER 2	6
LITERATURE REVIEW	6
2.1 Floods	6
2.1.1 Causes of flood	6
2.1.2 Flood triggers and conditioning factors.....	6
2.2 Rainfall-runoff models	7
2.2.1 Streamflow synthesis and reservoir regulation (SSARR model)	7
2.2.2 TANK model.....	8
2.2.3 Nedbor-Afstromning-Model (NAM)	8
2.2.4 Soil and water assessment tool (SWAT)	8
2.2.5 Topography based hydrological model (TOPMODEL).....	9
2.2.6 HEC-HMS model	10
2.3 Hydrodynamic models.....	10
2.3.1 MIKE 11 model.....	10

2.3.2	HEC-RAS model.....	11
2.4	Related works	12
2.5	Previous studies in the Chindwin river basin	13
2.6	Remarks on the literature review	15
CHAPTER 3	15
MATERIALS, METHODS, AND PROCESSING	15
3.1	Data Acquisition	16
3.2	Methods	17
3.2.1	Hydrologic model (HEC-HMS)	17
3.2.1.1	Loss method	19
3.2.1.2	Transform method	20
3.2.1.3	Baseflow method.....	20
3.2.1.4	Routing method	22
3.3.2	Hydraulic model (HEC-RAS) and flood hazard mapping	23
3.3.2.1	Steady flow and unsteady flow.....	24
3.3.2.2	Uniform and Non-uniform flow	25
3.3.2.3	Momentum equation.....	25
3.3.2.4	Continuity equation	25
3.3.3.5	Manning's Coefficient "n"	26
3.3.3.6	Geometric data.....	26
3.3.4	Geographic Information System (GIS)	26
3.3	Flood risk assessment	27
3.3.1	Flood hazard	29
3.3.2	Flood exposure	29
3.3.3	Flood vulnerability	30
3.3	Flood risk assessment	31
3.3.1	Generation of Triangulated Irregular Network (TIN)	31
3.4.2	Land use/land cover (LULC)	31
3.4.3	Type of soil.....	34

3.4.4 Rainfall data	35
3.4.4.1 Areal rainfall calculation	36
3.4.4.2 Design rainfall event.....	37
3.4.4.3 Delineation of river catchment	38
3.5 Processing in the HEC-HMS model	40
3.5.1 Calibration and validation for hydrologic model	42
3.5.2 Trial & error and objective function.....	43
3.5.3 Efficiency criteria method and error assessment.....	44
3.5.3.1 Nash Sutcliffe Efficiency (ENS)	44
3.5.3.2 Coefficient of Determination (R ²)	45
3.5.3.4 Coefficient of correlation (R)	45
3.5.3.5 Root Mean Square Error.....	46
3.5 Processing in HEC-RAS Model	46
3.6.1 Pre-processing in HEC-GeoRAS	47
3.5.2 Geometric data	48
3.6.3 Unsteady flow data.....	49
3.6.4 Flood inundation mapping.....	50
3.7 Remote Sensing	50
3.7.1 Google Earth Engine (GEE).....	52
3.7.2 Remotely sensed techniques for flood detection.....	52
3.7 Processing for flood risk assessment	55
3.7.1 Hazard mapping	55
3.7.2 Exposure map	55
3.7.3 Vulnerability mapping.....	59
CHAPTER 4	65
4.1 Hydrologic model (HEC-HMS)	65
4.1.1 Calibration and validation results.....	66
4.1.2 Simulation of design flood hydrography.....	68
4.2 Hydraulic model (HEC-RAS).....	69

4.2.1 Calibration and validation results	69
4.2.2 Simulation of flood scenarios	71
4.2.3 Flood hazard mapping	72
4.3 Validation for the flooded area	75
4.4 Flood risk assessment	77
4.5 Discussion	82
CHAPTER 5	85
5.1 Conclusion	85
5.2 Recommendations	86
5.3 Future Works	87
REFERENCES	88
BIOGRAPHY	99

LIST OF TABLES

	Page
<i>Table 1 Types and sources of data</i>	16
<i>Table 2 Area of LULC types in the study area</i>	33
<i>Table 3 Types and area of soil in the study area</i>	35
<i>Table 4 Physical characteristics of sub-basins in the Chindwin watershed area</i>	40
<i>Table 5 Demographic data of the study area</i>	60
<i>Table 6 Calibrated parameters of HEC-HMS model in Chindwin River Basin</i>	65
<i>Table 7 Results of calibration for the selected seven years of flood events</i>	67
<i>Table 8 Flood inundation area and depths of the 2, 10, 20, 50, and 100-year flood return periods</i>	75
<i>Table 9 Comparison of flood inundation area of simulated result and flood area from remote sensing</i>	77
<i>Table 10 Data of the peak discharge and storm inundation area for the selected return periods</i>	83

LIST OF FIGURES

	Page
<i>Figure 1 Location map of the Chindwin river basin.....</i>	<i>2</i>
<i>Figure 2 Causes of the flood triggers and flood-conditioning factors</i>	<i>7</i>
<i>Figure 3 Overall flow-charts of the flood inundation map and risk assessment</i>	<i>17</i>
<i>Figure 4 Flow-chart of the hydrologic model</i>	<i>18</i>
<i>Figure 5 Initial base flow recession</i>	<i>21</i>
<i>Figure 6 Process of base-flow model</i>	<i>22</i>
<i>Figure 7 Lag method.....</i>	<i>23</i>
<i>Figure 8 Flow-chart of the hydraulic model and flood inundation mapping</i>	<i>24</i>
<i>Figure 9 The general process of GIS, HEC-GeoHMS, and HEC- HMS</i>	<i>27</i>
<i>Figure 10 Flow-chart of flood risk</i>	<i>28</i>
<i>Figure 11 Process of TIN model generation (a) Digital Elevation Model (DEM) and (b) Triangulated Irregular Network (TIN).....</i>	<i>31</i>
<i>Figure 12 Land use/land cover map</i>	<i>32</i>
<i>Figure 13 Graph of land use/land cover area</i>	<i>33</i>
<i>Figure 14 Soil map</i>	<i>34</i>
<i>Figure 15 Pie chart of soil type</i>	<i>35</i>
<i>Figure 16 Location of rain-gauge and water level stations in the study area.....</i>	<i>36</i>
<i>Figure 17 Thiessen polygons for aerial rainfall calculation</i>	<i>37</i>
<i>Figure 18 The overview steps of HEC-GeoHMS</i>	<i>38</i>
<i>Figure 19 The process of terrain analysis</i>	<i>39</i>
<i>Figure 20 HMS schematic basin model</i>	<i>41</i>
<i>Figure 21 Method selection window for basin model development</i>	<i>42</i>
<i>Figure 22 Pre-processing in HEC-GeoRAS</i>	<i>48</i>
<i>Figure 23 Geometric river data.....</i>	<i>48</i>
<i>Figure 24 Cross-section data with the editing interface</i>	<i>49</i>
<i>Figure 25 The unsteady flow data option</i>	<i>50</i>

<i>Figure 26 Remote sensing system</i>	51
<i>Figure 27 Flow-chart of flood mapping in Google Earth Engine (GEE)</i>	53
<i>Figure 28 Processing the flood computation using the sentinel-1 data for 2015 flood event at Homalin Area in Chindwin River</i>	54
<i>Figure 29 Processing the flood computation using the sentinel-1 data for 2017 flood event at Homalin Area in Chindwin River</i>	54
<i>Figure 30 Population density map</i>	56
<i>Figure 31 General flow chart of crop mapping</i>	56
<i>Figure 32 Crop map of Chindwin river basin</i>	57
<i>Figure 33 (a) Location of schools and (b) Buffering of schools</i>	58
<i>Figure 34 (a) Location of hospitals and (b) Buffering of hospitals</i>	59
<i>Figure 35 (a) Location map of the road network and (b) Buffering the road network</i>	59
<i>Figure 36 Illustration of statistical, demographic data of study area (Census 2014).</i>	60
<i>Figure 37 Demographic maps for (a) Age composition (more than 65 years old) and (b) Age composition (less than 14 years old)</i>	62
<i>Figure 38 Overall steps of urban area computation in Google Earth Engine</i>	63
<i>Figure 39 (a) Literacy map of township-level and (b) Location map of the urban area</i>	63
<i>Figure 40 (a-g) Calibration results of HEC-HMS model</i>	67
<i>Figure 41 Validation results of the HEC-HMS model for 2015 and 2017 flood events</i>	68
<i>Figure 42 Design flood hydrograph with the selected return periods</i>	69
<i>Figure 43 Calibration result of HEC-RAS model for 2012 flood event</i>	70
<i>Figure 44 Validation result of HEC-RAS model for 2015 and 2017 year flood events</i>	71
<i>Figure 45 Maximum flow profile of 50-year return period (only main channel)</i>	71
<i>Figure 46 3D perspective view of floodplain and channel (50 year return period)</i>	72
<i>Figure 47 (1)Flood inundation map for 2015, and (2) Flood inundation map for 2017 modeled by HEC-RAS</i>	72

<i>Figure 48 (a-f) Flood inundation maps for the 2, 5, 10, 20, 50, and 100 year return period floods</i>	<i>74</i>
<i>Figure 49 The relationship of flood extent and depth of the 2, 5, 10, 20, 50, and 100 year return period floods</i>	<i>75</i>
<i>Figure 50 Flood area computed from the Sentinel 1 satellite data in Google Earth Engine for (1) 2015 flood area and (2) 2017 flood area</i>	<i>76</i>
<i>Figure 51 Flood comparison between flood inundation map by RAS model and flood map by remote sensing technique for (a) overlapped area of 2015 flood, and (b) overlapped area of 2017 flood</i>	<i>77</i>
<i>Figure 52 Flood hazard map of Chindwin river basin</i>	<i>78</i>
<i>Figure 53 Flood exposure map of Chindwin river basin</i>	<i>79</i>
<i>Figure 54 Flood vulnerability map of Chindwin river basin</i>	<i>80</i>
<i>Figure 55 The overall process of flood risk assessment</i>	<i>81</i>
<i>Figure 56 The result of flood risk assessment for Chindwin river basin</i>	<i>82</i>
<i>Figure 57 Flood risk assessment in village tract level for Chindwin river basin</i>	<i>84</i>

CHAPTER 1

INTRODUCTION

Flooding is a kind of natural disasters in the globe, and it can cause lots of damage to the Earth's surface, including human lives and infrastructures [1]. It can happen as a hazard if it has a potential threat to people, animals, and their welfare in a watershed area. Thus, the flood inundation map has become essential for flood risk management, and it also provides vital information to the residents to be aware of the vulnerabilities [2].

Due to the southwest monsoon season in Myanmar, floods also happen in June to September since the westerly depression system, and the tropical cyclone system may turn into macroscopic rainstorms especially, in low land areas and Ayeyarwaddy river basin. [3]. These floods have caused the most prominent natural disaster in Myanmar in terms of the population increased, and the disruption to socio-economic activities [4].

In this study, hydrologic and hydraulic models are applied to carry out the rainfall-runoff simulation and flood hazard maps of the Chindwin river basin to be achieved the awareness of the flooded area in that area. Moreover, the flood risk assessment is analyzed by the integration of hazards, exposures, and vulnerabilities for flood risk management of the study area. Thus, the flood hazard mapping and flood risk assessment are helpful for flood risk management.

1.1 Study Area

Figure 1 shows the location of the Chindwin river basin situated in the northwest of Myanmar and partly included the eastern part of India. It is the most significant catchment area of the Ayeyarwady river system. The coordination of the Chindwin river basin lies between 21°24' and 27°20'N latitude and between 93°25' and 97°05'E longitude with the catchment area 113484 km². The terrain condition of the study area is being varied within the 150 m influenced by the high land terrain region of the high mountain ranges and flat land terrain of agriculture. As the terrain elevation is a huge difference, the significant sub-basins of the Chindwin River system are formed, such as U Yu and Myitha at the upstream and Kalawe at downstream, respectively.

The catchment area of Chindwin River is, in general, hilly topography at the north and west in alignment while the central and south of the basins are low land terrain. The highest topography is more than 3,700 m (Mean Sea Level). The basin is standing from north to south with different topography. Firstly, the river passes through the Hukawn valley, which is a vast valley and basin admits the mutinous area with the elevation of 2300 m and then goes through the different topography in various of above 1000 m at the north and around 50 m at the south of the study area. Many towns have encountered in the basin, and some of the big towns are Monywa, Mawlaik, Homalin, Hkanhti, Kalay, Gangaw, etc.

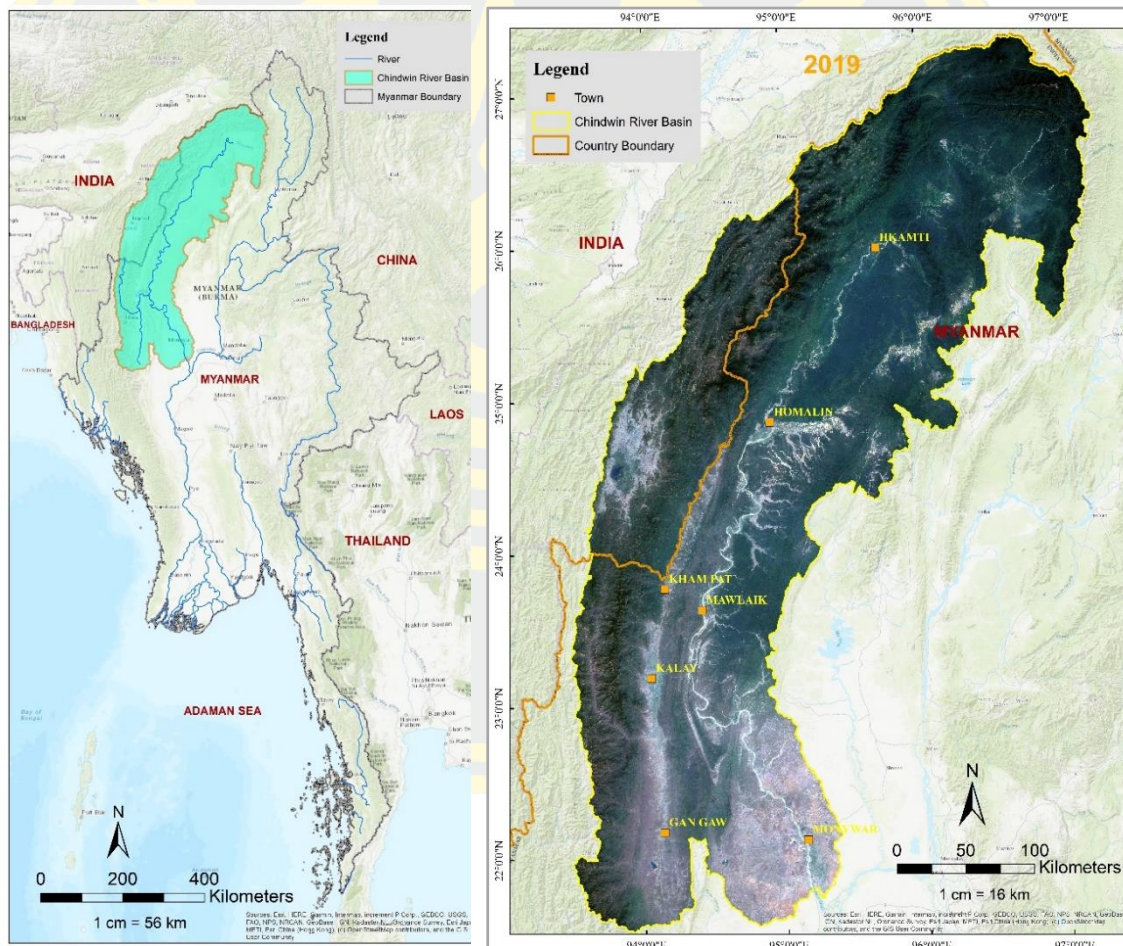


Figure 1 Location map of the Chindwin river basin

1.2 Problem statement

The study area is quite a big area with a different topographic condition, and it can be representative of the central river basin, Ayeyarwaddy, which is the most significant river system in Myanmar. Here, Myanmar has the effects of monsoon throughout the country every year. Annual monsoon of floods and seasonal floods occurred mainly in the tense of heavy rain and big temporal scale in the study area [5]. It is naturally with large segments of rivers, streamlets, and tributaries, and it could be ranked as the biggest river of the Ayeyarwaddy River system.

According to the historic floods, some devastating impacts were recorded primarily in 2015 and 2011 floods. These floods had impacted the lives and properties of humans, especially livestock, agriculture, infrastructures, and so on. The challenges of river flooding are getting more and more dangerous due to human intervention in the floodplain at an ever-increasing scale [6].

Research Objectives

Overall, the main objectives of this research are summarized as follow:

- To simulate the rainfall-runoff process of flood events by using the hydrologic model
- To determine the design flow hydrography using the hydraulic model
- To predict the flood inundated depths and extents of the selected scenarios
- To validate the flood maps from remote sensing techniques with the flood inundation maps and
- To assess the risk of flood by considering the factors of flood exposures, hazards, and vulnerabilities in the Chindwin river basin.

Research questions

- What is the amount of rainfall-runoff volume in simulation for the selected flood events?
- How many maximum flood inundation areas in the Chindwin river basin during the peak storm events?

- What are the maximum rainfall-runoff volume, the surface flood extent, and the depth of the different return periods?
- How to validate the flood hazard maps with the data of remotely sensed techniques and field observation from the government office?
- What are the factors required to evaluate the flood hazard, exposure, and vulnerability maps?
- How many village tracts flooded in the analysis of risk assessment in the study area?

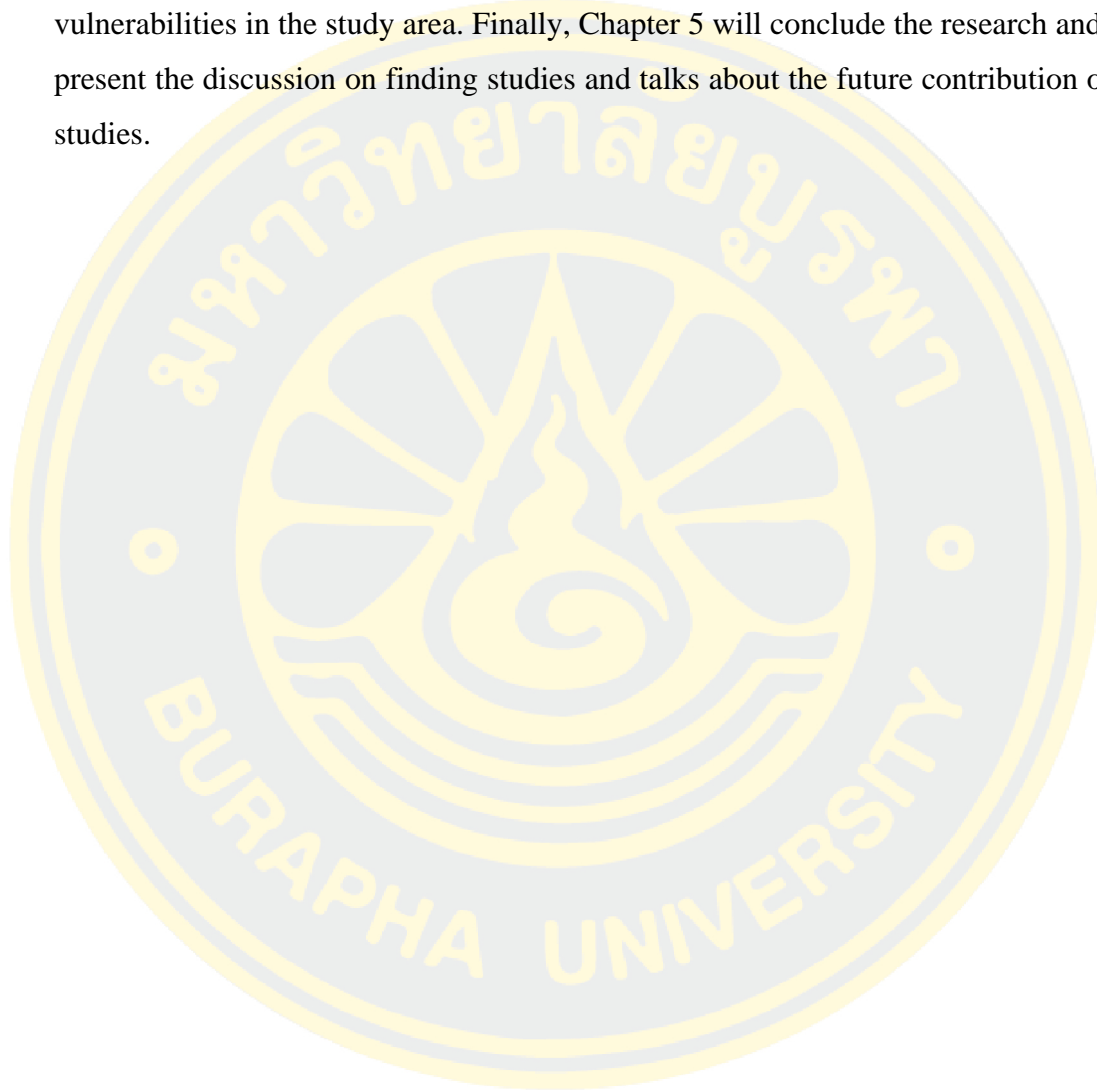
Scope of research

- Required datasets for modelling, the rainfall, water level, discharge, and cross-section data were collected from five Met stations in the entire watershed area.
- Spatial data such as population map, land cover map, soil data, digital terrain model, etc. were extracted from the open accesses databases.
- The rainfall-runoff simulation was produced by applying the HEC-HMS. Moreover, the flood hydrograph was also calculated.
- Flood hazard maps for the selected storm events and return period flood were simulated by using with HEC-RAS model
- The residential land and crop mapping were computed with Sentinel-2 satellite data in the cloud-based system of google earth engine (GEE). Moreover, the flood areas of 2015 and 2017 year were calculated in GEE to validate the simulated maps from the hydraulic model.
- Flood risk assessment was carried out in consideration of the related factors such as the flood hazard, the exposure, and the vulnerability layers.

Thesis structure

This study relates to the process of flood hazard mapping and flood risk assessment for the Chindwin River Basin in Myanmar. There are five chapters in this thesis. Chapter 1 presents the overview of the flood, the general review and characteristics of the research area, problem statement, and research problem and objectives. Chapter 2 will provide the literature review of hydrologic and hydraulic models for flood hazard mapping, the related works, and previous studies in the study area. Next, Chapter 3 will describe the method, data, and processing of the whole research. Moreover, the handling, data preparation, and model development will present in this chapter. In

Chapter 4, the main experiment result and discussion are mainly described such as the results of model validation and calibration in the HEC-HMS and its return period, the results of validation for flood inundation mapping in the hydraulic model, and the flood risk assessment by consideration of flood hazard, flood exposure and flood vulnerabilities in the study area. Finally, Chapter 5 will conclude the research and also present the discussion on finding studies and talks about the future contribution of the studies.



CHAPTER 2

LITERATURE REVIEW

2.1 Floods

The different types of floods are occurred across the world, such as urban flood, river flood, flash flood, and coastal flood. Among them, urban floods are the most significant and destroying thing in flood risk due to the high flood exposures and vulnerabilities [7]. In a riverine flood, it is relatively connected with the high water volume increasing as the heavy rain is getting longer. The flood can also be produced in the unfavorable condition of an area such as land cover, soil, geomorphology, elevation, slope, and so on. And it also has impacts on human societies and their properties because the rivers are essential for cultivation and Civilization [8][9].

Flash flood is rapid flooding due to the heavy intensity of precipitation in the low land area. [10]Coastal floods mainly occurred in the region of seashore line when the high pressure of onshore winds push water from the sea onto land, and this can create the form of storm surges related to storm surge, tsunami, tidal waves, etc. [9].

People are living in flood plain areas and along the side of the river system due to the full fill their foods for cultivation, transportation, fishing, etc. As the overpopulation has become more prominent, the people are living in more floods in return period area and low land terrain region, and it is happening the flood risk in recent years and future [11].

2.1.1 Causes of flood

Generally, the river floods have happened in the condition of the excessive heavy rainfall and over-discharged in the area. By a combination of high tides and waves at the low land area can produce the estuarine and coastal floods [12].

2.1.2 Flood triggers and conditioning factors

Figure 2 shows some trackers of the flood and the flood-intensifying elements. There are so many flood-trigger and conditioning factors in a river flood, and one of them, the intensive heavy rainfall, is the leading tracker of the river flood by combination with the conditioning-factors such as the geomorphology, elevation,

human activities, etc. In the cases of estuarine and coastal flood-intensification, the flood is occurred due to the storm surge, tsunami waves, etc. [12].

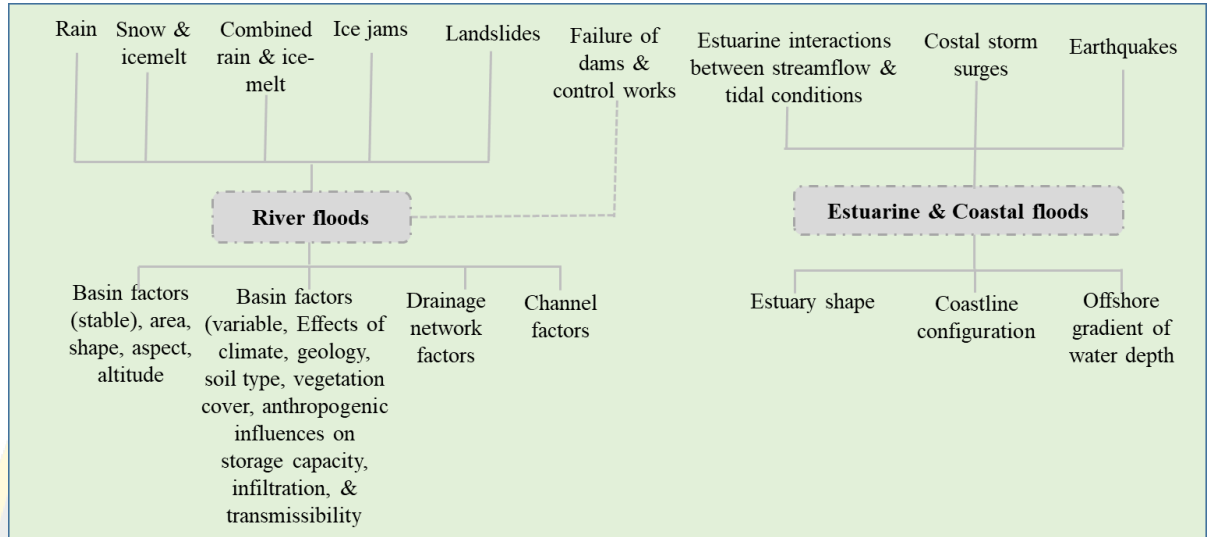


Figure 2 Causes of the flood triggers and flood-conditioning factors

Source: [12]

2.2 Rainfall-runoff models

There are various rainfall-runoff transformation models transformed to form the rainfall data by combination with factors of soil classes, vegetation condition, moisture content, and humidity, characteristics of underground water, and geomorphological characteristics of each sub-basin [13][14]. And it is also required to consider the facts of routing, flow transformation, loss in the determination of excess overflow[14].

[15] In which there are generally two types of the catchment of the model processing in the rainfall-runoff simulation, and they are the event models and continuous-process models. Some of the rainfall-runoff models are described below.

2.2.1 Streamflow synthesis and reservoir regulation (SSARR model)

This model was originally introduced by the American Society of Civil Engineers to design for the conditions in the Columbia River in the Northwest United States. Later on, it was developed to simulate the stream synthesis model in any basin. Presently, this model can be analyzed for a hydrologic and reservoir regulation model [16].

In the SSARR model, the distributed, physically-based model incorporating novel approaches for the sub-surface, run-off, and the base flow can be computed [17]. It is suitable for the big watershed area for rainfall-runoff simulation.

2.2.2 TANK model

It is a conceptual representation firstly published by Sugwara, Japan (1961), to model the variable source flow assumed in the unit area of the basin by utilizing the various data of soil, precipitation, etc. [18][19]. The Tank model is a simplified application, but it can support the excellent outcome in rivers analysis [20].

Evapotranspiration is associated with subtraction from the basin. The runoff from the side outlet of a storage tank (q) is proportional to the water head over that outlet, and the infiltration (p) is proportional to the water depth [18]. These relations can be mentioned as below:

$$q = a(h - z), p = bh \quad 2.1$$

Where h is the water depth, z is the height of the discharge outlet from the base of each basin, a is the runoff coefficient, and b is the infiltration coefficient.

2.2.3 Nedbor-Afstromning-Model (NAM)

NAM means the rainfall-runoff model, and it was developed by the Hydrological Section of the Institute of Hydrodynamics and Hydraulic Engineering of Denmark. It is a conceptual, deterministic, lumped model. It can estimate the precipitation-runoff simulation at a watershed area based on the rainfall, evapotranspiration, and temperature [21].

Moreover, NAM is appropriate to proceed with the rainfall-runoff simulation in the condition of moisture content in various water storage. As the NAM is also the lumped model, the values should be defined on average for parameters and variables for the whole basin. NAM model can be utilized to run the process of the individual storm event in the different conditions of weather and hydrologic formation [22].

2.2.4 Soil and water assessment tool (SWAT)

In the 1990s, SWAT was developed by the United States Department of Agriculture (USDA) – Agriculture Research Service (ARS). SWAT is a river basin scale, and continuous-time models and an extension of ArcGIS application to predict

the quality of runoff and underground water and predict the environmental issues of land use, land management system, and climate changes in a small basin to river basin-scale model. The SWAT is very useful, especially in the assessment of soil erosion for management, non-spatial pollution source, and regional management in a basin [23]. The author also mentioned the SWAT could be applied in the simulation of the biomass production and evapotranspiration [24].

There are two methods in the SWAT model for simulation of discharge, and they are Green & Ampt infiltration method, and the Soil Conservation Service (SCS) curve number method.

The Green-Ampt method is to determine the rate of infiltration in a basin [25]. The precipitation is an essential requirement and incorporated with a sub-daily scale. The method of SCS curve number is widely applied for a surface runoff simulation. It requires the datasets of the precipitation, weather, solar radiation, humidity, land use, and moisture content of the soil. The model can use the SCS curve number process to estimate the surface runoff when daily rainfall data and the Green-Ampt infiltration method were chosen for the simulation of discharge.

In the calculation for the overall water balance condition in a basin, the equation 2.2 can be used to achieve the accurate forecast in nutrient, water, and sediment circulation and it is an essential requirement for the simulation of the hydrologic circle [26].

$$SW_t = SW_0 + \sum_{i=1}^t (R_v - Q_s - W_{seepage} - ET - Q_{gw}) \quad 2.2$$

Where SW_t is the humidity of the soil, SW_0 is the base humidity, R_v is the rainfall volume of water, Q_s is the surface runoff, $W_{seepage}$ is seepage of the water from the soil to underlying layers, ET is the evapotranspiration, Q_{gw} is the groundwater runoff, and t is the time in days.

2.2.5 Topography based hydrological model (TOPMODEL)

The TOMDEL is also a conceptual hydrologic model by the determination of the analysis of watershed topography. However, some researchers also use it as a physical-based model [27]. This model can apply an individual or multiple sub-basins

using the grided elevation data. The geomorphology, topography, and soil condition are very considerable in the TOPMODEL application [26].

TOPMODEL have studied the flood frequency analysis in a various range of hydrologic field [27]. In the studies of [28], he explored the importance of spatial resolution in the digital elevation model (DEM) for the runoff simulation.

2.2.6 HEC-HMS model

It was introduced by the U.S Army Corps of Engineers and designed to estimate the hydrologic modelling for the river watershed area. It is the deterministic mathematical model that can calculate the various factors of the hydrosphere, including precipitation, evapotranspiration, infiltration, and surface runoff. It also takes account of controlling factors such as land use, topography, soil condition, elevation, humidity, etc. [29][30].

This application can be widely used in modelling of a flood hydrograph, water supply, and watershed runoff in a different geographic area, whether it is big or small watershed area because it is a general simulated method for many kinds of the watershed area. Any part of the process can then be done with a mathematical model that can be modelled in the different environmental conditions. The interface of the application is integrated into the work environment, including a database, data entry option, computational platform, and output featured tools [30].

2.3 Hydrodynamic models

It is physical modelling to determine water surface area & depth, and streamflow velocities. Hydraulic modelling is used for the determination of the design and operation issues in the structures [31] [32]. It enhances the use of a designed model for complicated in the different forms of river or stream flow in hydraulic structures. So many programs related to hydraulic modelling, which have purposely introduce to be ease of simulation in model design and operating system of engineering structures [32].

2.3.1 MIKE 11 model

MIKE 11 model is a professional hydrodynamic tool for river, stream, and water bodies and which was developed by the Danish Hydraulic Institute (DHI) in 1987 [33].

It can be applied as 1 D hydrodynamic model for the applications of precipitation-runoff, transportation of sediment, water quality, flooding, flash reservoir break, etc.

MIKE 11 can be in cooperation with Geographic Information System (GIS) as the ArcGIS program for flood inundation mapping or post-processing in the different flood scenarios at the watershed area [34]. It becomes an integrated system in hydrology and hydraulic fields improved by the Danish Hydraulic Institute (DHI) into a near real-time flood estimating tool [35].

2.3.2 HEC-RAS model

HEC-RAS, the Hydrological Engineering Centre-River Analysis System, is a physically hydraulic modelling tool. It can be performed the steady and unsteady flow, 1-Dimensional (1D), and St Venant Equation. This model can be returned into the promising results in comparison with 2D models [36] while controlling the simplify and employing geometric parameterization derived from spatial data [37].

Steady flow: It is applied for calculation of water surface profile for steady gradually varied stream and can be used for a single condition such as one item in channel reach, dendritic network structure, or a full of stream network [38].

Unsteady flow: It is required to perform an unsteady water surface profile calculation and composed of: (1) boundary conditions (external and internal), and (2) initial conditions.

- (1) Boundary Conditions must be structured at all of the open ends of the river system being modelled. Upstream terms of the river system can be modelled with the following types of boundary conditions: flow hydrograph, stage hydrograph, current, and stage hydrograph. Downstream ends of the river system can be shaped with the following types of boundary conditions: rating curve, Normal Depth (Manning's equation); stage hydrograph; flow hydrograph; stage, and flow hydrograph. Boundary conditions can also be established at internal locations within the river system. The following types of boundary conditions can be specified at internal cross-sections: lateral inflow hydrograph, uniform lateral inflow hydrograph; groundwater interflow; and internal stage and flow hydrograph [39].

- (2) Initial Conditions are required to construct the initial conditions (flow and stage) at all nodes in the system at the beginning of the simulation. Besides, it is needed to define the starting water surface elevation in any storage areas that are identified [39][40].

2.4 Related works

The author studied the computation of the degree and spatial area of the potential flood impacts by integrating into the GIS environment, a combination of surface runoff and hydraulic models [41]. The HEC-HMS and HEC-RAS models were utilized to simulate the river flow and floodplain evolution in the Bostanli river basin. Rainfall data was mainly used for the estimation of surface runoff using the SCS CN method for loss rate in all catchments. The author mentioned as the study area would be a positive impact and decrease the flood peak rate in the potential flood hazard after the dam construction as planned.

In this studies, the authors studied the flood extent monitoring with the HEC-RAS model to obtain the information of the near-real-time approach in Marinkina River, Philippines. Moreover, the authors developed the three significant steps of flood model setup, automation, and online visualization and which can be handled with the script for automatic calculation in the flood analysis. The input data of geometric were extracted from the 1 m spatial resolution digital elevation model, which was generated from the LIDAR technology [42]. At the same time, the river cross-section was created from field observation data and then interpolated into raster data in better resolution.

The author applied to perform the flood hazard mapping in the use of HEC-HMS and HEC-RAS models for hydrologic and hydraulic models, respectively, in the Bago river basin, Myanmar. In the loss model calculation for surface runoff simulation, the SCS Unit Hydrograph Method was utilized. In hydraulic modelling, the unsteady flow method was used with a river cross-section data, Manning's values, and flow data to analyze the river channel [43].

The author conducted the comparative studies for the flood hazard between DEM STEREO (30 m spatial resolution) and DEM (4 m resolution) generated from stereoscopic images of the Pleiades in a semi-arid mountainous area. The generation of geometric data used in the hydrodynamic model is essential for river analysis, and the

DEM of the Pleisades proved that the excellent and high accuracy of the outcome has resulted [44].

In the research of [45], the author simulated the flood inundation mapping with HEC-RAS in Sri Lanka, the lower Kalu-River basin, and also produced the different return periods of the flood events. The flood events simulated by the model validated with the remotely sensed techniques using the microwave data of the ALOS/PALSAR HH dataset. He described as the comparative studies of the simulated flood map by model and microwave remote sensing data were beneficial to study in the flood extent overlapping.

The author applied the various methods of remote sensing, HEC-HMS, HEC-RAS, and GIS techniques to produce the flood risk assessment for Lagos Island and part of Eti-Osa local government areas in Lagos State, Nigeria. The flood hazard maps were calculated from a combination of hydrologic and hydraulic models, and then, the results were checked with the flood map derived from the remote sensing data. The author continued to conduct the flood risk information on the classes of the infrastructures in the study area. The ground validation on buildings was carried out the GPS sampling at the flood events, and the overlaying process resulted in the areas of flood risk in the GIS platform. The author suggested the development of flood plain can help better management in flood risk [14].

The authors studied the flood risk on the whole country of Myanmar to indicate the flood risk index in the township level. They mentioned as the time-series satellite data can derive the flood area and produced as the hazards in consideration of the historic flood frequency (Joint Research Center). In the reduction of flood risk, the proper management is required, and they describe the equation for flood risk assessment index as $FRI = FHI \times FEI \times FVI$ [46].

2.5 Previous studies in the Chindwin river basin

There are limited research papers in the study area, especially the studies related to the hydrologic and hydraulic models due to the various dataset requirement and the vast watershed area. Some of the related research is described below.

The author studied the approach of neural network-based regionalization to estimate the homogenous hydrological regions in the Chindwin River basin. However, the author didn't present the surface runoff simulation and river flow analysis. The homogenous hydrological areas of the study area were detected by clustering and utilizing the artificial neural network (ANN) model, and the four clusters of homogenous regions were produced [47].

The studies of [48] experimented with forecasting the flood event-based-model for rainfall-runoff simulation using the Flussgebietsmodel (FGM). This model is based on the unit hydrograph as a fundamental requirement in the hydrologic process, and it can mainly be classified as the urban region and rural areas for the flood determination. In the flood routing of FGM, the Kalinin-Milyukov method was applied to analyze the base flow in the Chindwin river basin. According to the result, the peak discharge and the magnitude of the peak discharge were correlated between rainfall and runoff with acceptable accuracy in the FGM model.

The author examined the water quality impact and landscape pattern changes (between 1990 -2013) due to deforestation and mining activities. The effects of these factors were computed with the remote sensing technology and compare the previous condition and current condition. The author found the findings of the rate of deforestation increased since 200, from 140 to 359 km²/year. The main controlling factor of deforestation is mining activities, and it is leading to the water quality impact. Moreover, the author noticed the increase in levels of turbidity and electrical conductivity in different periods. However, the author didn't mention the flood increased by the impact of deforestation and mining activities [49].

The researcher carried out the comparative studies between the RRI model and the HEC-RAS model for the flood inundation maps in the different return periods. Both models classified as a similar risk area at Homalin Township, but the water level by the RRI model was slightly more than the HEC-RAS model predicted [50].

The author also examined the surface runoff simulation and the flood inundation maps using HEC-HMS and HEC-RAS models for the upper Chindwin watershed area. The author compared the simulated flood hazard area of the selected

storm event in 2015 and the flood map derived from the remote sensing, and the result was presented the near correlation of the flood extent in the validation [51].

The author mentioned the flood quartiles of the different return periods using a Multiple linear regression approach (MLRA) and Artificial Neural Network (ANN) based on the digital elevation model [52]. An MLRA is a model to fit the relationship between one or more explanatory variables and a response variable in observed data. An ANN is big processing in the information database system that is composed of several processing elements with the neuron the layers. Each layer neuron operates the logical parallelism. The author found that the performance of the ANN model for flood forecast is one day ahead than the MLRA.

2.6 Remarks on the literature review

As the literature review is presented with the previous studies and related works for the flood hazard mapping and risk assessment, it is assumed that to produce the hazard maps is a better correlation using the hydrologic and hydraulic models. Moreover, the validation is essential to validate the flood extent and depth. For disaster management, at least, the village track levels are required for the flood risk assessment.

CHAPTER 3

MATERIALS, METHODS, AND PROCESSING

This chapter will describe the sources of data collection required in processing and analyzing, and also present the flow charts of the hydrological model, hydraulic

model, remotely sensed techniques for flood mapping, and flood risk assessment. Moreover, the detailed data processing for model developments with the illustration and the related attribute tables was also presented.

3.1 Data Acquisition

Data is fundamental to analyze the rainfall-runoff model and analyze the flood hazard maps for The Chindwin river basin. Moreover, to conduct the flood risk assessment, so many datasets are required. All of the materials and sources of data are presented in Table 1.

Table 1 Types and sources of data

No	Data Type	Description	Source
1	Digital Elevation Model	DEM SRTM 30m DEM ALOS PALSAR 12.5 m	USGS Earth Explorer Copernicus Open Access Hub (ESA)
2	Land Use/Cover map (Satellite Imagery)	Sentinel 2 Optical Data (2019)	https://scihub.copernicus.eu/dhus
3	Soil map	(SSURGO) Soil Map	United States Department of Agriculture
4	Precipitation Data	Daily precipitation (1967-2019)	Department of Metrology and Hydrology (DMH)
5	Discharge Data	Daily Discharge (2011-2019)	
6	Water level Data	Daily Water Level (2011-2019)	
7	Rating Curve and IDF	Homalin, Mawlaik & Kale Stations	
8	River Cross Section	Homalin, Mawlaik & Kale Stations	
9	Flood Extent Map	Sentinel 1 Radar Data	https://scihub.copernicus.eu/dhus
10	Population	Population Density	Department of population (Census 2014) (http://www.dop.gov.mm/en)
11	Cropland	Sentinel 2 Optical Data (2019) (Remote Sensing Technique)	https://scihub.copernicus.eu/dhus
12	Urban Area	Sentinel 2 Optical Data (2019) (Remote Sensing Technique)	https://scihub.copernicus.eu/dhus
13	School	School location	Myanmar Information Management Unit (MIMU)

14	Hospitals	Hospital locations	UTM 2000, Myanmar Survey Department
15	Roads	Road network	OpenStreetMap Contributors

3.2 Methods

In this research, the overall work-flow of flood hazard mapping, and flood risk assessment is shown in Figure 3.

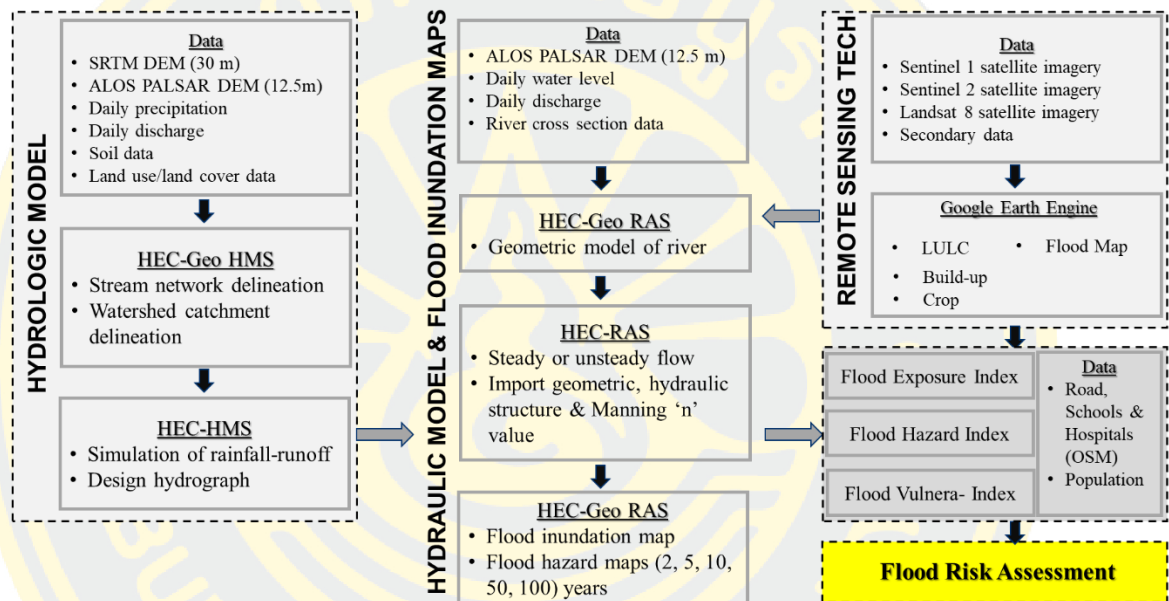


Figure 3 Overall flow-charts of the flood inundation map and risk assessment

3.2.1 Hydrologic model (HEC-HMS)

To estimate the rainfall-runoff simulation, the hydrologic model was applied, as shown in Figure 4.

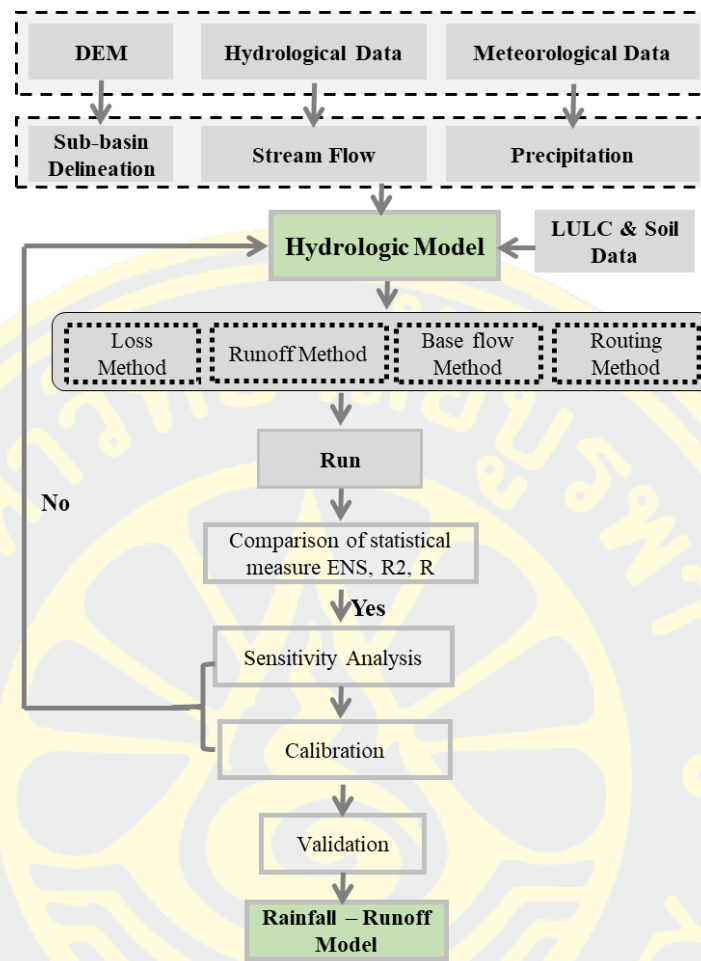


Figure 4 Flow-chart of the hydrologic model

In the modelling of the rainfall-runoff model with HEC-HMS, four essential components are needed to run the primary model, and they are (1) basin model, (2) Meteorological model, (3) control specification, and (4) time-series data.

(1) Basin model: It is the mainframe of the hydrologic model and also presents the watershed, sub-basins, junctions, reaches, reservoirs, outlets, and river segments. They are connected with a node-link system spatially from the upstream database to the downstream till the outlet.

(2) Meteorological model: It is used to calculate and estimate the amount of precipitation, evapotranspiration, temperature, sunshine, humidity, and snowmelt required by the sub-basin element.

(3) Control specification: it is to define the time frame of the simulation period and individual time. The beginning and end times, plus the computational time interval, identify the control specifications for an HEC-HMS model run. The separate specification is created in the attribute table of observed precipitation, discharge data, etc. with time interval to fulfill the hydrologic processing.

(4) Time-series data: created database of meteorological elements and discharged data are defined with the specific period for the event.

Moreover, to transform the data from the precipitation into the rainfall-runoff model, four basic models are essential in HEC-HMS, and they are the loss, transform, base flow and routing models [30].

3.2.1.1 Loss method

It is the amount of water loss during the storm event that is transformed from runoff, infiltration, or evapotranspiration in the watershed area [53][32]. The loss methods can be applied in HEC-HMS, as presented in Table 2.2.

In the loss model, the initial and constant rate loss method is selected because it is elementary and useful for the hydrologic model in the condition of a lack of detailed soil information. It is also appropriate for the flow-frequency studies [53]. The constant rate determines the rate of infiltration that will occur after the initial loss is satisfied, and it is directly connected with the impervious area.

This model considers the high potential rate of rainfall loss, f_c , in a storm event [53]. Here, P_t is the mean areal precipitation depth during a time interval (t) to t+D, the excess, pe_t , during the interval is given by:

$$pe_t = \begin{cases} P_t - f_c & \text{if } P_t > f_c \\ 0 & \text{otherwise} \end{cases} \quad 3.1$$

Equation 2.2 for loss models represents the interception and depression storage for the process of absorption in precipitation by surface covers such as soil and land use land cover in a basin, and a consequence of depression in catchment geomorphology respectively [53].

3.2.1.2 Transform method

[54] This mentioned that the rainfall from a storm event would be converted in the runoff transformation, such as decreasing in the runoff, affect each sub-basin, and represents the subsurface model.

The actual subsurface in the basin is calculated with a base-flow method [55]. There are six processes in base flow. They are (1) Constant/Monthly, (2) Linear reservoir, (3) Nonlinear Boursin Esq, (4) Bounded Recession, (5) Recession curves methods, and (6) the Recession method because of the availability of its input data was chosen for this research to model Chindwin river basin.

In the SCS unit hydrograph, it is considered in the process of a large number of natural unit hydrograph for the big catchment area. The parameters are required the peak discharge and the time to peak [53]. Some researchers suggest the following equation.

$$U_p = C \frac{A}{T_p}$$

3.2

Where U_p is the unit hydrograph peak discharge, A is the watershed area, T_p is the time-to-UH peak, and C is the conversion constant (2.08 in SI and 484 in Foot-pound system).

3.2.1.3 Baseflow method

Recession method in HEC-HMS is utilized to present the catchment base flow and the channel from natural storage in a watershed [56][30]. The relationship of Q_t (the base flow at any time t) is as:

$$Q_t = Q_0 k^t$$

3.3

Where Q_0 is the initial base flow (at time zero), and k is an exponential decay constant.

Figure 5 illustrates the relationship between the base-flow, direct surface runoff, and infiltration. The shaded area represents the base-flow in Figure 3.3. As the HEC-HMS program, k is described as the ratio of the base-flow at time t to the base-flow one day earlier. The starting base-flow value, Q_0 , is an Initial of the model [57][30].

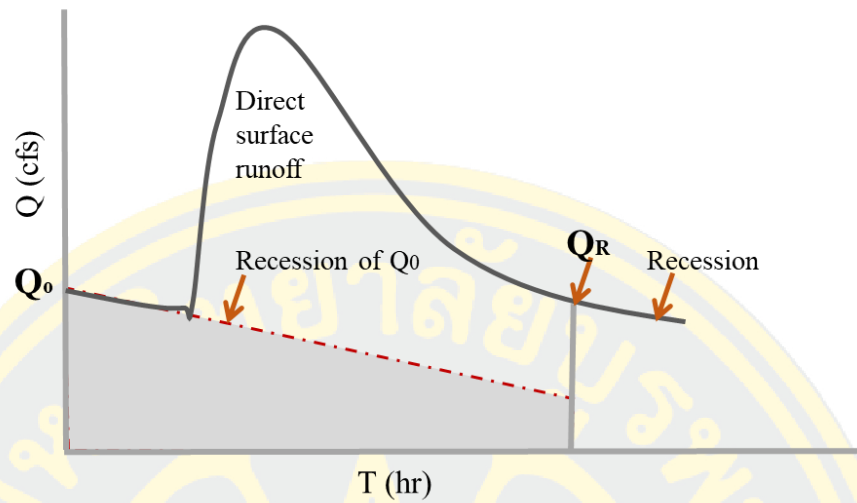


Figure 5 Initial base flow recession

In this model, the recession base-flow model is used both at the start of simulation of a storm event and later in the event as the delayed subsurface flow reaches the stream or river channels [57][58], as illustrated in Figure 6.

The base-flow is regarded as the initial base-flow recession [59]. After that, base-flow is not computed directly but is considered as the recession flow less the direct-surface-runoff. When the direct-surface-runoff eventually reaches zero, the total flow and base-flow are identical.

After the threshold flow occurs, the stream-flow hydrograph ordinates are defined by the recession model alone, even though there is no exceeding the threshold value in the direct runoff with initial base-flow recession [60]. It may arise the second time in the hydrograph if the subsequent precipitation is high. In that process, begins on the second rising limb are calculated by increasing with direct runoff to the initial recession [53].

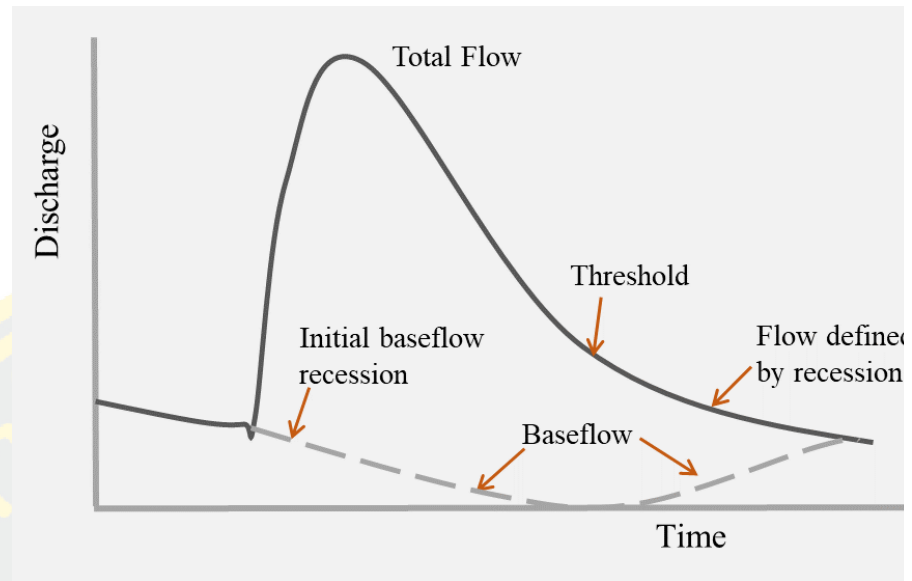


Figure 6 Process of base-flow model

3.2.1.4 Routing method

It is the movement of the runoff from the different watershed outlets along the river or streamlines, and finally, goes through to the outlet or sink of the whole basin system [53]. The routing options include the Muskingum, Modified Puls, Kinematic Wave, and Muskingum-Cunge and lag methods in the HEC-HMS model [54][61].

The lag routing method only represents the translation of flood waves, and the outflow hydrograph is simply the inflow hydrograph. However, this flow is originally started by the specified duration. So, this may not access any representation of the attenuation or diffusion process [62]. Consequently, it is also suitable for shorter stream reach with an estimated travel time that does not vary flow depth. The flows are not attenuated, and the shape is not changed.

$$Q_t = \begin{cases} I_t & \text{if } t < \text{lag} \\ I_{t-\text{lag}} & \text{if } t \geq \text{lag} \end{cases}$$

3.4

Where, Q_t is the outflow hydrograph ordinate at time t , I_t is the inflow hydrograph ordinate at time t , and Lag is the time by which the inflow ordinates are to be lagged.

Figure 7 illustrates the results of the application of the lag model. In Figure 3.5, the upstream (inflow) hydrograph is the boundary condition. The downstream

hydrograph is the computed outflow, with each ordinate equal to an earlier inflow ordinate, but lagged in time.

The lag model is a particular case of other models, as its results can be duplicated if parameters of those other models are carefully chosen [53].

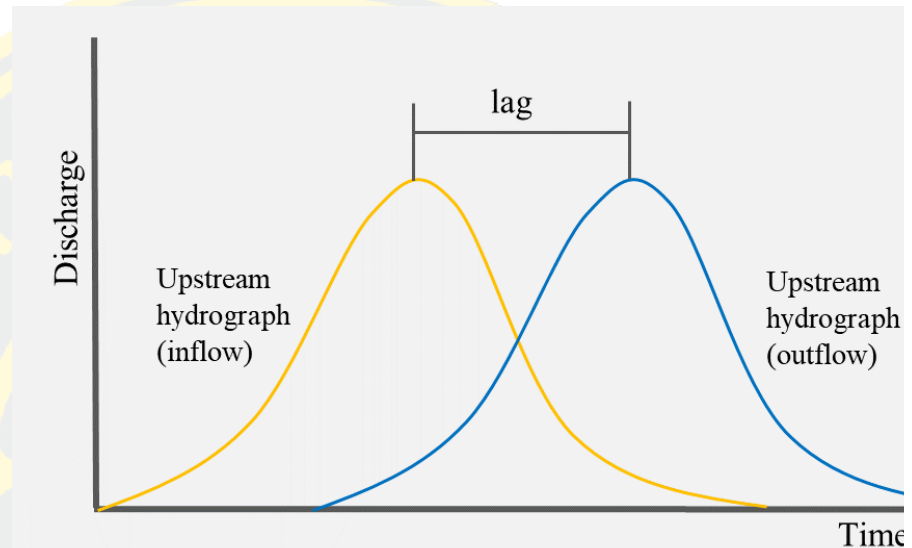


Figure 7 Lag method

3.3.2 Hydraulic model (HEC-RAS) and flood hazard mapping

Figure 8 shows the detailed process of the flood inundation mapping using the flood observed data from the hydrologic model and computed the hydraulic condition in the study area.

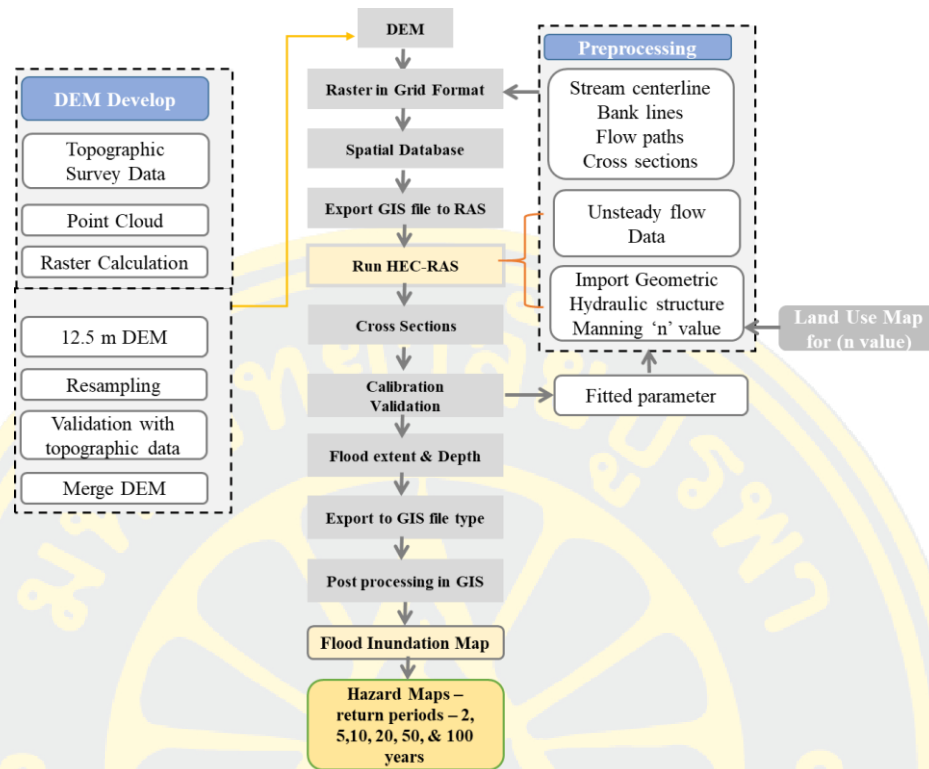


Figure 8 Flow-chart of the hydraulic model and flood inundation mapping

3.3.2.1 Steady flow and unsteady flow

Steady flow: It is applied for computation of water surface profile for steady slowly changed the flow rate and can be used for a single condition such as one item in channel reach, dendritic system, or a full network of channels [38].

Unsteady flow: It is required to perform an unsteady water surface profile calculation and composed of: (1) boundary conditions (external and internal), and (2) initial conditions. In this study, the unsteady flow was selected to determine the flow model due to the variable datasets and uncertainties.

- (1) [61] Boundary Conditions must be structured at all of the open ends of the river system being modelled. Upstream ends of the river system can be shaped with boundaries of flow hydrograph; stage hydrograph; flow and stage hydrograph while downstream ends of the river system with the following types of boundary conditions: rating curve, Normal depth (Manning's equation); stage hydrograph; flow hydrograph; stage and flow hydrograph [39].

- (2) Initial Conditions are required to construct the initial conditions (flow and stage) at all nodes in the system at the beginning of the simulation. Besides, it is necessary to identify the starting water surface elevation in water bodies [39].

2.3.2.2 Uniform and Non-uniform flow

If the water river depth, flow rate and velocity do not vary in the area, this open channel flow can be assumed as uniform flow [63].

Open channel flow is said to be uniform if the depth, the discharge, and the mean velocity do not change with area [63]. The channel flow is quickly varied if the location changes; this flow type can be said as a non-uniform flow [64].

2.3.2.3 Momentum equation

It is a vector equation that is applied in the longitudinal direction of the water bodies. The final formation of the differential momentum equation for the control volume [65][66]. The final derivation of the momentum equation is

$$\frac{\partial Q}{\partial t} + \frac{\partial QV}{\partial x} + g A \left(\frac{\partial z}{\partial x} + S_f \right) = 0 \quad 3.5$$

Where V is the velocity of the flow, g is the acceleration due to gravity, A is an area of the flow, $\delta z / \delta x$ is the water surface slope, and S_f is friction slope [66].

2.3.2.4 Continuity equation

In the steady flow processing, the continuity equation implies that flow must be found between adjacent cross-sections [67][68].

$$Q = V_1 A_1 = V_2 A_2 \quad 3.6$$

Where A_1 is the cross-sectional area normal to the direction of flow at the downstream cross-section, A_2 is the cross-sectional area normal to the direction of flow at the upstream cross-section, Q is the flow rate/ discharge, V_1 is the average velocity at the downstream cross-section, and V_2 is the average velocity at the upstream cross-section.

3.3.3.5 Manning's Coefficient "n"

The roughness coefficient is an essential parameter to decide the flow condition and which can be considered the uncertainty of hydraulic parameters [69]. The common equation of the Manning number is below.

$$Q = K S_f^{\frac{1}{2}} \quad 3.7$$

$$K = \frac{1}{n} A R^{\frac{2}{3}} \quad 3.8$$

Where K is a conveyance of the section (m³/sec), n is Manning's roughness coefficient (m⁻¹/3s), R is the hydraulic radius for subdivision (m), A is flow area of subdivision (m²), and S_f is friction slope.

Manning's roughness value is varied depending on the length and width of a river or stream [69]. And it also varies with the surface water depth [70]. Various values of Manning's coefficient can be different conditions for velocity and water depth. It is very applicable to analyze the water depth and flood extent in the hydraulic analysis. [69].

3.3.3.6 Geometric data

The geometric data is the spatial data that needs to be inputted into the hydrodynamic model that includes (1) river networks, (2) river cross-sections, (3) the reach length, and (4) hydraulic structure data [15]. Besides these, hydraulic loss coefficients in terms of N values and expansion and contraction coefficients are also needed in the determination of cross-section data [71][72].

3.3.4 Geographic Information System (GIS)

GIS has become a useful and essential tool in hydrologic and hydraulic modelling for a few decades for the field of the studies of the management of water resources and flood risk management [73][74]. It can be applied in these fields due to the requirement of spatial and temporal data for a more in-depth analysis, especially in the development of watershed management [73]. As the climate has been changed day by day, water resource management and proper sustainability of the environment are scientifically demanded nowadays. In such kinds of challenges on the water resource management, GIS is the most advanced one in the sustainability of water cycle and

flood risk management because the water in its occurrence is varied spatially and temporally throughout the hydrologic cycle [75].

HEC-GeoHMS is a geospatial hydrology plug-in of the GIS platform introduced by the U.S Army Corps of Engineer in the hydrological modelling [76]. It can perform the visualization of the spatial information, delineation of basins and streams, data conversion between GIS platform and HEC-HMS model, etc. Figure 9 illustrates the overview process of the GIS environment and HEC-HMS to model the precipitation-runoff simulation in the watershed area.

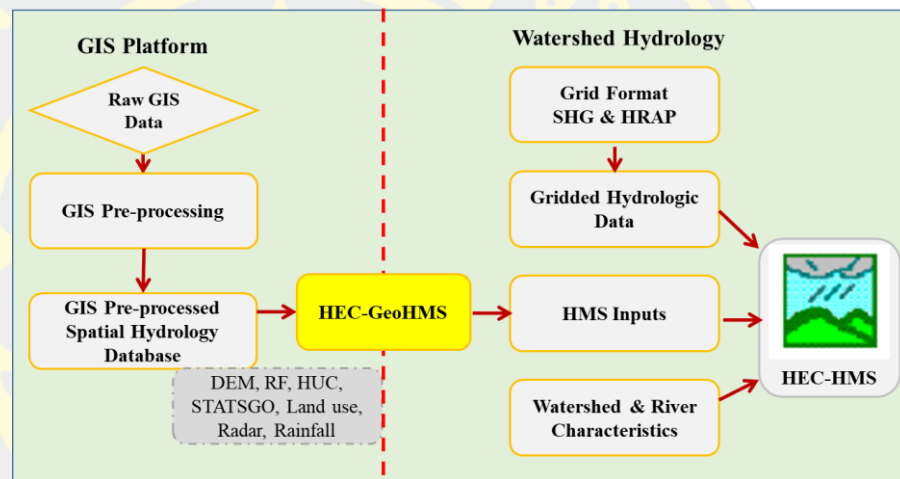


Figure 9 The general process of GIS, HEC-GeoHMS, and HEC- HMS

Source: [76]

And another geospatial tool, HEC-GeoRAS, serves as the interface between GIS and the simulation model HEC-RAS to develop the hydrodynamic model and analyze the geospatial data. Moreover, it can be reconnected to the GIS platform for further data processing by combination with the hydraulic model and spatially and statistically databases. A widely used approach is watershed modelling that divides the drainage basin into discrete units possessing similar rainfall-runoff and physical characteristics [76].

3.3 Flood risk assessment

In [77], it needs to understand the causes of the potential flood disasters by accounting the vulnerabilities of people and their properties, and natural flood hazards in the area. It also described the assessment of the expected damage due to the flood in

terms of four primary steps, and they are flooded frequency, flood hazard, flood exposure, and damage record.

Flood risk usually rises from massive rain events like a typhoon, intensive rainstorms, while dyke breach and storm surges are also frequent in a particular area [78]. The research mentioned that the potential damage things could be recognized as the flood risk consequences, and it is essential to determine the risk scale level in the assessment area [79].

In the risk assessment for flood, the flood hazard map is considered from the modelling of hydrologic and hydraulic models. And the data for flood exposure and flood vulnerability maps will be applied from the satellite imagery computation, open-source data, and statistical data from government offices and so on. The detailed process of the flood risk assessment map is shown in Figure 10.

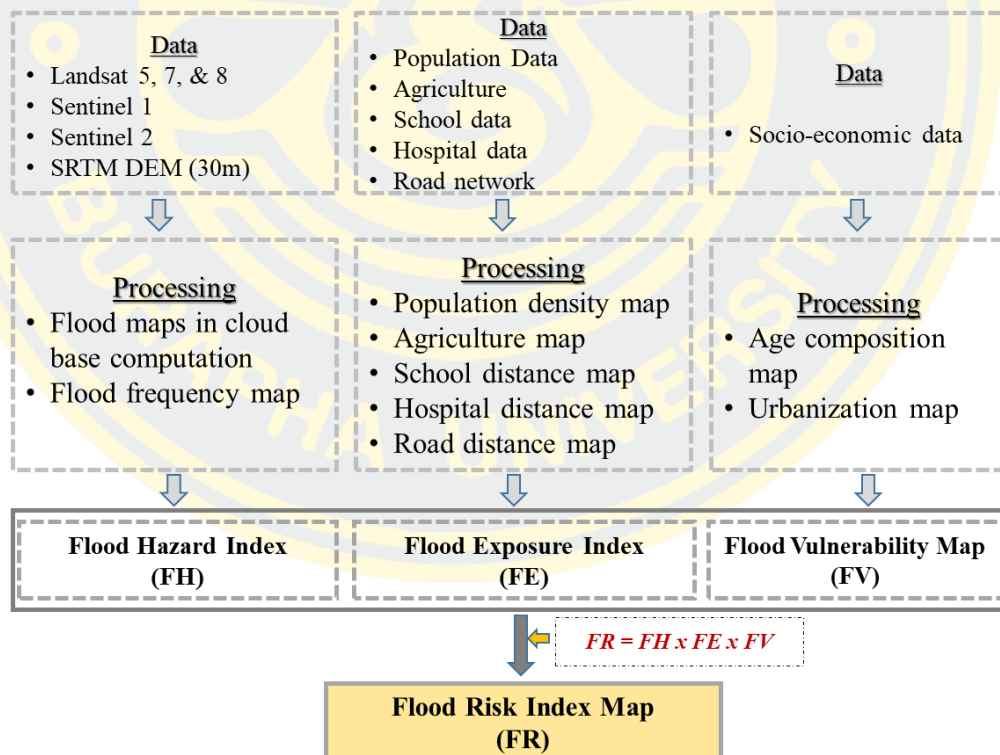


Figure 10 Flow-chart of flood risk

In risk assessment, the various sources of datasets are considered such as satellite-derived datasets, flood inundation model, open-source data, field observed data

from the government (DMH), aerial statistical data and so on. The flood risk map is calculated using Equation 3.9.

$$FR = FH \times FE \times FV \quad 3.9$$

3.3.1 Flood hazard

Flood hazard has been studied in various methodologies such as simple binary models, GIS techniques, spatial coexistence models, historic flood hazards using remote sensing techniques, etc. [80][81]. In flood risk mapping, the trend of historic floods is the key to analyze the recent flood risk and also can estimate future floods [81].

3.3.2 Flood exposure

Without the exposure of socio-economy and valuable assets in the flood plain area, the flood risk will be reduced [82]. There are various factors to consider flood exposures. The selected sectors for exposure factors are population density, crops, and urban, which directly impact to area from the flood and hospital, schools, and road networks are the potential relief to the people exposed to flood events [47].

Land use/land covers are the ones of the flood exposures to account for the intensity of flood risk assessment because a flood can directly affect them. Consequently, the properties and productivity of agriculture and settlements can be destroyed [83]. Besides, the necessary facilities of the road networks, schools, and hospitals are serving to release the flood risk during the flood events and mitigation plan because they can support the local people as a shelter in emergency cases [84]. Whether the distance of the road is fared or near, the condition of flood risk can be mitigated to assess the hospitals for treatment and the schools for the temporary shelter. The population is the main controlling factor of flood exposure due to the threat of human lives and their properties. Moreover, the secondary effect as the diseases can be followed [85].

Exposure is the ratio of susceptible properties' value to the total properties value of human being. It can be happened depending on the values at the location in the flood-prone area. Due to different understandings of vulnerability, some researches single out exposure as a direct risk factor in the specific analysis [86] [87].

In consideration of flood risk assessment, it is required to identify the flood exposure of the river basin. Generally, flood exposure datasets were prepared and collected from the various sources of computational satellite data, open-source data, and statistical data from the government.

$$FE = Wp \frac{C + U + Sd + Hd + Rd}{5} \quad 3.10$$

Where FE is flood exposure, Wp is population data, C is the crop, Sd is school distance, Hd is hospital distance, and Rd is road distance [46].

3.3.3 Flood vulnerability

Even though the same intensity of flood extent and depth happened in the flood-prone areas, the impacts were different because of various levels of resilience. The more resistance of people is strong, the lesser the adverse consequences are, while the more strength of people is weak, the bigger the negative impacts are. In this task, two components of flood vulnerabilities are applied, such as the urban area and age of people, even though there are plenty of indicators to vulnerabilities [88][89][90].

The vulnerability of the flood is the grade of loss (from 0% to 100%) due to the destroying phenomenon [91], i.e., the exposure of human and facilities to floods and the susceptibility of the elements to suffer from flood damage [92].

There are three leading physical and social indicators of literacy (>25 years old), age (< 14 years and > 65 years old), and urbanization used as the flood vulnerabilities. They were collected from the statistical datasheet from Myanmar Census 2014 survey data presented in Table 3.7 and contained data on the township scaled level. And they were converted from the statistical data into geospatial data for further GIS processing. The composition of these vulnerabilities is mentioned below as equation 3.11.

$$FV = \frac{A (< 14) + A (65 <) + U + L}{4} \quad 3.11$$

Where, FV is vulnerability, A (<14) is age range (Less than 14-year-old), A (65<) is age range (more than 65-year-old), U is urbanization, and L is literacy (more than 25).

3.3 Flood risk assessment

3.3.1 Generation of Triangulated Irregular Network (TIN)

Developing of Triangulated Irregular Network (TIN) is significant for flood inundation model as the data pre-processing in HEC-GeoRAS and used it in HEC-RAS for further geometric data creation. Firstly, 12.5 m Digital Elevation Model (DEM) of ALOS PALSAR was downloaded from Alaska Satellite Facility for earth data (<https://search.asf.alaska.edu>). And it is exported into the GIS platform and generated into the TIN model by using the 3D analyst tool. It illustrates as a pair of the non-overlapping continuous surface with triangular facets of varying dimensions.

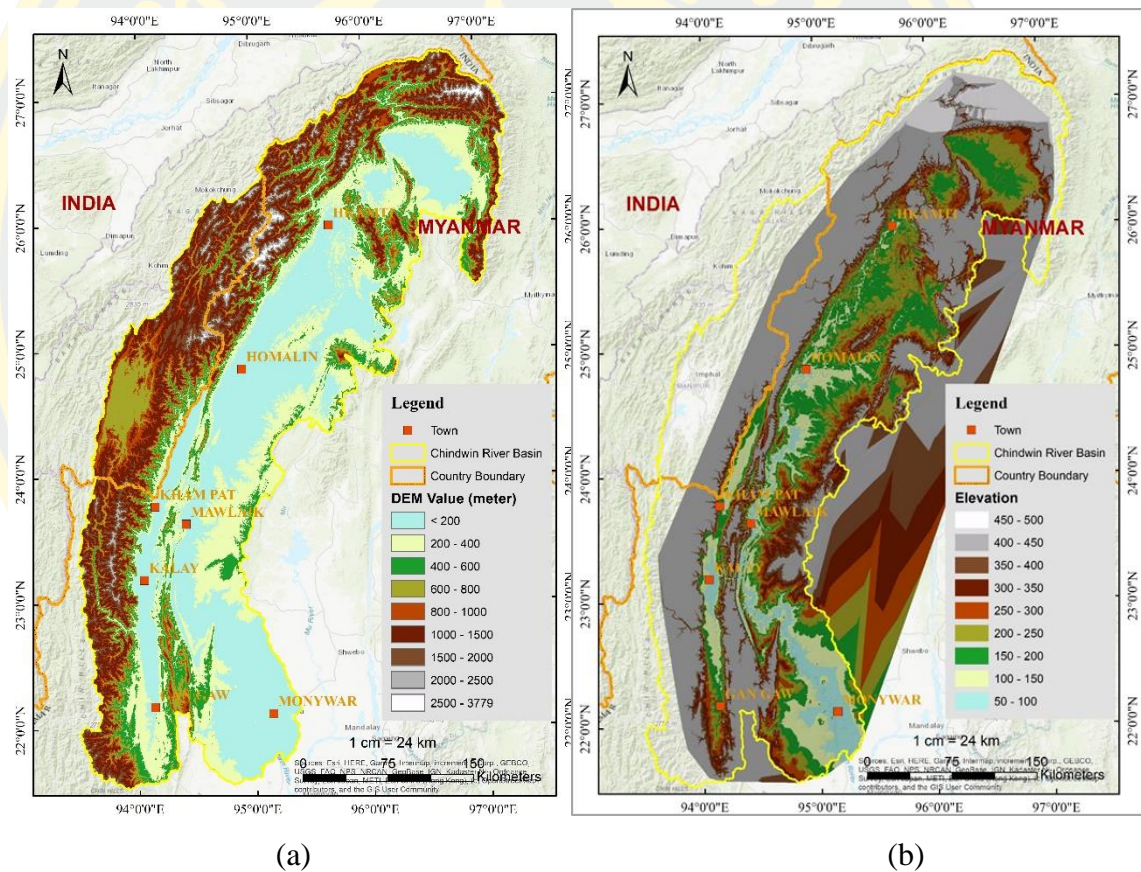


Figure 11 Process of TIN model generation (a) Digital Elevation Model (DEM) and (b) Triangulated Irregular Network (TIN)

3.3.2 Land use/land cover (LULC)

In modelling of rainfall-runoff simulation, the LULC is necessary for the water infiltration rate through into the soil layer in the river basin. Finally, some amount of precipitation is accumulated in the river. This land use/land cover (Figure 12) was extracted the data, which was classified from the Moderate Resolution Imaging Spectroradiometer (MODIS) at [93]. There are a total of 14 classes in the Chindwin

River Basin, and the most prominent area in all types is an evergreen broadleaf forest with 52.75 % of the total area, as presented in Table 2.

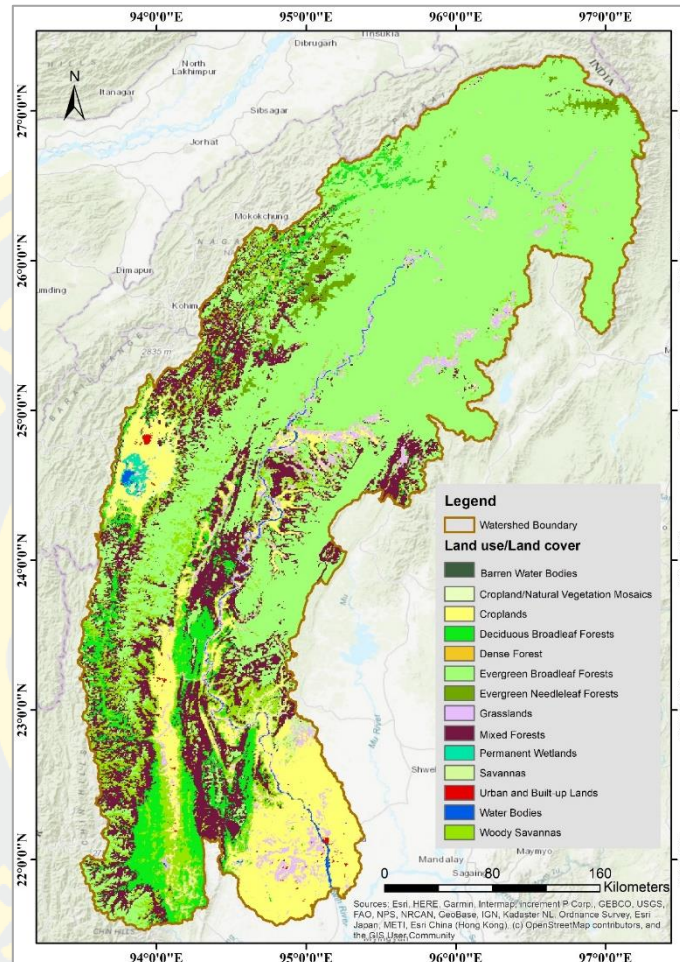


Figure 12 Land use/land cover map

Source: [100]

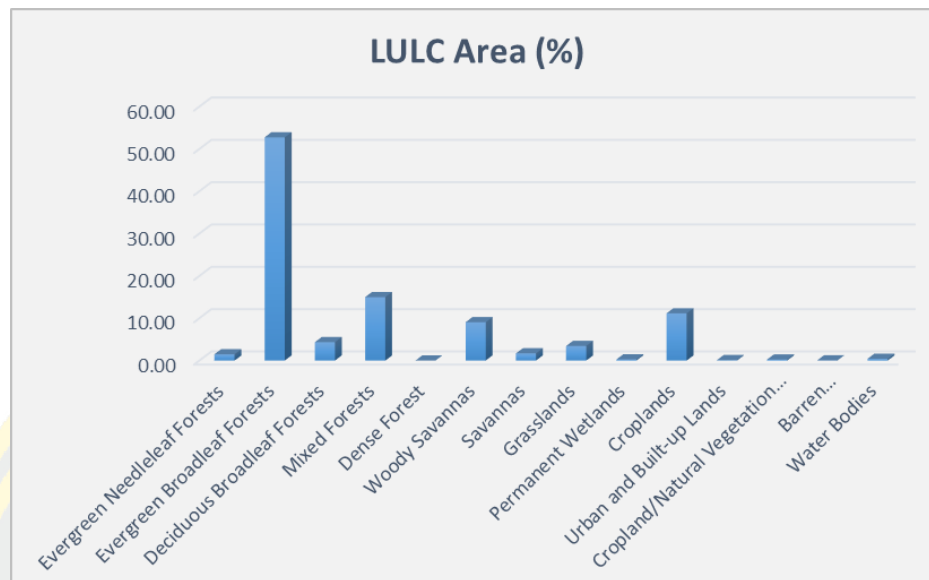


Figure 13 Graph of land use/land cover area

Table 2 Area of LULC types in the study area

No.	LULC Class	Area (km2)	Area (%)
1	Evergreen Needleleaf Forests	1,657	1.49
2	Evergreen Broadleaf Forests	58,803	52.75
3	Deciduous Broadleaf Forests	4,852	4.35
4	Mixed Forests	16,701	14.98
5	Dense Forest	4	0.00
6	Woody Savannas	10,095	9.06
7	Savannas	1,895	1.70
8	Grasslands	3,859	3.46
9	Permanent Wetlands	293	0.26
10	Croplands	12,431	11.15
11	Urban and Built-up Lands	119	0.11
12	Cropland/Natural Vegetation Mosaics	273	0.24

13	Barren Water Bodies	54	0.05
14	Water Bodies	446	0.40
Total		111,482	100.00

3.4.3 Type of soil

Figure 14 shows the soil classes in the study area. It was collected from [94] Digital Soil Map of the world (DSMW) (www.fao.org) and extracted with the Chindwin River basin. Seven types of soil occur in the river basin, and the largest area of soil type is orthic Acrisol, with 59.17 % in the total area, while the smallest area of soil type is the pellic vertisols soil, 0.52%. The types of soil and their attributes are listed in Table 3.

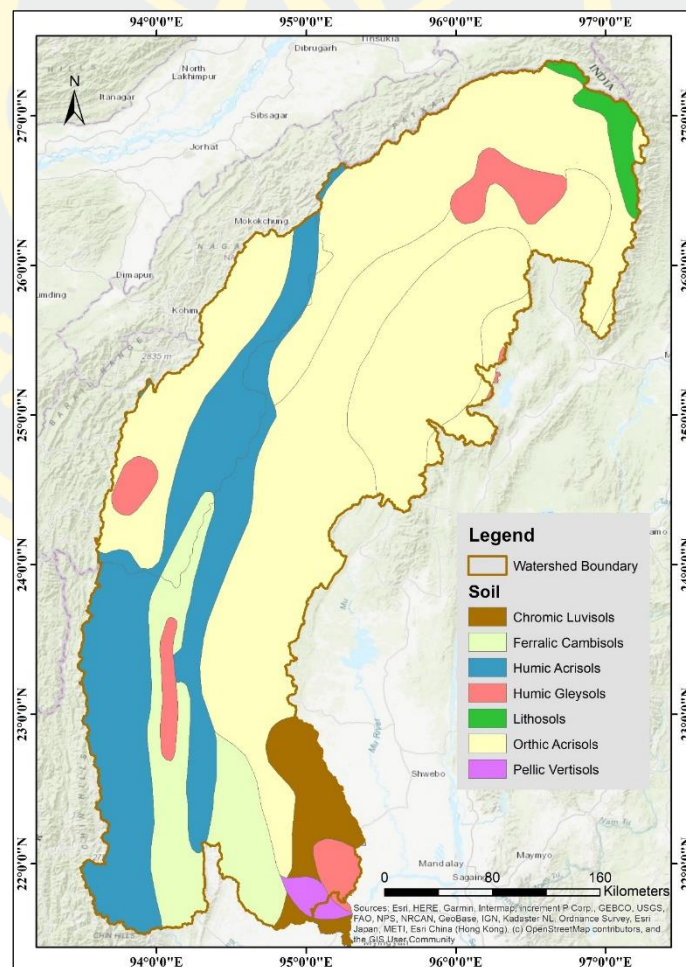


Figure 14 Soil map

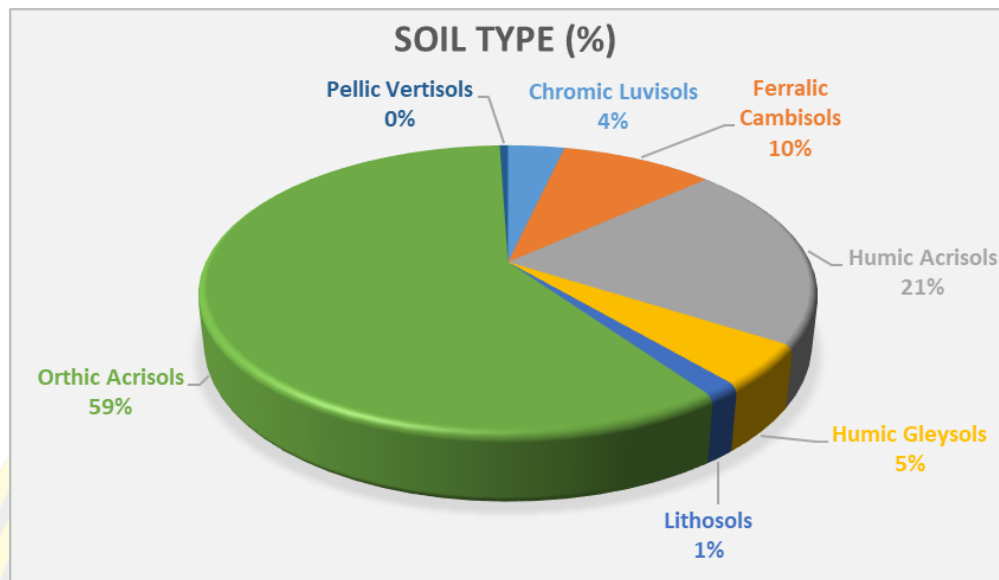


Figure 15 Pie chart of soil type

Table 3 Types and area of soil in the study area

Sr. No.	Name	Area (km2)	Area (%)
1	Chromic Luvisols	4,048	3.57
2	Ferralic Cambisols	11,021	9.71
3	Humic Acrisols	23,616	20.81
4	Humic Gleysols	5,358	4.72
5	Lithosols	1,707	1.50
6	Orthic Acrisols	67,143	59.17
7	Pellic Vertisols	591	0.52
Total		113,484	100.00

3.4.4 Rainfall data

Rainfall is the main factor for hydrologic models. There are five rain-gauges and water level stations in the study area, namely Hkamti, Homalin, Mawlaik, Kalewa, and Monywa stations, as shown in Figure 16 for the station's location in the study area. Daily rainfall data of all stations were recorded from the Department of Meteorology and Hydrology (DMH) for many years as historical rainfall data, and it may be a frequency-based hypothetical or design rainfall event. HEC-HMS model can process

the hydrologic model by utilizing the primary precipitation data, especially for the flood event periods.

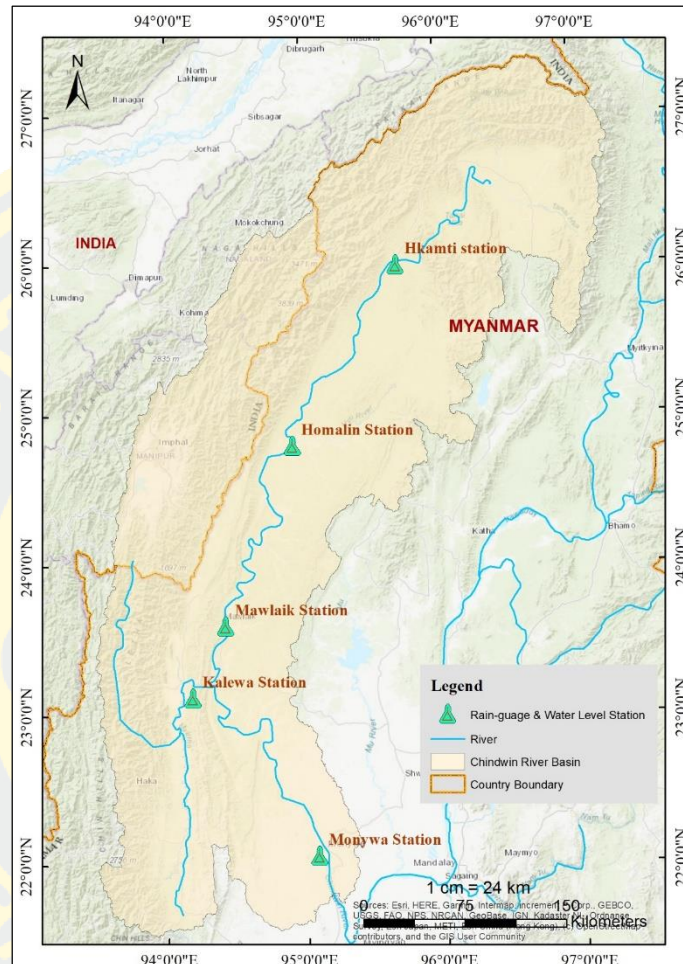


Figure 16 Location of rain-gauge and water level stations in the study area

3.4.4.1 Areal rainfall calculation

As the study area is pretty big and limited rain gauges were established in the study area, the determination of areal rainfall is significant for consideration of precipitation to each sub-basin in the main watershed area. Here, Thiessen polygons were calculated based on the area-based weighing to cover the whole watershed area, and it was generated from a set of five rain-gauge stations. The polygons are bounded strictly based on the location of point sources in the Chindwin river basin, as shown in Figure 17. Weights accessed from the intersection of the Thiessen polygons of gages and the sub-basin. The average rainfall (R_{areal}) over the area can be computed from equation 3.12.

$$R_{\text{areal}} = \sum_{i=1}^n \frac{R_i A_i}{A_t} \quad 3.12$$

Where R_i is the rainfall at station i , A_i is the polygon area of station i , A_t is the total catchment area, and n is the number of stations.

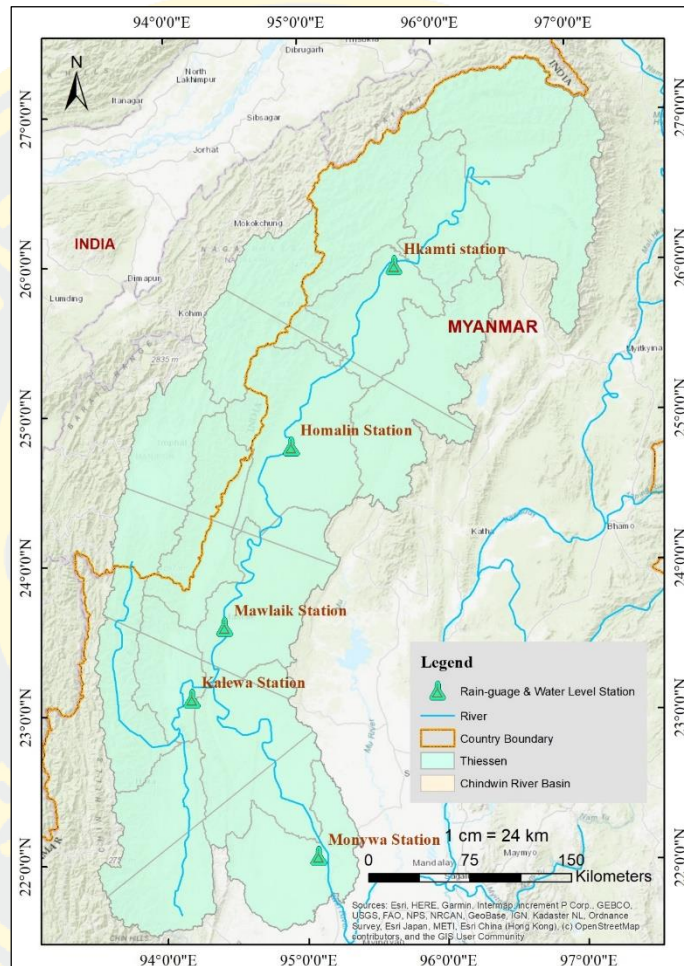


Figure 17 Thiessen polygons for aerial rainfall calculation

3.4.4.2 Design rainfall event

It is also known as Intensity-Duration-Frequency (IDF) because of its storm frequency for precipitation in the hydrologic field. Firstly, the development of IDF curves needs to be considered some theoretical frequency distribution to the extreme or abnormal rainfall amounts for fixing. And the logical step is continued with the variable parameters distributed in duration by a functional relation. According to the relationship of these fitted parameters, the intense precipitation for any duration and return period

can be computed. Two different distributions are applied in this research, and they are the Log Pearson Type III method and Log-Normal method [95].

In this study, the rainfall depth of area is estimated for different return periods using observatory rainfall data of Homalin station. The result of the Log Pearson Type III method was chosen to compute rainfall intensity with duration. Ratio to 24-hour rainfall with duration was taken from the mean rate of “n” hour to “24” hour rainfall for basins. The rainfall intensity and total rainfall with the necessary duration can be selected from the table of IDF. The IDF tables and curves are shown in Appendix I.

3.4.4.3 Delineation of river catchment

In the simulation of the hydrologic model in HEC-HMS, stream network and catchments are required. So, the representation of the stream network is pre-processed using the 12.5 m of DEM in HEC-GeoHMS plug-in, which is the extension tool of the GIS platform. DEM was utilized to analyze the stream network and sub-basins of the Chindwin river basin. The detailed processing of terrain analysis is shown in Figure 18.

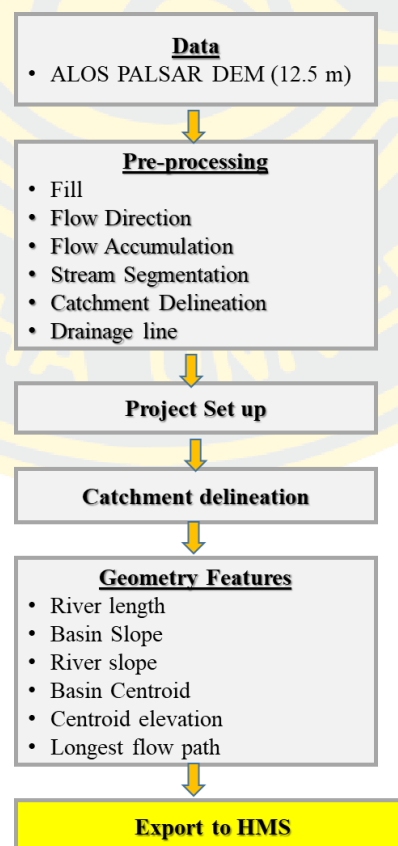


Figure 18 The overview steps of HEC-GeoHMS

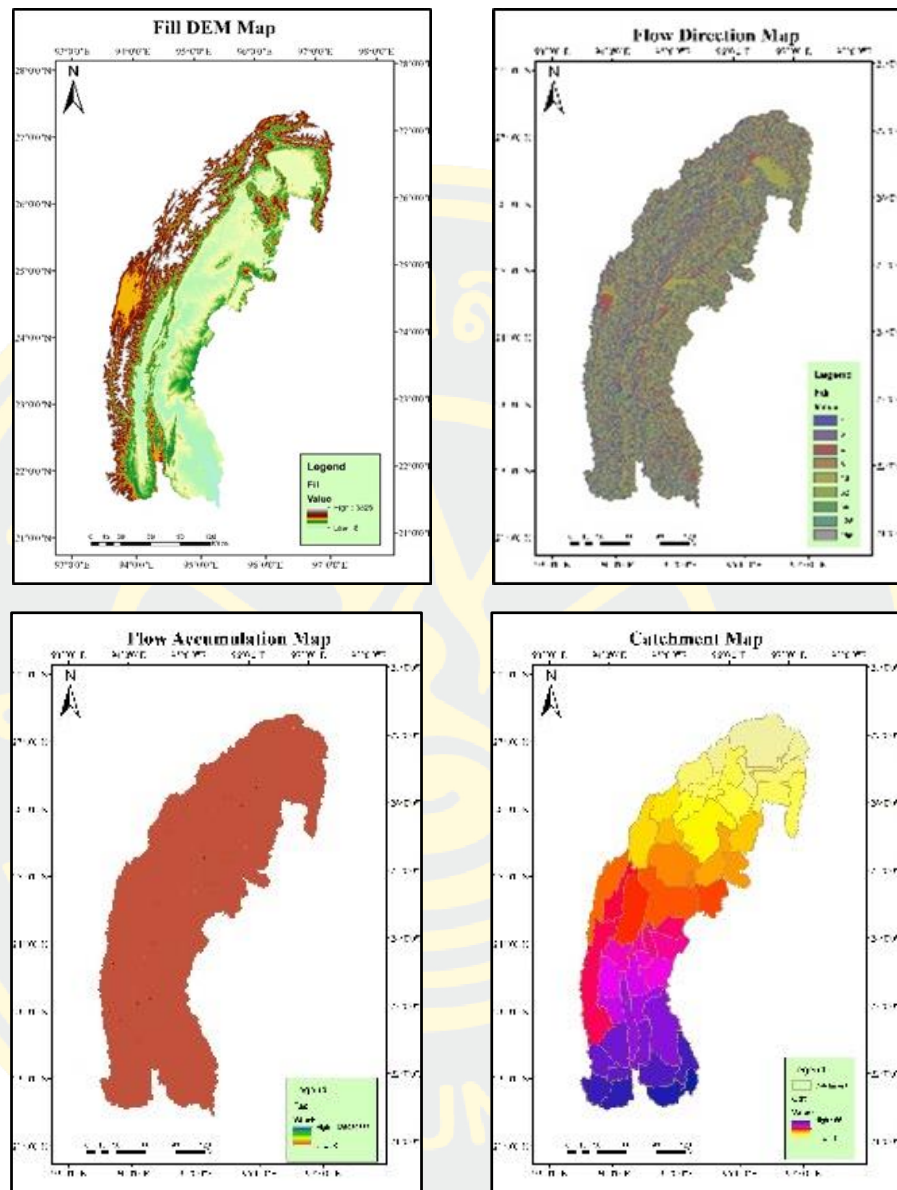


Figure 19 The process of terrain analysis

As mentioned in the process (Figure 19) above was done, the area of total catchments has resulted in 113,484 km². The small polygons of basins were either merged or subdivided with the patterns of stream network and size of basins in the primary watershed accordingly. And then, geometric features such as stream network and sub-basins were quarried and computed the length of their properties. Basin slope used the slope grid of raster DEM format to identify the average gradient for sub-basins. The longest flow stream was calculated as the length between endpoints from upstream

to downstream elevations. And also, the centroid elevation, the basin centroid, and the centroid flow path were processed. All of the geometric features were exported to HEC-HMS for further hydrologic modelling.

3.5 Processing in the HEC-HMS model

After preparing the stream network delineation and sub-basin generation, these geometric data were imported to the HEC-HMS model for surface runoff simulation. There are four methods in the HEC-HMS model, such as the Loss method, runoff method, base flow method, and routing method. In the modelling of surface runoff, one of the above techniques has appropriately chosen in a meteorological model to prepare the boundary conditions that act on the watershed area, control specification utilized for controlling of the simulation period. And time-series data was used to store the data such as rainfall, discharge, and so on. The models included in the HMS are mathematical models. They are representing the behaviour of the components of the hydrologic system.

Observed flow data were created in the excel sheet and input the data to HEC-HMS and summary data, time series-data and graphs can be seen in the model. HMS computes runoff depth and volume for observed and modelled hydrographs and can be compared in the summary table of the element. Graphical results provide a mechanism for visual analysis by superimposing the observed hydrograph over the modelled hydrograph.

Table 4 Physical characteristics of sub-basins in the Chindwin watershed area

Sr. No.	Sub-basin Name	Basin Shape Length (km)	Basin Shape Area (km ²)	Slope	Upstream Elevation (m)	Downstream Elevation (m)	River Length in sub-basin (km)
1	W560	144.92	6503.17	0.0134	3242	230	224.47
2	W590	63.89	5207.87	0.0084	1601	185	168.32
3	W630	120.21	6780.79	0.0119	2526	185	196.49
4	W650	77.20	8039.19	0.0085	2287	161	215.56
5	W700	58.28	5352.60	0.0064	1674	168	189.10
6	W740	119.62	7301.31	0.0044	996	161	250.54
7	W760	68.06	9423.88	0.0078	1904	230	236.21
8	W800	111.37	10239.69	0.0052	2464	124	299.44
9	W820	71.29	6237.35	0.0086	2701	129	214.72

10	W840	223.49	11854.12	0.0073	1698	120	451.95
11	W870	110.41	8177.30	0.0016	539	102	267.42
12	W970	90.57	9236.72	0.0193	2648	102	339.65
13	W980	38.68	3998.45	0.0026	933	65	132.25
14	W1080	104.72	8475.68	0.0058	1141	61	185.06
15	W1090	86.42	6656.64	0.0116	2744	124	226.76

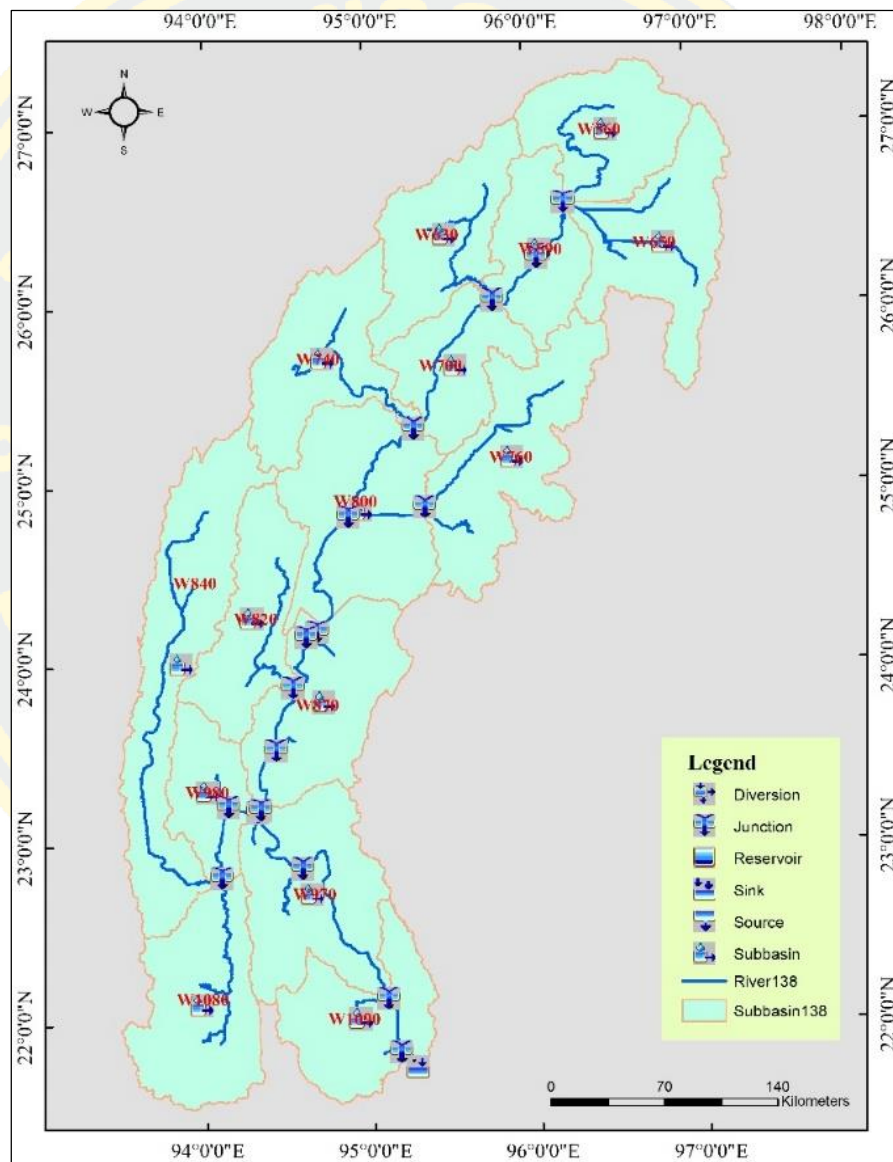


Figure 20 HMS schematic basin model

Figure 21 describes the method selection window in the basin model of HEC-HMS. Methods in basin model were chosen, such as sub-basin name, loss method, transform process, and base flow method. In the study area, there are 15 sub-basins, 16

reaches, and 17 junctions. Required parameters and data were calculated in various ways and put them in this basin model.

The screenshot shows the 'Subbasin' tab of the HEC-HMS software. The 'Basin Name' is 'Res_Tr_1' and the 'Element Name' is 'W650'. The 'Description' field is empty. The 'Downstream' field is set to 'J179'. The 'Area (KM2)' is '8039.1'. The 'Latitude Degrees', 'Latitude Minutes', 'Latitude Seconds', 'Longitude Degrees', 'Longitude Minutes', and 'Longitude Seconds' fields are all empty. The 'Canopy Method' is set to '--None--', the 'Surface Method' is set to '--None--', the 'Loss Method' is set to 'Initial and Constant', the 'Transform Method' is set to 'SCS Unit Hydrograph', and the 'Baseflow Method' is set to 'Recession'.

Figure 21 Method selection window for basin model development

The meteorological model is the main factor in the hydrologic model because the precipitation data and discharged data were put in it by defining the meteorological boundary condition for sub-basins. There are seven rain-gauge stations among the 15 sub-basins of the study, and the data is needed to cover the area.

Control specification in HEC-HMS can set up the duration time and the interval of modelling. The starting and ending period depended on the rainfall event's time in the Monywa runoff station.

3.5.1 Calibration and validation for hydrologic model

There are two essential steps, such as model calibration and validation in hydrologic modelling due to the uncertainty data abilities and to match the computed data and observed data.

In model calibration, the automatic and manual steps are handled in the parameters of the initial loss, constant rate, impervious, initial discharge, recession constant, lag time, and threshold ratio are considered through the calibration process. These parameters are adjusted the data till nearly matching between computed data and

observed data, especially the highest precipitation event in the study area. In model validation, the parameters are tested until the acceptant accuracy, which is more accurate than the calibrated data.

Model calibration and validation are essential in rainfall-runoff modelling as uncertainty in model predictions can be reduced if models are properly calibrated.

3.5.2 Trial & error and objective function

In the calibration of the data, trial & error, and objective function are needed for better experiment results, and they are two conventional methods. Trial and error function in calibration is generally the methods that controlled by manual while the objective function is mostly related to the automatic control method.

Optimization trials are used for optimizing the initial processing of the model parameters in the HEC-HMS. The auto-calibration process does not cover the desired optimum results. Therefore the model was handled with both manual and auto-calibration. In the objective function, the quantitative measure in calibration is applied to measure the level of changes between computed and observed hydrographs. The availabilities of accurate services in HEC-HMS optimization are about seven, and five of them are listed as below.

- (1) Peak-Weighted Root Mean Square Error (PWRMSE): This function gives more weight to significant errors than small errors, and it provides higher overall weight to error near the peak discharge.

$$\text{PWRMSE} = \sqrt{\frac{\sum_{t=1}^N (Q_o(t) - Q_M(t))^2 \frac{Q_o(t) + Q_A}{2Q_A}}{N}} \quad 3.13$$

$$Q_A = \frac{1}{N} \sum_{t=1}^N Q_o(t) \quad 3.14$$

Where, Q_t , Q_M is the observed flow at time t , and Q_A is the average observed flow.

- (2) Sum of absolute residuals (SAR): The this function accesses the equal weight to both small and large errors.

$$SAR = \sum_{t=1}^N |Q_o(t) - Q_M(t)| \quad 3.15$$

- (3) Sum of squared residuals (SSR): It measure gives a higher weight to significant errors and lesser importance to small mistakes and uses the squared differences as the measure of fit.

$$SSR = \sum_{t=1}^N (Q_o(t) - Q_M(t))^2 \quad 3.16$$

- (4) Percent error in peak flow (PEPF): It measures only considers the grade of simulate peak flow and does not calculate for total volume or timing of peak.

$$PEV = 100 \left| \frac{V_o - V_M}{V_o} \right| \quad 3.17$$

- (5) Percent error in volume (PEV): It only considers the simulate volume and does not assume for the grade or timing of peak flow.

$$PEPF = 100 \left| \frac{Q_o(\text{peak}) - Q_M(\text{peak})}{Q_o(\text{peak})} \right| \quad 3.18$$

The equations and descriptions mentioned above are referred to as the HEC-HMS Technical Reference Manual [30].

3.5.3 Efficiency criteria method and error assessment

In this research, the sensitivity analysis of the model was applied to figure out the critical parameters with the efficiency criteria, and error parameter computations, and each of the requirements have their weakness to determine the data. Even though there are various types of efficiency criteria and error computation, the following facts are applied in my research.

3.5.3.1 Nash Sutcliffe Efficiency (ENS)

The ENS is mostly utilized in the hydrologic model and to estimate the hydrological the discharge model. If the ability of ENS value is 1, it can be said the better matching of the discharge model for observed data while the efficiency of ENS = 0 is correct as of the mean of observed data. However, over the prediction of model

simulation during the peak flow period and an under-prediction during low flow conditions is an unfortunate result.

$$ENS = \frac{\sum_{i=1}^n (Q_{oi} - \overline{Q_o})^2 - \sum_{i=1}^n (Q_{oi} - \overline{Q_{ci}})^2}{\sum_{i=1}^n (Q_{oi} - \overline{Q_o})^2} \quad 3.19$$

Where ENS is Nash Sutcliffe Efficiency, Q_{oi} is observed value at the i time interval, Q_{ci} is Simulated value at the i time interval, and $\overline{Q_o}$ is Average of the observed value [66].

3.5.3.2 Coefficient of Determination (R^2)

This function can predict the correlation between simulated data and observed data. The range of it is from zero to one. The closer to the zero, it is a weak correlation, and the closer to the one, it can be better and perfect matching. The formula is mentioned as below.

$$R^2 = \left[\frac{\sum (Q_{si} - \overline{Q_{si}}) (Q_{oi} - \overline{Q_o})}{\sqrt{\sum (Q_{si} - \overline{Q_{si}})^2} \sqrt{\sum (Q_{oi} - \overline{Q_o})^2}} \right]^2 \quad 3.20$$

Where R^2 is coefficient of determination, Q_{oi} is observed value at the i time interval, Q_{si} is simulated value at the i time interval, $\overline{Q_o}$ is the average value of the observed discharge, $\overline{Q_{si}}$ is average value of the simulated discharge, and N is a number of sample data [66].

3.5.3.4 Coefficient of correlation (R)

The linear correlation between computed and observed data can be estimated in the Coefficient of Correlation, in which the value ranges from minus one to plus one. The +1 correlation value of Coefficient Correlation is a better linear relationship, -1 correlation is a decreasing linear relationship, and finally, 0 value means that there is no linear relationship among the variables [66].

$$R = \frac{\text{cov}XY}{S_x S_y} \quad 3.21$$

$$\text{cov } XY = \frac{\sum_{i=1}^n [(X_i - \bar{X}) \times (Y_i - \bar{Y})]}{(n-1)} \quad 3.22$$

$$S_x = \sqrt{\frac{\sum_{i=1}^n (X_i - \bar{X})^2}{(n-1)}} \quad 3.23$$

$$S_y = \sqrt{\frac{\sum_{i=1}^n (Y_i - \bar{Y})^2}{(n-1)}} \quad 3.24$$

Where R is the coefficient of correlation, X_i is the observed value at the i time, Y_i is the simulated value at the i time, \bar{X} is the average of the perceived value, \bar{Y} is average of the simulated value, n is the number of sample data, S_x is a standard deviation of observed data, and S_y is the standard deviation of simulated data.

3.5.3.5 Root Mean Square Error

Its value is the parameter error test, and its value approached the zero means the least error parameter.

$$\text{RMSE} = \sqrt{\frac{\sum_{i=1}^n (X_i - Y_i)^2}{n}} \quad 3.25$$

Where RMSE is the root mean square error, X_i is the observed value at the i time, Y_i is the computed value at the i time, and N is the number of sample data.

3.5 Processing in HEC-RAS Model

In the HEC-RAS model, the primary processing is to simulate the flow profiles and floodplain model in depth and extent using the data of rainfall computed by hydrologic model, flow discharge, geometric data, and cross-section and so on. Cross-section profiles derived from the TIN model are critical and also needed to validate with the field observation and cross-section measurement from the government office (DMH). To run the HEC-RAS model, four file types are considered. They are (1) geo-database management in the model, (2) geometric files are required with their attributed table, (3) the model is set up with supercritical, subcritical or mixed flow to run the simulation and (4) defining the flow boundary in unsteady flow is required.

3.6.1 Pre-processing in HEC-GeoRAS

Pre-processing in HEC-GeoRAS is required to connect with the hydraulic model (RAS mapper). In my study, the length of the Chindwin River is more than 968 km, and it originated from the Hukahung basin and ended at the outlet of Monywa city. Generally, the primary data is Digital Elevation Model (DEM), and it is converted into the TIN model for better geometric data preparation and they are the flow path lines, stream centerlines, bank lines, and XS cut lines. There is the main streamline of Chindwin River, and other tributaries as U Yu and Monwya are conducted. U Yu tributary started from the east of the river basin and ended at the junction of Main River at Homalin city. For the Monywa tributary, it is started at the west side of the river basin near the Kale city and poured into the main river near the Monywa city.

The essential geometric data is cross-section creating for flood plain mapping because it controls the flood extent according to their elevation section and the intensity amount of rainfall for the flood events. These cross-section lines are traced from the left bank to the right overbank by facing the downstream and were perpendicular to the flow path lines.

Stream centre lines were created from upstream to downstream of the Chindwin river according to a topology rule of HEC-RAS. A junction, U Yu Tributary, was formed where endpoints of three reach connected. Left and right bank lines were also digitized, but the direction of these lines was not significant. Then, the flow path centerline that defines the central flow direction of the river is automatically created, and in the same layer, the limits of the flooded land are digitized.

Finally, geometric data was imported into HEC-RAS for hydraulic modelling. According to the TIN value, the Z value of stream centerlines is recognized as a 3D cross-section. Moreover, the manning's N value can be considered to each cross-section. After completion of all the above-described steps, the geometry file is ready to be exported into HEC-RAS as a GIS export file.

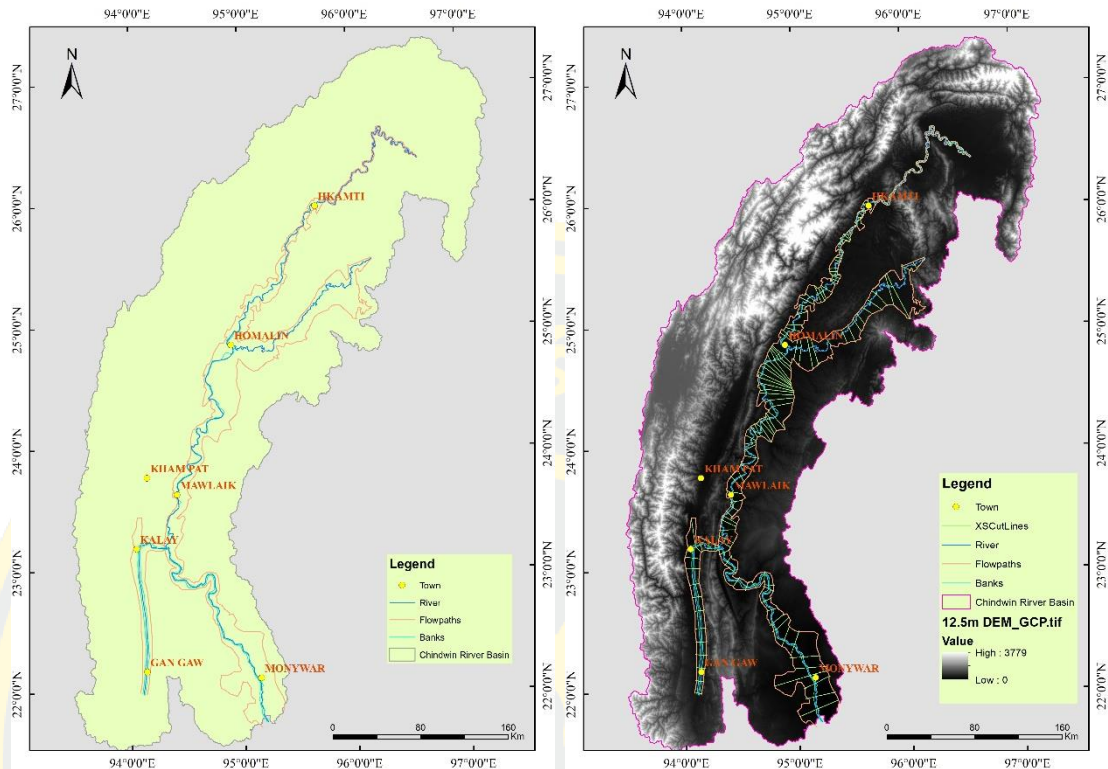


Figure 22 Pre-processing in HEC-GeoRAS

3.5.2 Geometric data

Figure 23 shows the geometric data, including with river, cross-section, cut lines, cross-section surface lines, cross-section bank station, and reach length, which is imported and created in HEC-GeoRAS as a pre-processing data set.

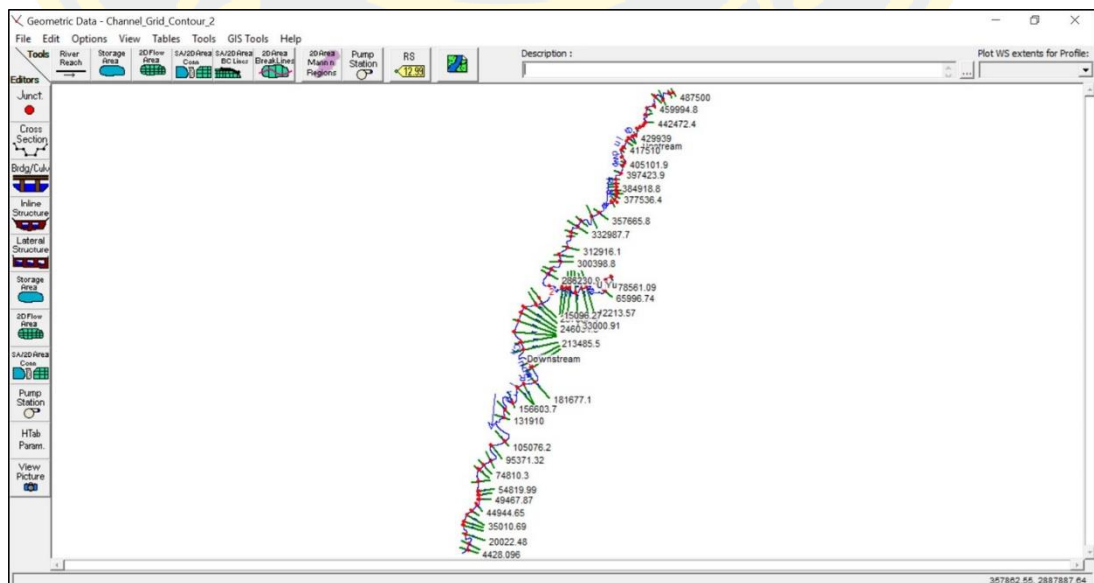


Figure 23 Geometric river data

Cross-section plays an essential role in flood simulation because it controls the flood depth and flood extent based on the amount of precipitation and discharge along the river and tributaries lines. In creating the cross-section, it should be covered throughout the whole river lines and flood conditioning area by checking with the historic flood event of remote sensing and topographic consideration. Moreover, the cross-sections are required to consider the following facts, such as cross-section connectivity, the elevation of station equality, proper Manning n value for each cross-section line.

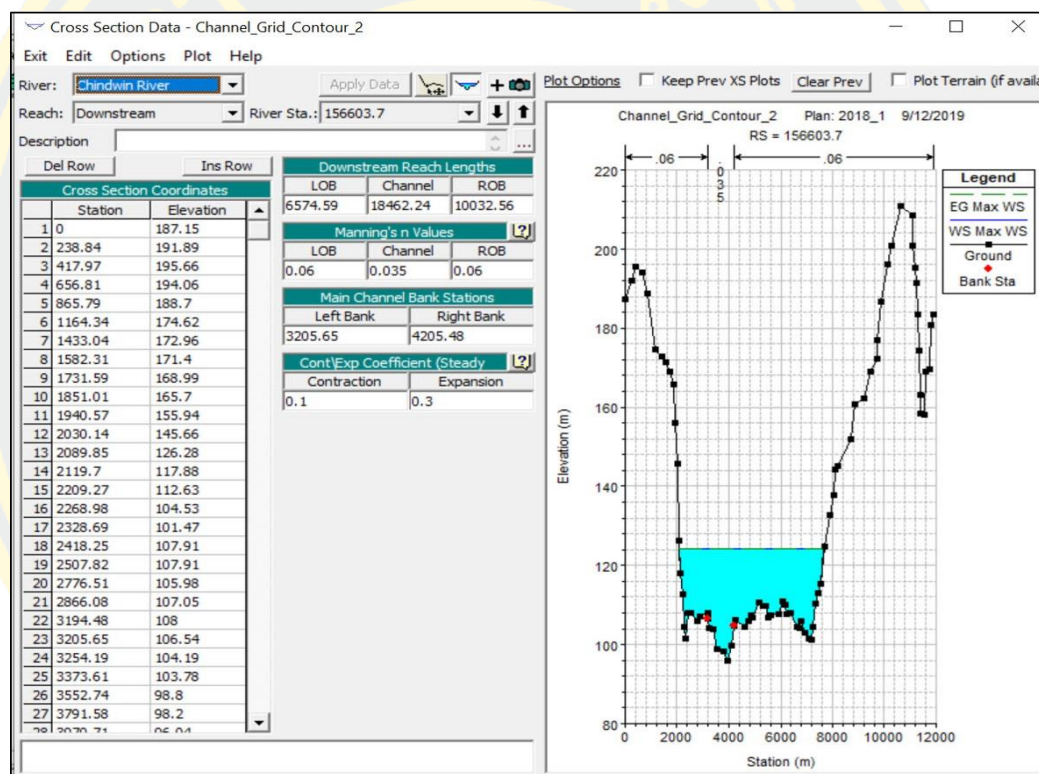


Figure 24 Cross-section data with the editing interface

As mentioned above, the cross-section is significant for hydraulic modeling. Here, the accurate cross-section data should be done with the Manning N value. Manning N value is the different condition of surface roughness along the riverbank of both the river line side. Land use/land cover and geomorphology are the keys to Manning N value.

3.6.3 Unsteady flow data

To develop the hydraulic model, unsteady flow data is required in the HEC-RAS model to simulate the flood hazard mapping with flood depth and extend for

studied flood events. Generally, two main conditions are necessary, such as boundary condition and initial condition. The unsteady flow simulation was developed with a series of discharge data along concerning the time of occurrence. In this study, the upstream boundary conditions were chosen as flow hydrograph and downstream boundary conditions as flow hydrograph with Normal depth, respectively.

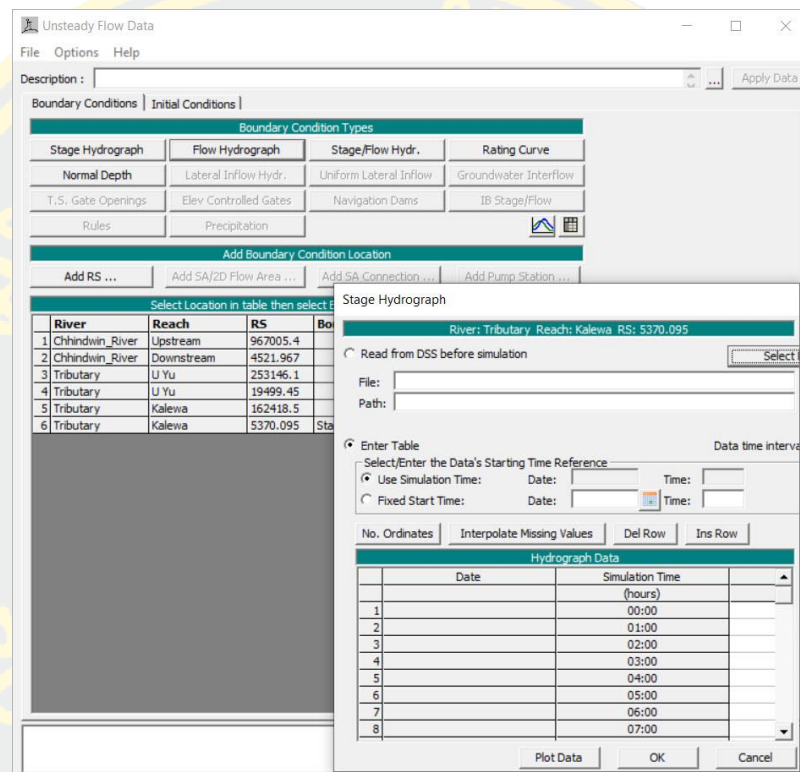


Figure 25 The unsteady flow data option

3.6.4 Flood inundation mapping

It is the final step of the hydrologic and hydraulic model. HEC-RAS is the simulation model for flood extent and surface depth of the flood plain area. In the visualization and validation of the flood area, the GIS environment is required. Firstly, the results of the HEC-HMS model were exported into the GIS platform. The connecting file type between RAS and GIS platforms is specially formatted GIS exchange (*.sdf) file, and it is converted into a raster file.

3.7 Remote Sensing

Remote sensing is a technique in a combination of science and art in acquiring the information of the thing or area from a distance without in touch with the thing or

area under investigation [96]. Figure 26 shows the process of the remote sensing system, and the primary requirement of remote sensing is the radiation and the electromagnetic spectrum. The electromagnetic spectrum is mentioned by the ranges of shorter to longer wavelengths of radiation [97].

Generally, there are four kinds of resolution, namely spatial, temporal, spectral, and radiometric resolutions. The spatial resolution means the length of one side of a single-pixel between two objects. The spectral resolution is identified as the width of each band acquired by a sensor that can classify the narrowest area of wavelength intervals for a band. Temporal resolution is the time of revisiting a specific place during the satellite rotation. And finally, the radiometric resolution is the level of quantization divided by the radiance in each band [98].

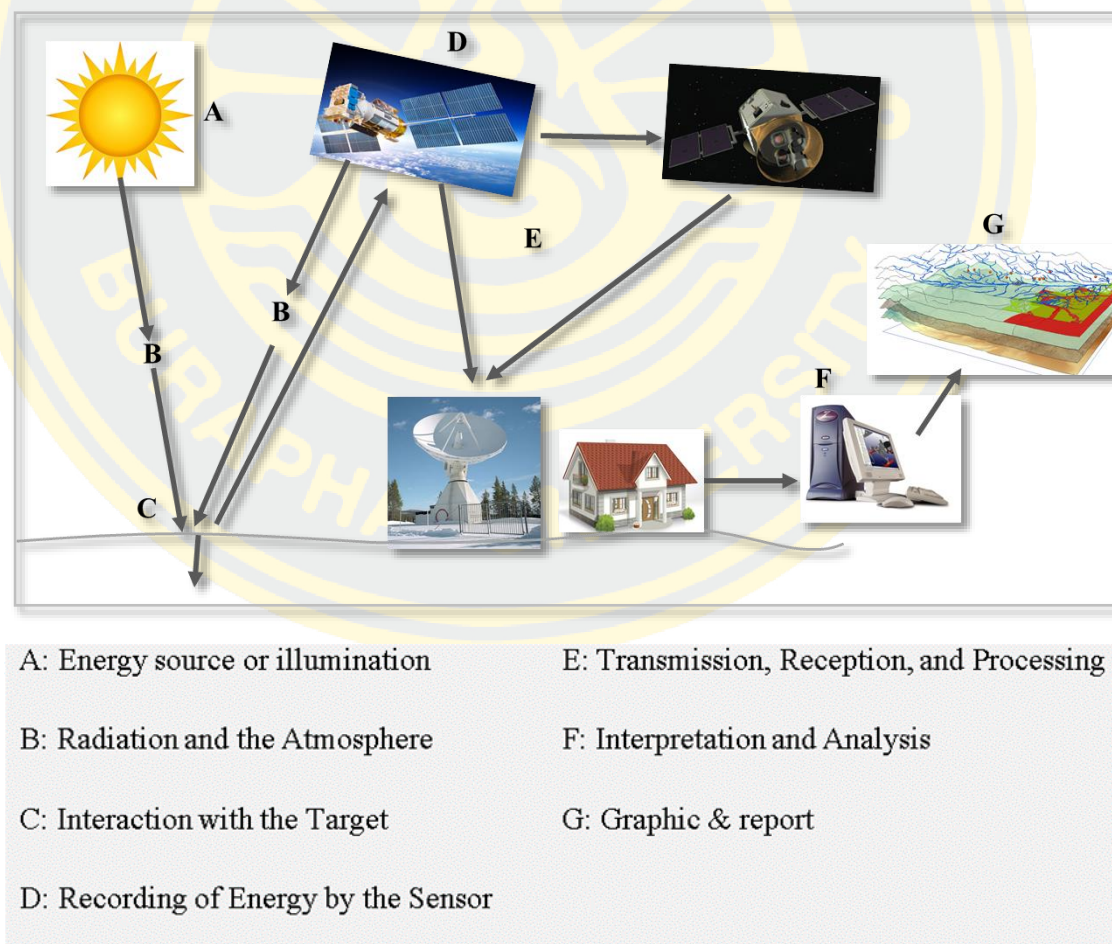


Figure 26 Remote sensing system

In the remote sensing system, basically, there are two main kinds of sensors, namely active sensor and passive sensor [97]. The passive sensor can only collect the objects or areas during the natural radiation from solar energy. However, an active sensor emits its radiation toward the target for investigation without the aid of solar energy radiation. It can acquire the data in any weather condition and condition of no lighting due to its radiation from the platform [98].

3.7.1 Google Earth Engine (GEE)

It is a cloud-based system which provides the many satellite images and geospatial dataset that can be enabled to perform geospatial image processing and analysis by using machine learning algorithms. It is freely accessible to various users such as scientists, academic researchers, non-profit, business organizations, and so on [99]. Due to the cloud-based computation of a massive dataset of satellite images,

Since GEE operates the huge file size, it reduces the data processing period and the positive effect on the capacity to perform large scale computation [100].

3.7.2 Remotely sensed techniques for flood detection

General data processing of SAR satellite images was computed in google earth engine (GEE), and the steps are as below Figure 27.

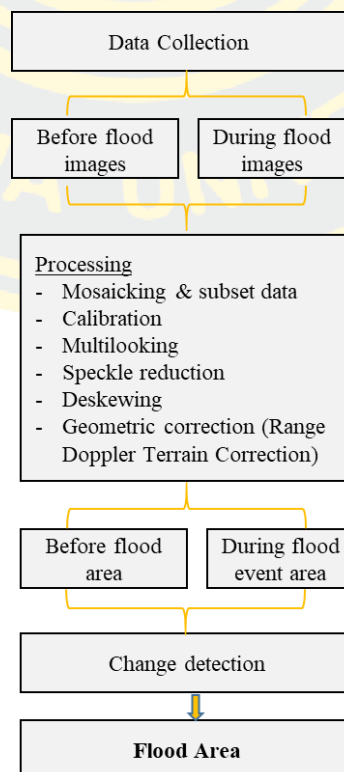


Figure 27 Flow-chart of flood mapping in Google Earth Engine (GEE)

Satellite data of Radar were collected from the google earth engine, which is the cloud-based system, and so many satellite data are available in it [101]. To calculate the flood area, the two different periods of data are required before the images of the flood events and during the flood event. After that, the raw images were processed for each period. As the study area is covered with more than the three satellite scenes, and they were mosaicked and subset with the study area. Due to the various scenes at different incident angles and relative levels of brightness, the first calibration of processing was carried out, and this step is vital for the quality of SAR data.

The satellite products have noise and pixel size errors, and these will be reduced in Multilooking processing. The images will be better with a nominal image pixel size. To lessen the amount of speckle at blurred features or reduce resolution in condition, the speckle reduction processing is more effective. Deskewing and terrain correction were also done for geometric correction, especially for terrain due to the different Doppler time and needed to be done before processing [102].

After processing the two different periods of satellite image were calculated to extract the flood area from the data of the before-flood period by subtracting during the flood event, especially for the flood peak period. Finally, the only flood area was exported into the .tiff file and can be performed in the GIS platform. The processing of the selected flood events (2015 and 2017) were illustrated in Figure 28 and 29 which are mentioned the image processing before flood period and after flood period using the Sentinel-2 data.

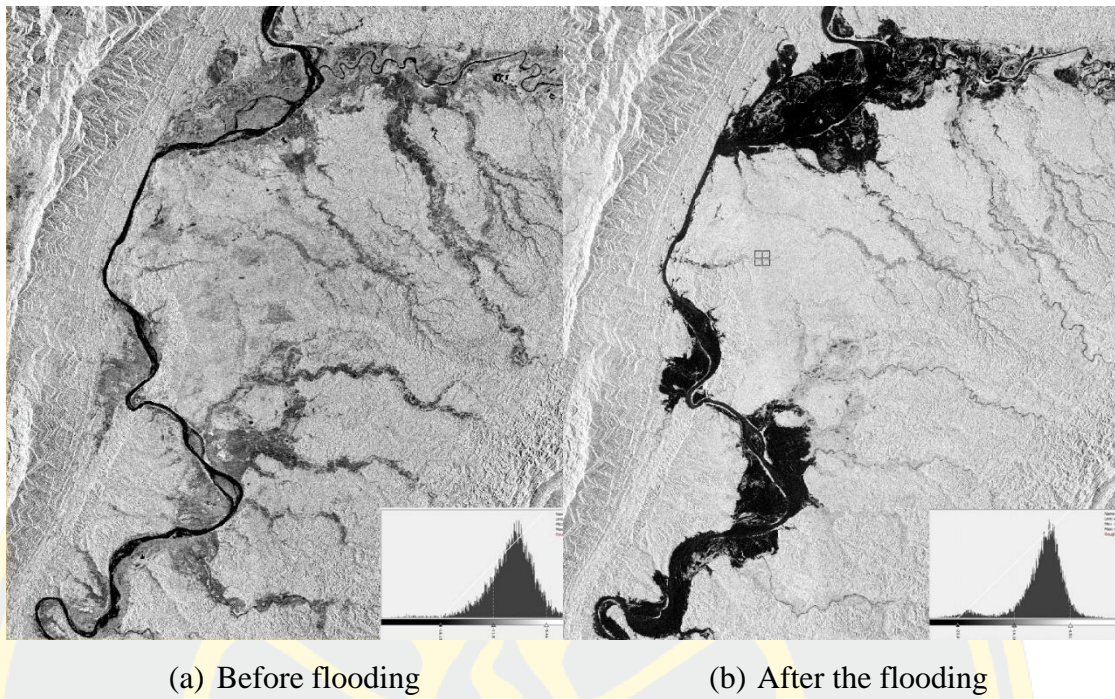


Figure 28 Processing the flood computation using the sentinel-1 data for 2015 flood event at Homalin Area in Chindwin River

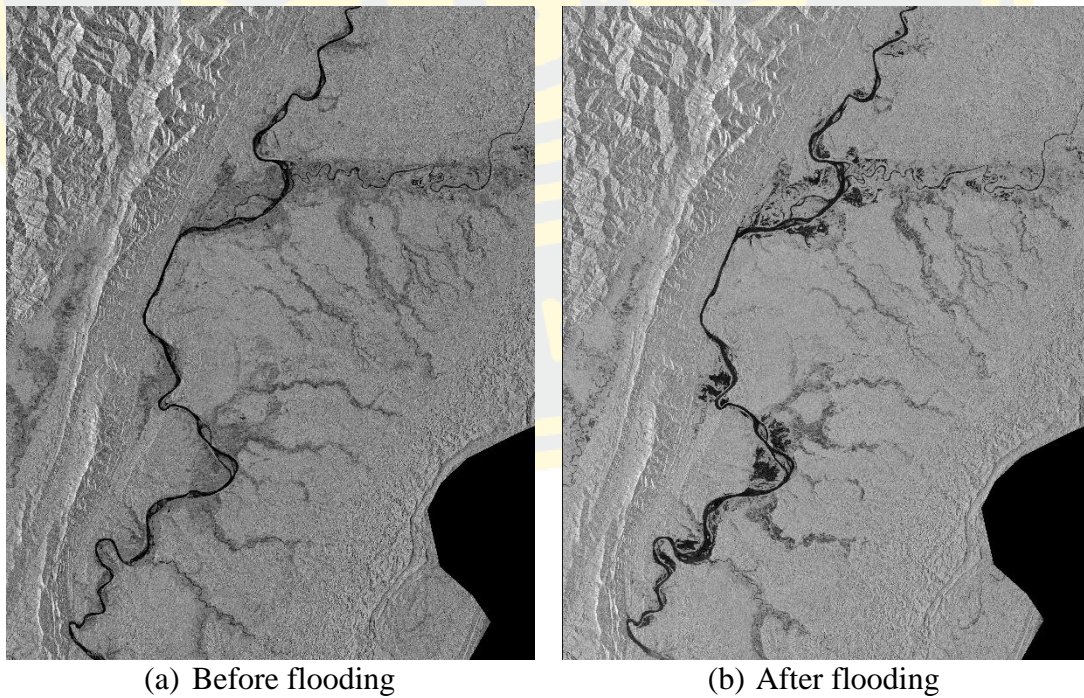


Figure 29 Processing the flood computation using the sentinel-1 data for 2017 flood event at Homalin Area in Chindwin River

3.7 Processing for flood risk assessment

In the evaluation of the flood risk, plenty of datasets are required, namely the flood hazard, flood vulnerabilities, and flood exposures first. Moreover, it is too complicated in consideration of hydrology and hydraulic conditions of the river system, which can be the potential to harm the lives and damage the properties during the flood [103].

3.7.1 Hazard mapping

In this study, the flood hazard maps are modelled in different return periods using the hydrological model and hydraulic model for the different return periods for the flood maps in the previous section. For flood risk assessment, 50 years flood inundated model was used as the flood hazard area to estimate the future flood risk condition.

3.7.2 Exposure map

Population dataset was collected from the Columbia University Earth Institute (<https://energydata.info/organization/about/columbia-university-earth-institute>) and extracted the data with the study area, as described in Figure 30. It is in the geo-tiff file with the pixel value of population data in the Chindwin River basin. Downstream is a more populated area than the upstream of the river where is the most mountainous area.

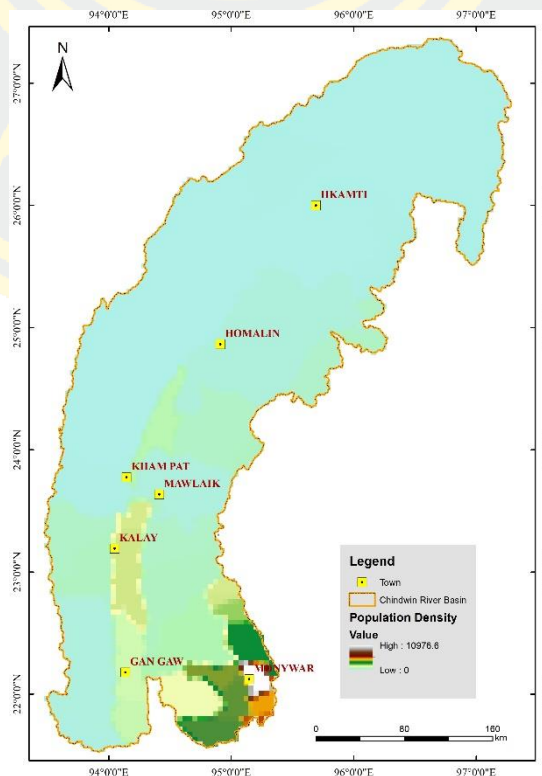


Figure 30 Population density map

The cropland was calculated in cloud-based computation, Google Earth Engine (GEE), using the Sentinel-2 optical satellite imagery of the 2019 year, as shown in Figure 31 which is provided the general flow chart of crop mapping. Generally, there are four main steps namely, data collection, pre-processing, processing and result. Firstly, the Sentinel-2 satellite data which have spectral bands of Top of Atmosphere (TOA) reference from the satellite data in GEE. In the pre-processing steps for Sentinel-2 included shadow and cloud removal, geometric correction, mosaicking, and subset. Cloud and shadow removal is an essential step because of the negative influence cloud shadow can have on data analysis especially in the optical remotely sensed data for further data classification. Moreover, the geometric correction was also processed. Mosaicking and data subset were applied according to the boundary of the study area.

The ground truth data were collected from the true data of Sentinel-2 optical image for the crop land computation in GEE. And the sampled data were trained by using the random forest method (RF) to explore the crop land and non-crop land area in the code of 0 and 1 data. Here 1 data of grid code is the crop land and the other, 0 data is non-crop area as shown in Figure 32. Finally, it was exported into .tiff file for further processing in the GIS platform.

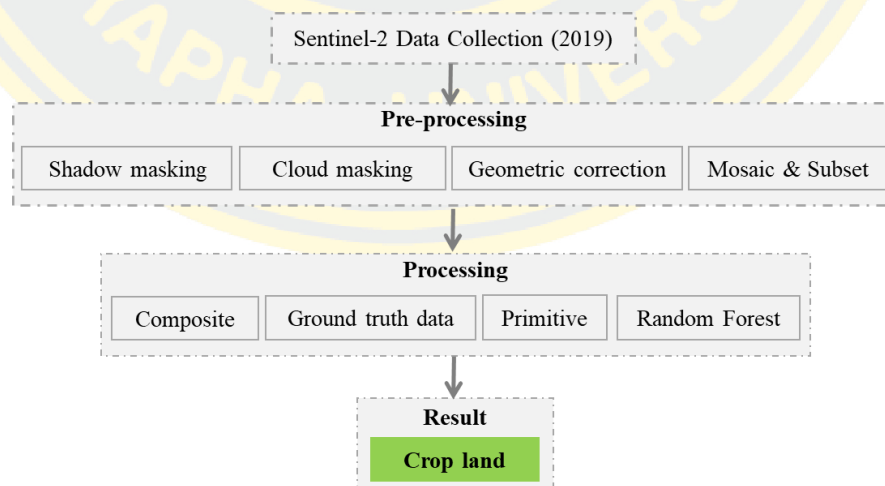


Figure 31 General flow chart of crop mapping

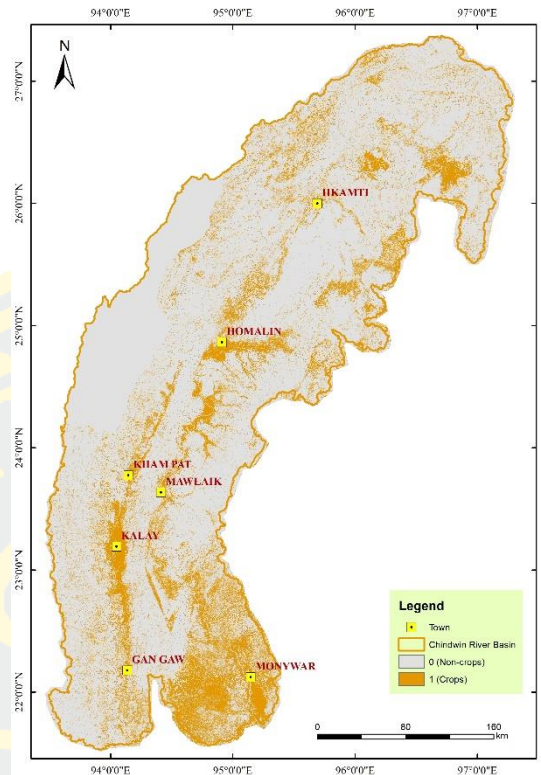


Figure 32 Crop map of Chindwin river basin

The locations of the schools were assessed from the database of [104] Myanmar Information Management Unit (MIMU), and the area outside of Myanmar, the school locations were lacking data as Figure 30. These spatial point sources were buffered into a different distance from the schools to account for one of the flood exposures, as shown in Figure 33.

The location of Hospitals (Figure 34) was spatially created from the Myanmar UTM Topographic Map (Survey Department) and buffering the data with various distance from the sources. The maximum length is about 100 km and converted into a raster format, as illustrated in Figure 3.34.

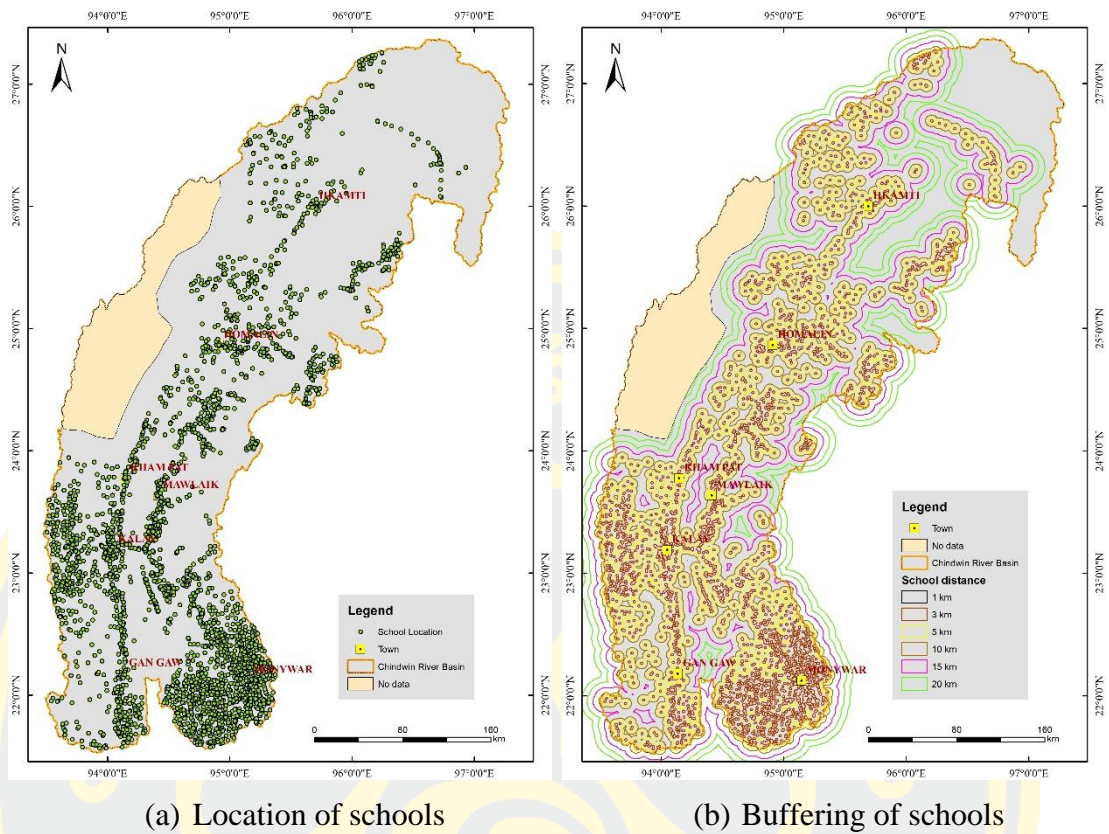


Figure 33 (a) Location of schools and (b) Buffering of schools

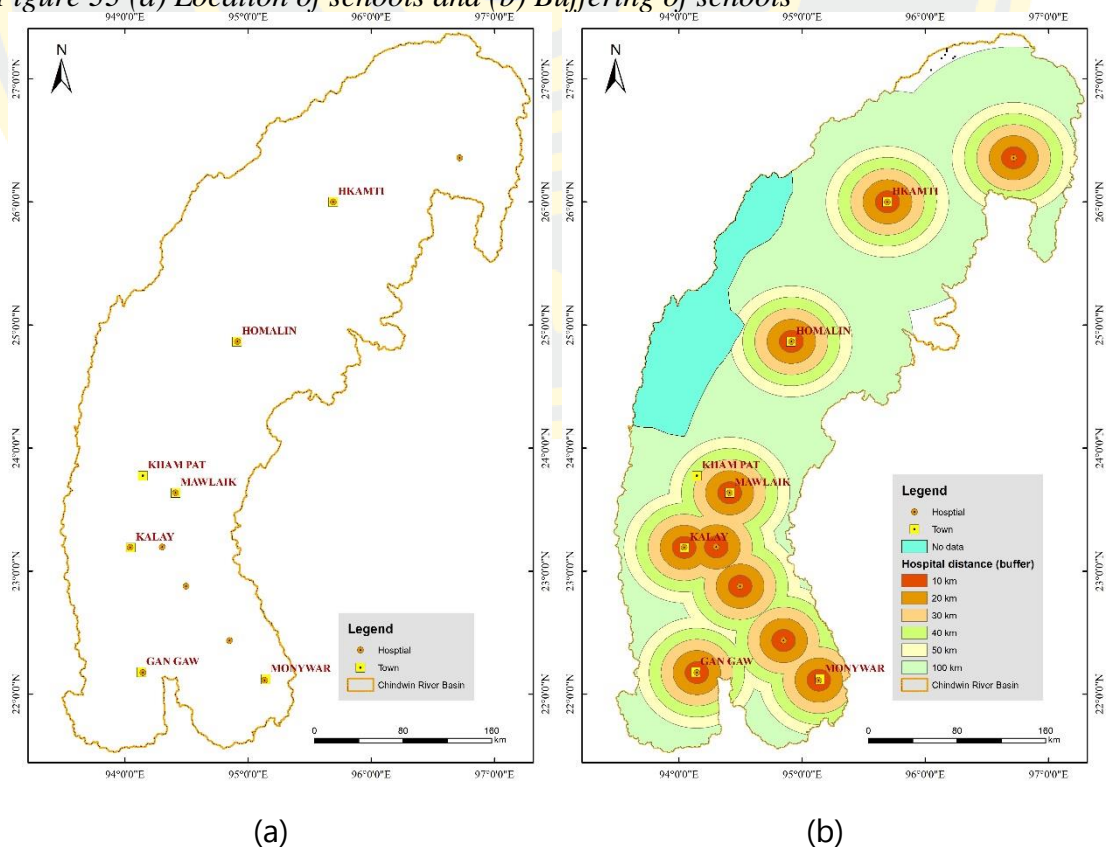


Figure 34 (a) Location of hospitals and (b) Buffering of hospitals

Road Network is also one of the factors which can reduce the flood risk. The datasets were assessed lines feature from the Open Street Map (OSM) [105] and selected the only road network. The line patterns of the road networks were clipped and buffered the road distance to access the road directly. And these buffered data were also converted into a raster format, as shown in Figure 35.

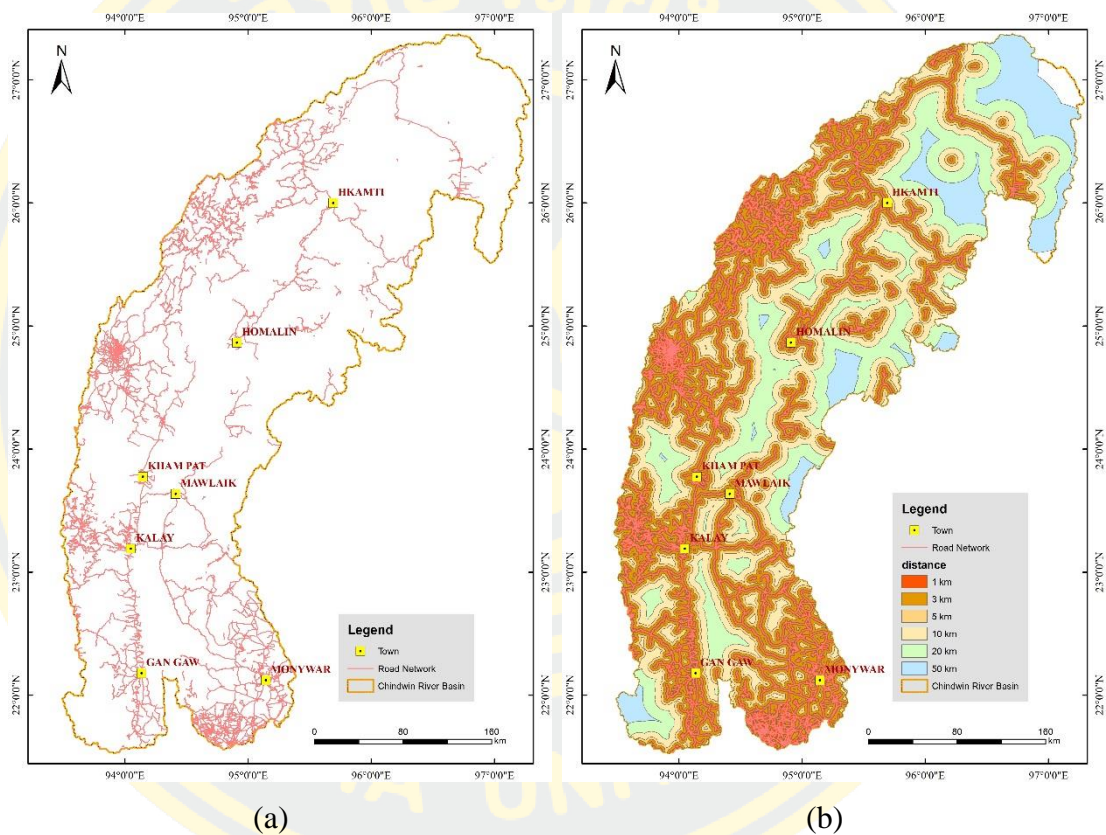


Figure 35 (a) Location map of the road network and (b) Buffering the road network

3.7.3 Vulnerability mapping

Even though the same intensity of flood extent and depth happened in the flood-prone areas, the impacts were different because of various levels of resilience [46]. The more resistance of people are strong, the lesser the adverse effects are, while the more strength of people is weak, the bigger the negative impacts are. In this task, two components of flood vulnerabilities are applied, such as the urban area and age of people, even though there are plenty of indicators to vulnerabilities [88][90].

Figure 36 describes the demographic comparison graph of three layers for age composition (less than 14 & more than 65 years old) and literacy.

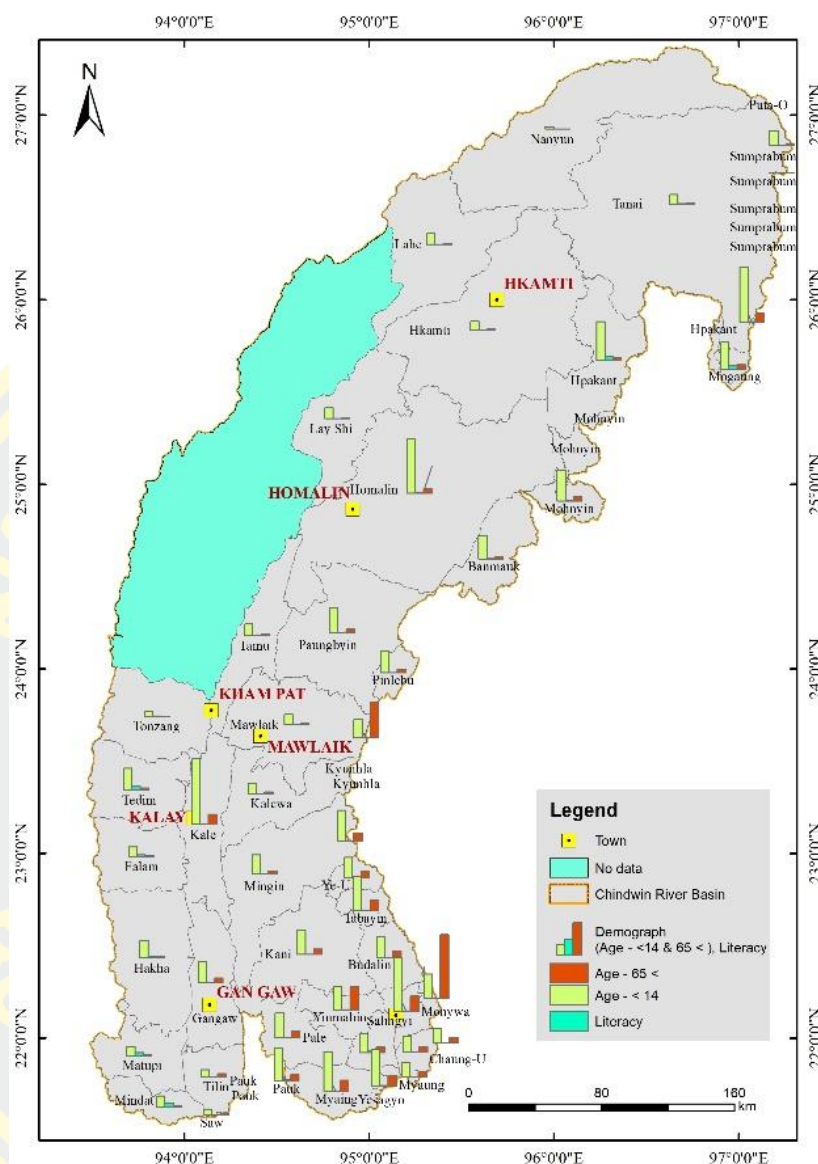


Figure 36 Illustration of statistical, demographic data of study area (Census 2014)

Table 5 Demographic data of the study area

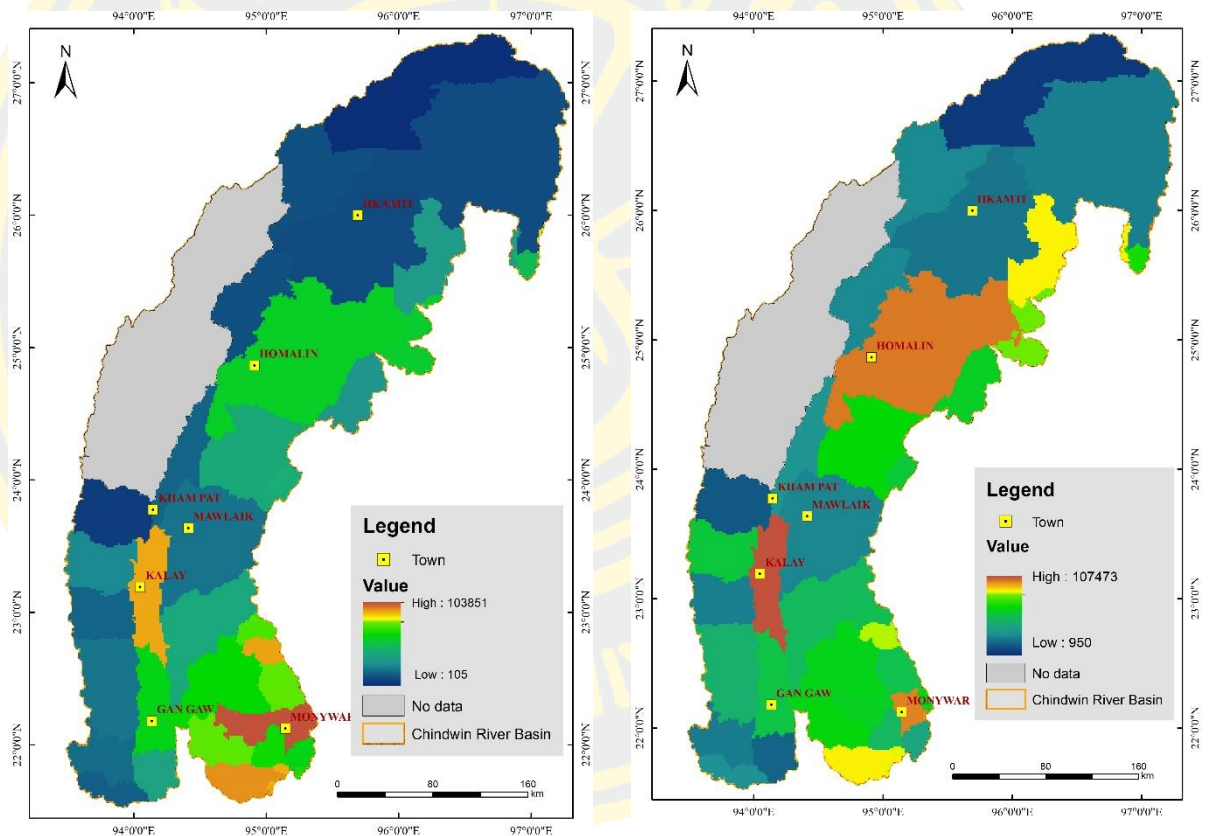
Sr. No.	State/Region	District	Township	No. of Age- <14	No. of Age- 65 <	No. of Literacy (Age 25 <)
1	Chin	Hakha	Hakha	28686	2878	3471
2	Chin	Falam	Tedim	35689	3534	6339
3	Chin	Mindat	Mindat	18139	2042	6731
4	Chin	Mindat	Matupi	15165	2474	5265
5	Chin	Falam	Falam	15447	2277	2732
6	Chin	Falam	Tonzang	9236	751	1335
7	Kachin	Mohnyin	Mogaung	43488	6751	5593
8	Kachin	Putao	Sumprabum	950	105	0

9	Kachin	Myitkyina	Myitkyina	91095	14345	1173
10	Kachin	Putao	Putao	23497	2942	65
11	Kachin	Myitkyina	Tanai	15524	1293	462
12	Kachin	Mohnyin	Mohnyin	50450	7732	606
13	Kachin	Mohnyin	Hpakant	63405	4624	5593
14	Magway	Pakokku	Myaing	65091	18028	515
15	Magway	Gangaw	Tilin	11221	5011	293
16	Magway	Pakokku	Pauk	54771	10837	1901
17	Magway	Pakokku	Yesagyo	59541	16730	409
18	Magway	Gangaw	Saw	9226	2758	108
19	Magway	Gangaw	Gangaw	34649	8340	293
20	Sagaing	Monywa	Chaung-U	25640	8330	236
21	Sagaing	Yinmabin	Yinmabin	38594	37757	151
22	Sagaing	Shwebo	Ye-U	33312	10145	84
23	Sagaing	Kale	Kalewa	16475	2733	21
24	Sagaing	Mawlaik	Paungbyin	40908	5597	70
25	Sagaing	Hkamti	Lay Shi	17623	1536	17
26	Sagaing	Hkamti	Lahe	17623	1536	33
27	Sagaing	Yinmabin	Pale	40549	10484	471
28	Sagaing	Monywa	Budalin	33943	10479	146
29	Sagaing	Kale	Mingin	31665	5446	83
30	Sagaing	Tamu	Tamu	19302	2289	40
31	Sagaing	Hkamti	Nanyun	3653	240	99
32	Sagaing	Monywa	Monywa	87869	24976	725
33	Sagaing	Kale	Kale	107473	16847	262
34	Sagaing	Katha	Banmauk	37932	4252	254
35	Sagaing	Sagaing	Myaung	24483	9168	144
36	Sagaing	Yinmabin	Salingyi	30957	9049	2831
37	Sagaing	Yinmabin	Kani	39463	8674	107
38	Sagaing	Shwebo	Taze	49450	13094	198
39	Sagaing	Mawlaik	Mawlaik	16390	2650	60
40	Sagaing	Katha	Pinlebu	36185	5779	174
41	Sagaing	Hkamti	Hkamti	14071	1254	413
42	Sagaing	Shwebo	Kyunhla	30245	58513	140
43	Sagaing	Hkamti	Homalin	89453	7953	1154
44	Sagaing	Shwebo	Tabayin	56153	17158	97
45	Sagaing	Monywa	Ayadaw	39538	103851	222
46	Sagaing	Sagaing	Myinmu	24483	9309	114

Source:[106]

Figure 37 (a) shows the township level map for the age composition (more than 65 years old) with the level of the flood vulnerability. The Kalay and Monywa townships in age composition (> 65 years old) are higher than other townships for the flood vulnerability. In comparison, the Homaline and Kalay townships are higher for the age composition (<14 -year-old).

For the literacy assessment, the Kalay and Homalin townships are also higher than other towns, while the northern part of the Chindwin river basin is found as low in township level, as shown in Figure 37 (b).



(a) Age composition (more than 65 years old)

(b) Age composition (less than 14 years old)

Figure 37 Demographic maps for (a) Age composition (more than 65 years old) and (b) Age composition (less than 14 years old)

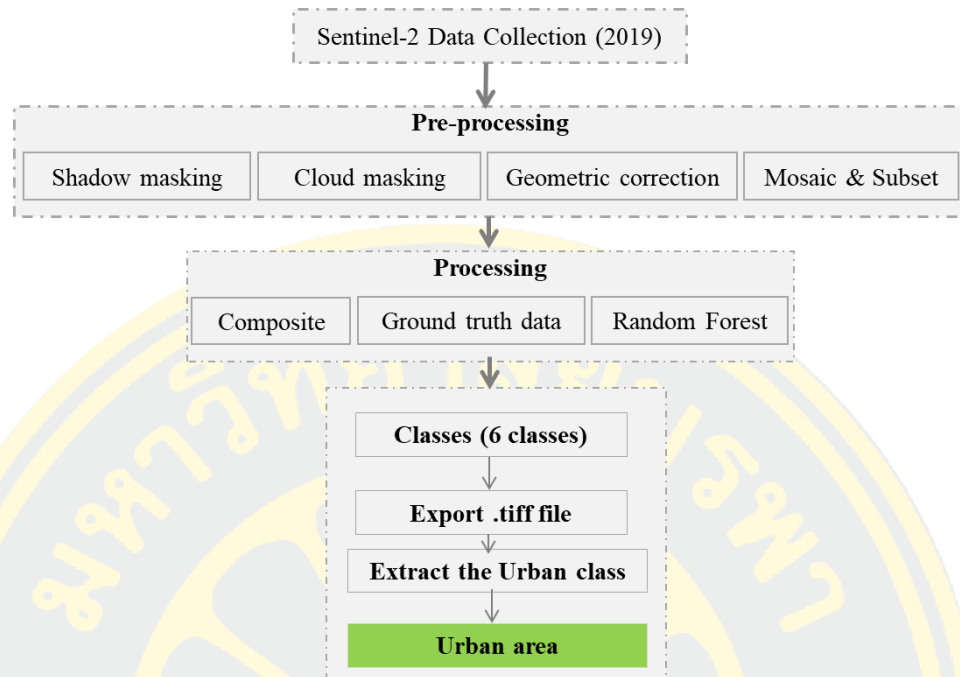


Figure 38 Overall steps of urban area computation in Google Earth Engine

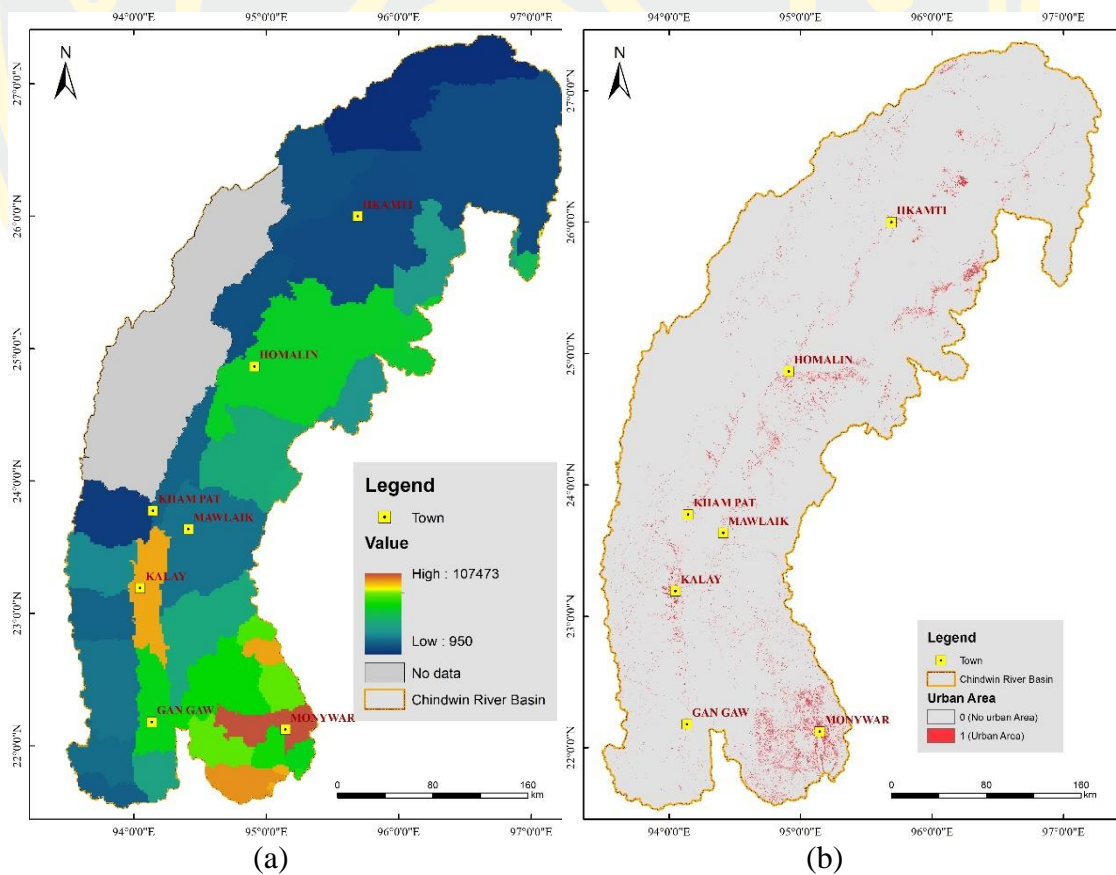


Figure 39 (a) Literacy map of township-level and (b) Location map of the urban area

The urban area (residential area) was computed from the cloud-based system (Google earth engine) using the Sentinel-2 satellite data for the 2019 year as the overall step of Figure 38. In the pre-processing steps for Sentinel-2 included shadow and cloud removal, geometric correction, mosaicking, and subset. Cloud and shadow removal is required due to the negative influence cloud shadow especially in the optical remotely sensed data for further data classification. Moreover, the geometric correction was also processed. Mosaicking and data subset were applied according to the boundary of the study area.

The ground truth data related six classes such as forest, agriculture, shrub, bare land, water bodies, the urban area (residential). The training data were randomly collected to cover the whole Chindwin river basin. And these samples were trained by using the random forest method (RF) to explore the six classes in google earth engine. And then it was exported into .tiff file and converted into shape file (.shp) in the GIS platform. Finally, the crop land of this study area were computed for one of the flood exposures. According to the result of Figure 35, it describes the condition of the urban area in the Chindwin river basin, and the high urbanization is found in the lower Chindwin river catchment, Kalay and Homalin townships, which can be assumed as a high vulnerability in flood risk assessment.

CHAPTER 4

EXPERIMENT RESULTS AND DISCUSSION

In this chapter, the experiment results of the four main sections will be discussed and presented. They are the results of the hydrologic model, the hydraulic model with its selected flood events of the flood inundation maps and the return periods, the flood validation maps derived from the remote sensing techniques in a cloud-based system, and finally, flood risk assessment by consideration of the flood hazard, flood exposure, and flood vulnerability.

4.1 Hydrologic model (HEC-HMS)

In this study, the HEC-HMS model was calibrated for different flood events to determine the best fit between the model and observation. Nine storm events of 2010, 2011, 2012, 2013, 2014, 2015, 2016, 2017, and 2018 have experimented with the hydrological model.

Table 6 Calibrated parameters of HEC-HMS model in Chindwin River Basin

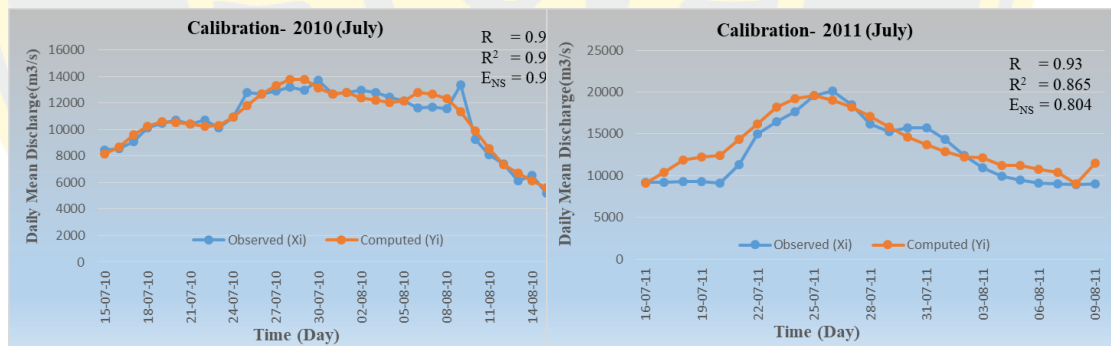
Sub-basin	Initial Loss (mm)	Constant Rate (mm/hr)	Impervious (%)	SCS Lag (min)	Base-flow rate (m3/s/km2)	Base-flow (threshold ratio)	Recession - Ratio to Peak
W1080	7.23	3.953	4.12	420	0.095	0.89	0.133
W1090	4.52	1.532	6.21	360	0.092	0.88	0.228
W560	6.14	1.930	4.21	1454	0.093	0.87	0.162
W590	7.19	3.972	4.23	480	0.093	0.94	0.200
W630	4.28	1.930	4.21	420	0.090	0.96	0.201
W650	5.21	3.498	5.29	180	0.093	0.93	0.185
W700	4.25	2.895	3.28	480	0.092	0.97	0.232
W740	4.9	3.923	8.13	480	0.092	0.83	0.235
W760	4.5	1.532	6.29	300	0.094	0.90	0.245
W800	7.81	3.015	3.25	360	0.095	0.60	0.344
W820	4.19	2.881	4.82	480	0.092	0.95	0.240
W840	4.9	3.890	8.23	480	0.095	0.86	0.203
W870	7.25	3.015	3.39	720	0.091	0.91	0.352
W970	4.8	3.819	3.25	1654	0.092	0.98	0.379
W980	4.25	2.881	3.52	480	0.094	0.97	0.234

Table 6 shows the final calibration parameters with data in HEC-HMS for the study area. In this rainfall-runoff simulation, HEC-HMS assigned to model the only flooded period of the selected years by accounting the following calibrated parameters such as initial Loss, constant--rate, impervious, SCS lag, base-flow rate, threshold ration in base-flow, and recession ration to the peak. These model parameters were calibrated using the trial and error method until a reasonable match between observed and computed hydrograph in event-based simulation.

4.1.1 Calibration and validation results

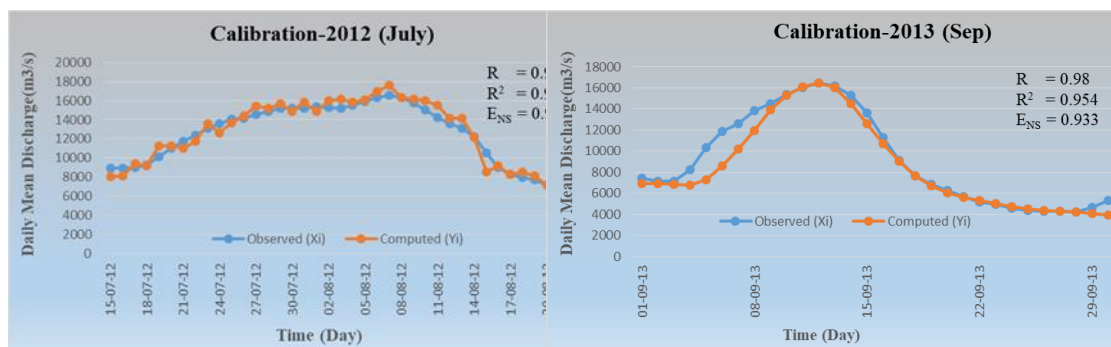
There are seven calibrations and two validations for flood events to determine the correlation between the computed and observed flows.

In the calibration of seven different flood events, the optimization trial option was applied using the Peak Weighted Root Mean Square Error (PWRMSE) objective function and the Univariate Gradient (UG) search algorithm method. Figure 40 shows the results of calibration for seven storm events, and each presented the results as the close correlation between the simulated and observed flows.

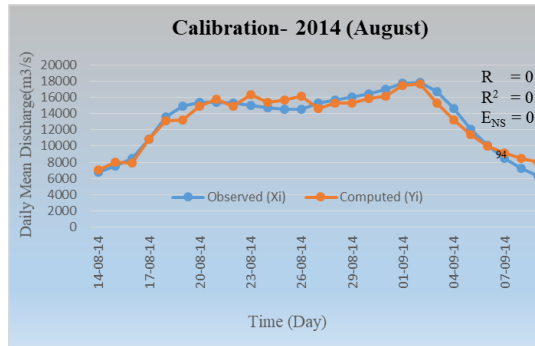


(a) Comparison of observed and simulated outflow for the calibrated year (2010-Jul to Aug)

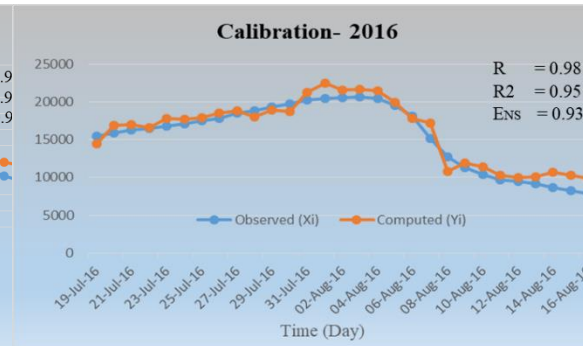
(b) Comparison of observed and simulated outflow for the calibrated year (2011-Jul to Aug)



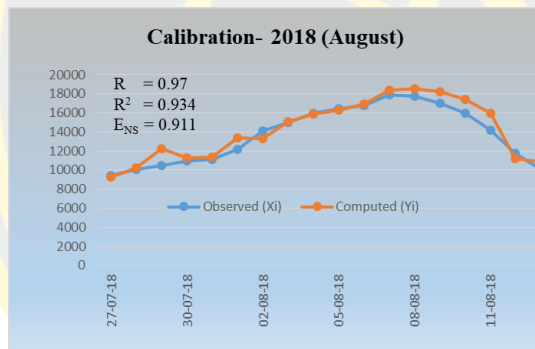
(c) Comparison of observed and simulated outflow for the calibrated year (2012-Jul to Aug)



(d) Comparison of observed and simulated outflow for the calibrated year (2013-Sep)



(e) Comparison of observed and simulated outflow for the calibrated year (2014- Jul to Sep)



(f) Comparison of observed and simulated outflow for the calibrated year (2016- Jul to Aug)

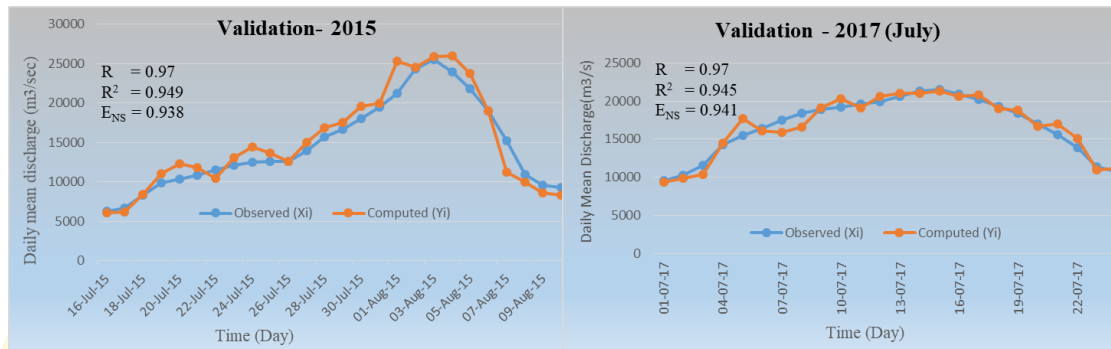
(g) Comparison of observed and simulated outflow for the calibrated year (2018- Jul to Aug)

Figure 40 (a-g) Calibration results of HEC-HMS model

Table 7 Results of calibration for the selected seven years of flood events

Year (Flood)	R	R ²	ENS
2010	0.96	0.94	0.94
2011	0.93	0.86	0.80
2012	0.98	0.95	0.94
2013	0.98	0.95	0.93
2014	0.97	0.94	0.94
2016	0.98	0.95	0.93
2018	0.97	0.93	0.91

Table 7 presents the results of the seven-year flood events for the calibration of the Chindwin River Basin, namely, Coefficient of Correction (R) Coefficient of Determination (R^2) and Nash Sutcliffe Efficiency (E_{NS}).



(a) Validation result of 2015 flood event (b) Validation result of 2017 flood event

Figure 41 Validation results of the HEC-HMS model for 2015 and 2017 flood events

Once the calibration was completed with seven selected flood events, then the final calibration parameters were taken as input data in the selected two storms flood events of (2015 and 2017) for the model validation, as shown in Figure 41. In the validation for 2015 flood event, the results of coefficient of correlation (R), the Coefficient of Determination (R^2), and Nash Sutcliffe efficiency (ENS) values are 0.97, 0.949, and 0.938 respectively while the validation results of coefficient of correlation (R), the Coefficient of Determination (R^2), and Nash Sutcliffe efficiency (ENS) for 2017 flood event were obtained as 0.97, 0.945, and 0.941. These relationships of both flood events indicated a closed and proper correlation between the observed and simulated flow.

4.1.2 Simulation of design flood hydrography

In this study, the 2, 5, 10, 20, 50, and 100 year return periods have computed the design flood hydrograph using the HEC-HMS model for the same duration. In the HEC-HMS model, the design rainfall hyetograph with selected return periods was input Meteorological Data file. SCS storm data was inputted to analyze the flows for 2, 5, 10, 20, 50, and 100-year storm events. Design flood hydrograph with the selected return periods was illustrated in Figure 42.

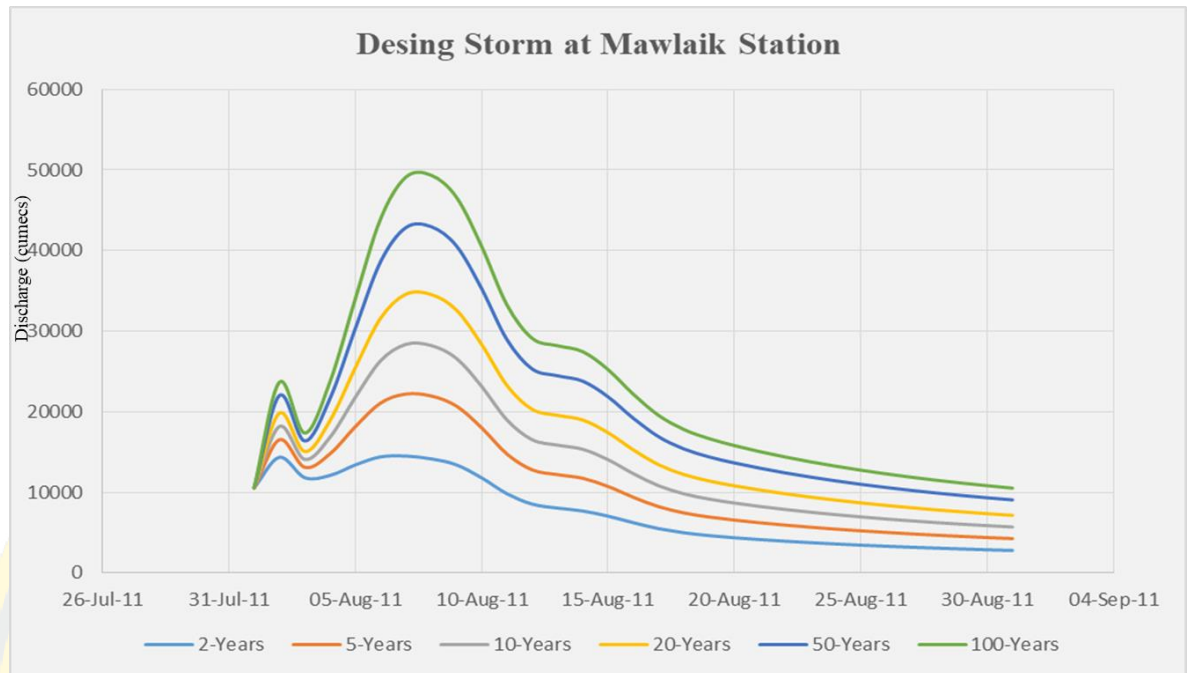


Figure 42 Design flood hydrograph with the selected return periods

4.2 Hydraulic model (HEC-RAS)

Simulation of storm events and different return periods modelled with the HEC-RAS was done. They are required to validate and calibrate for better accuracy assessment. The results of the models are described, as shown in Figure 43 and 44.

4.2.1 Calibration and validation results

HEC-RAS model produced the flood inundation map in the flood extent and flood depth for this study. The flood extent of the 2015 and 2017 flood events was checked with the flood map calculated in remotely sensed techniques using the Google Earth Engine while the flood depth was validated with the observed data from rain-gauge station (Appendix IV) and bed cross-section profile data (Appendix V) which are collected from Department of Meteorology and Hydrology (DMH).

In the calibration, the Manning Roughness Coefficient ‘n’ value is also crucial for the flood depth calculation, and it was assumed the values until the nearly same amount between observed and simulated data. The calibrated Manning of all cross-sections along the Chindwin River is generally ranging from 0.045 to 0.07.

Figure 43 shows that there is a negligible difference between the observed and computed values. The performance of the model was evaluated by three statistical tests,

namely, coefficient of correction (R), coefficient of determination (R^2), and Nash-Sutcliffe model efficiency coefficient (ENS) with 0.86, 0.72, and 0.81 respectively.

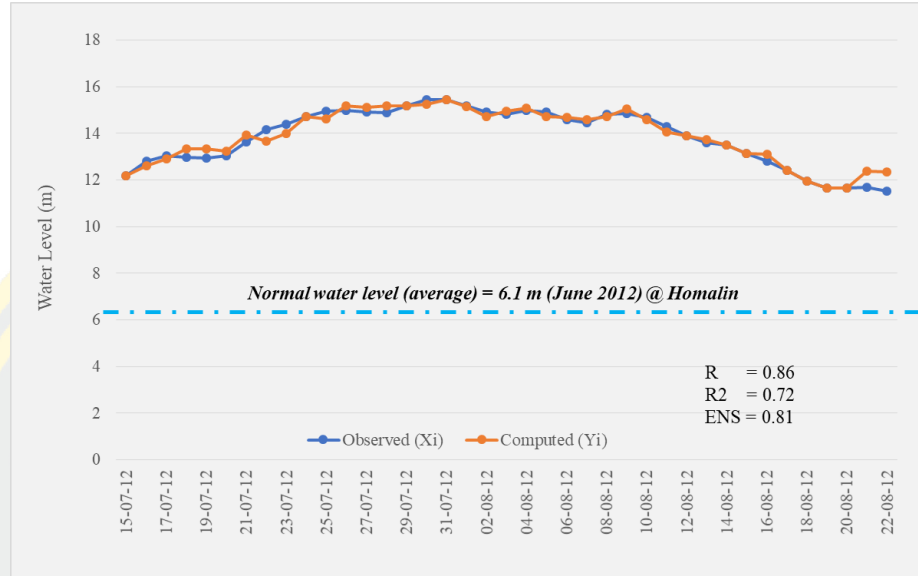
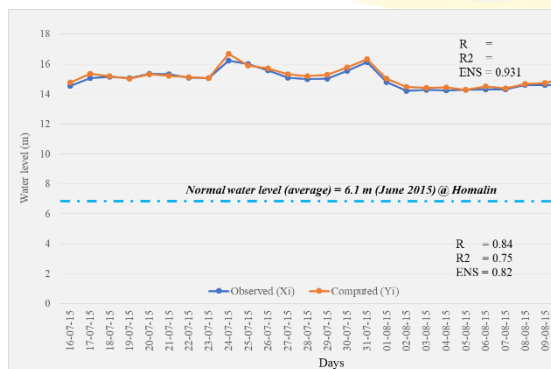
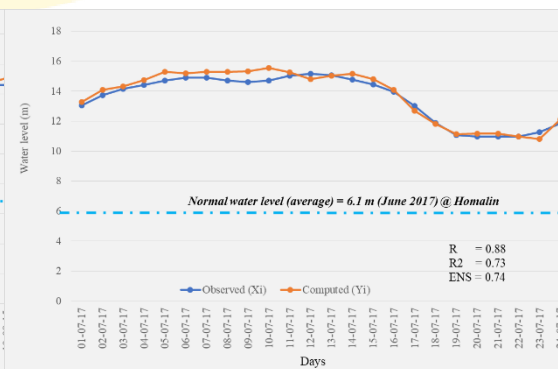


Figure 43 Calibration result of HEC-RAS model for 2012 flood event

The two storm events of 2015 and 2017 years were validated between observed and simulated water surface elevation. The difference between them was small, and it can be considered as acceptable values, as illustrated in Figure 44. The results of the calibration and validation process of the HEC-RAS model are seen to be fair with the Nash-Sutcliffe model efficiency coefficient (ENS), coefficient of determination R^2 , and Root Mean Squared Error value (RMSE). Therefore, the model is performed reasonably well with fitted Manning roughness coefficient 'n' and assumed friction slope.



(a) Validation result of 2015



(b) Validation result of 2017

Figure 44 Validation result of HEC-RAS model for 2015 and 2017 year flood events

4.2.2 Simulation of flood scenarios

Previously, the flood events were simulated with the HEC-RAS model, and it is also analyzed to know the future flood condition in the different return periods. In this study, the selected five return periods, 2, 5, 10, 20, 50, and 100-year, were calculated using the input data, which was derived from the HEC-HMS model. Figures 45 and 46 show the main river channel of the maximum flow profile and 3D perspective view of the flood plain and river channel for 50 year return period flood.

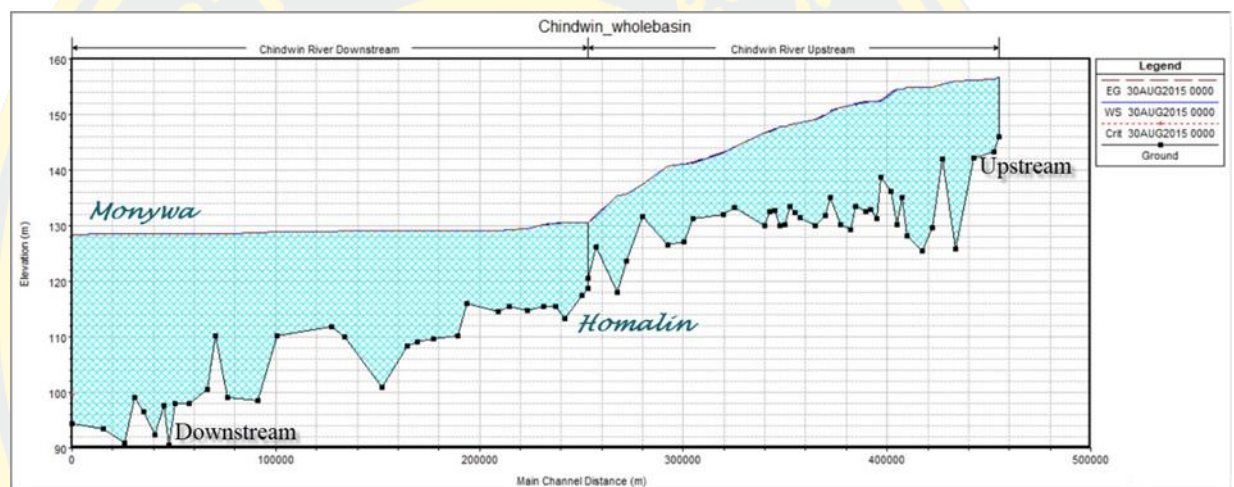


Figure 45 Maximum flow profile of 50-year return period (only main channel)

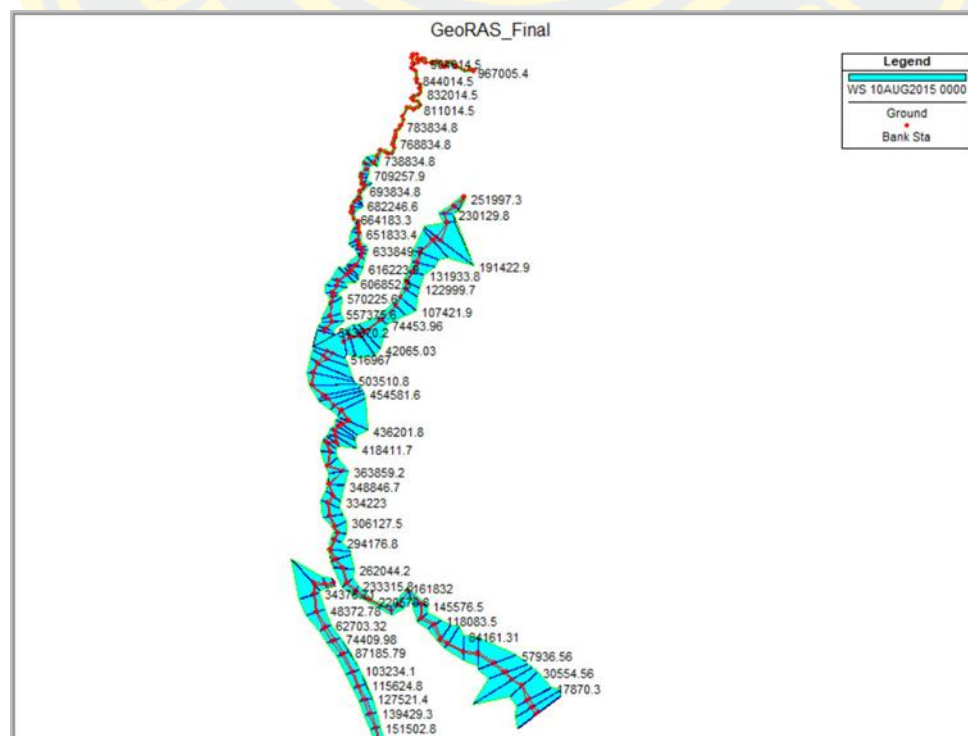


Figure 46 3D perspective view of floodplain and channel (50 year return period)

4.2.3 Flood hazard mapping

Flood hazard maps were analyzed for the selected flood events of 2015 and 2017. Firstly, the water level (flood) profile data and cross-section data simulated in HEC-RAS were exported into the GIS platform and generated as TIN based flood surface model.

According to the results of both flood events of 2015 and 2017, the flood extent of the study areas covered some parts of the Homalin city, Kalay city at tributary and the downstream regions such as Mawlaik and Monywa townships as shown in Figure 47. The depth of flood event was classified into the seven classes of flood inundation depth, named as < 2 m, 2.1-4.0 m, 4.1 – 6.0 m, 6.1 – 8.0 m, 8.1 – 10.0 m, 10.1 – 12.0 m, and > 12.0 m.

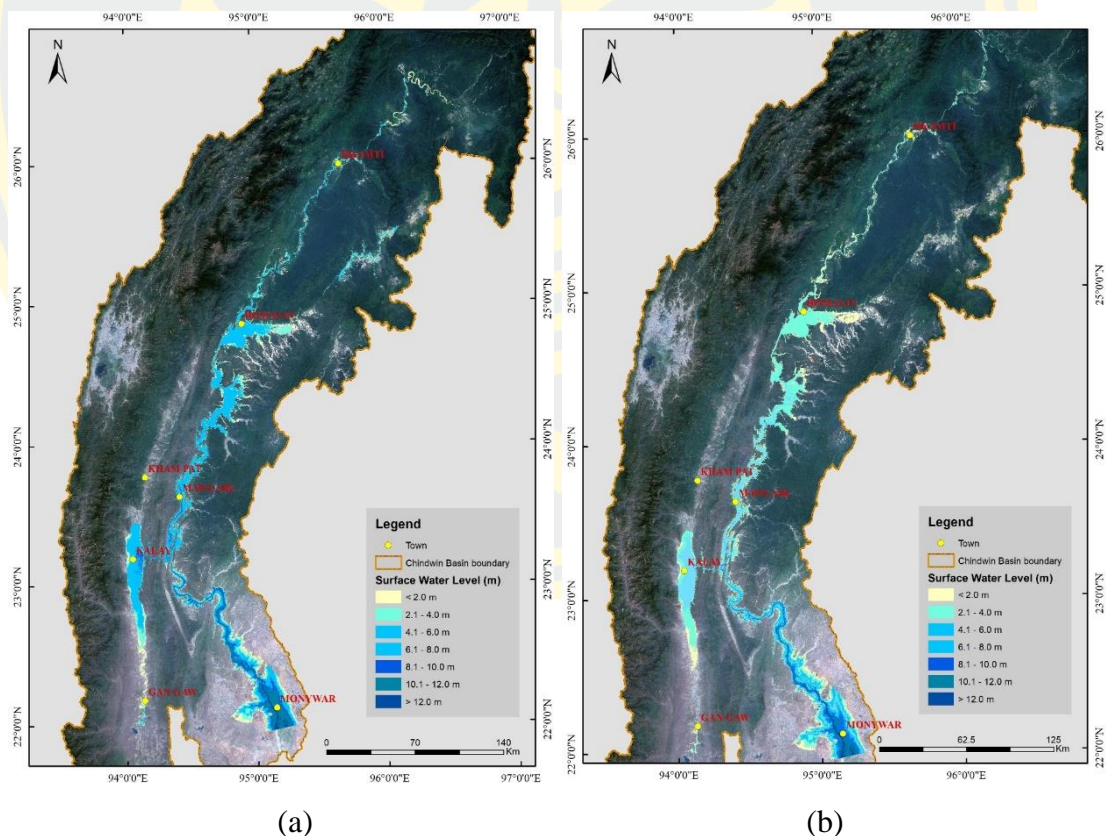
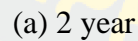


Figure 47 (1) Flood inundation map for 2015, and (2) Flood inundation map for 2017 modeled by HEC-RAS



(b) 5 year

Table 8 Flood inundation area and depths of the 2, 10, 20, 50, and 100-year flood return periods

Depth (m)	Area (km ²)					
	2 year	5 year	10 year	20 year	50 year	100 year
< 2.0	572.4	572.3	581.5	895.5	1312.1	1593.4
2.1 - 4.0	832.0	832.3	842.3	1362.6	1602.1	1794.9
4.1 - 6.0	1362.4	1362.5	1391.6	1402.5	1472.8	1593.6
6.1 - 8.0	726.0	732.2	742.4	752.3	991.3	1320.5
8.1 - 10.0	268.3	271.4	282.4	322.3	352.3	402.2
10.1 - 12.0	332.3	338.3	342.9	344.3	364.2	409.8
> 12.0	40.5	42.3	48.2	52.3	62.3	100.2
Total Area (km ²)	4133.9	4151.3	4231.3	5131.8	6157.1	7214.6

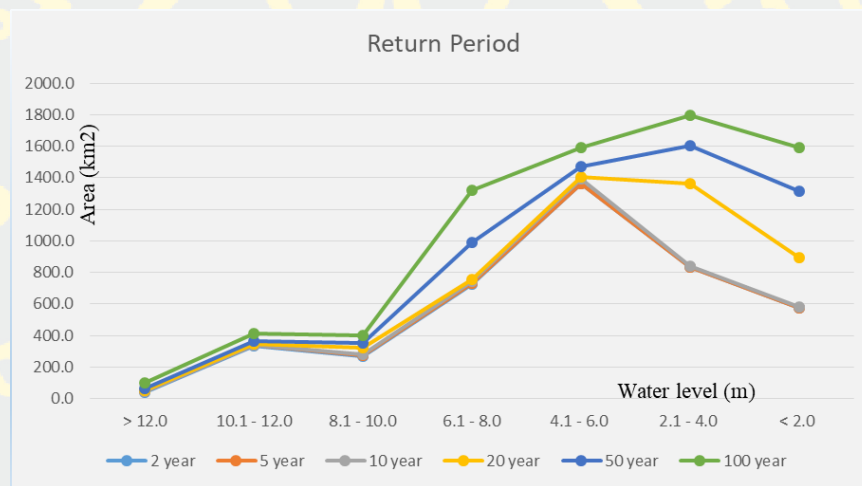


Figure 49 The relationship of flood extent and depth of the 2, 5, 10, 20, 50, and 100 year return period floods

4.3 Validation for the flooded area

In this research, remotely sensed techniques were also used to extract the flooded area of the different flood events from the satellite data of Sentinel-1. Use in remote sensing data aims to validate the flood area for the relevant flood events in this study.

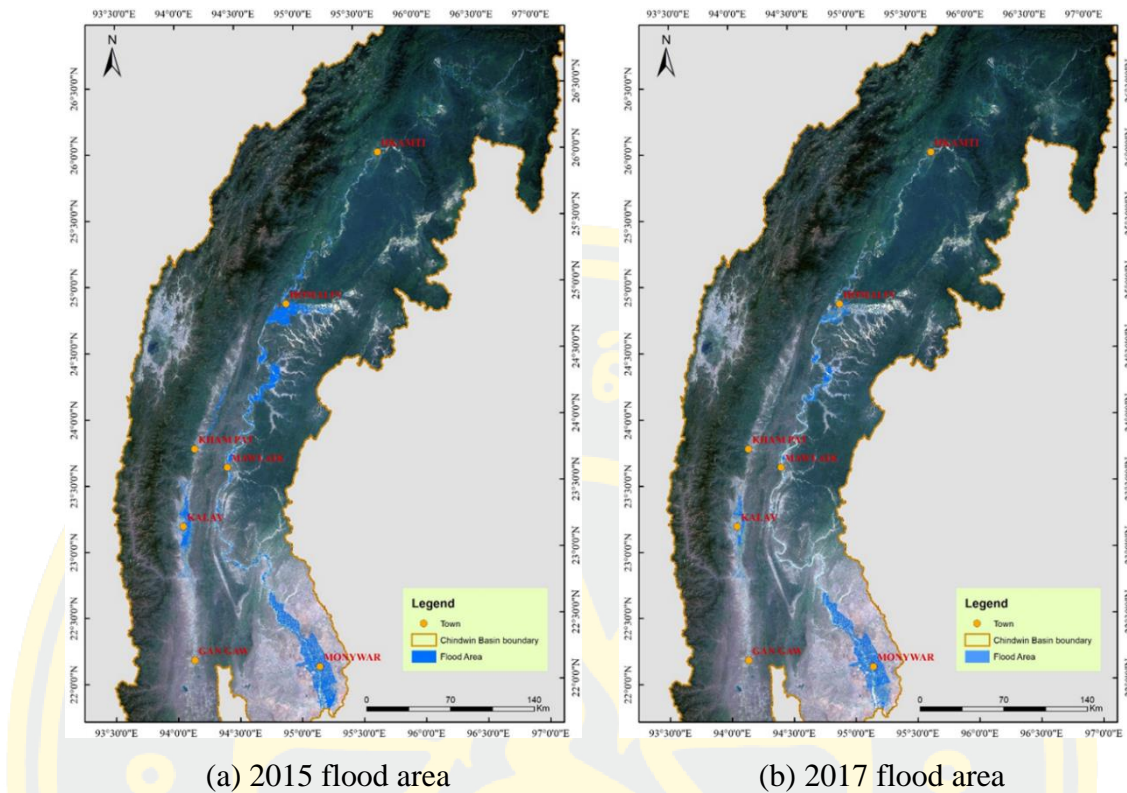


Figure 50 Flood area computed from the Sentinel 1 satellite data in Google Earth Engine for (1) 2015 flood area and (2) 2017 flood area

The results from flood inundation map simulated from the HEC-RAS model and the flood-prone area extracted from the remote sensing data (Sentinel 1) were validated for 2015 and 2017 flood events. According to the overlapped result between simulated map and map from sentinel one as presented in Table 9, 71.5% and 72.1% were the same for 2015 and 2017 flood events, and they are generally considered as the reasonably good validated check for the simulated maps. The comparison map between the simulated map and flooded map computed from remote sensing data are illustrated in Figure 51.

Table 9 Comparison of flood inundation area of simulated result and flood area from remote sensing

4.4 Flood risk assessment

Figure 52 was modeled for the 50-year return period and used as the flood hazard map in this flood risk assessment. It was classified into four classes, and higher

flood hazard has commonly occurred in the lower Chindwin river basin and Kalay flat land topography.

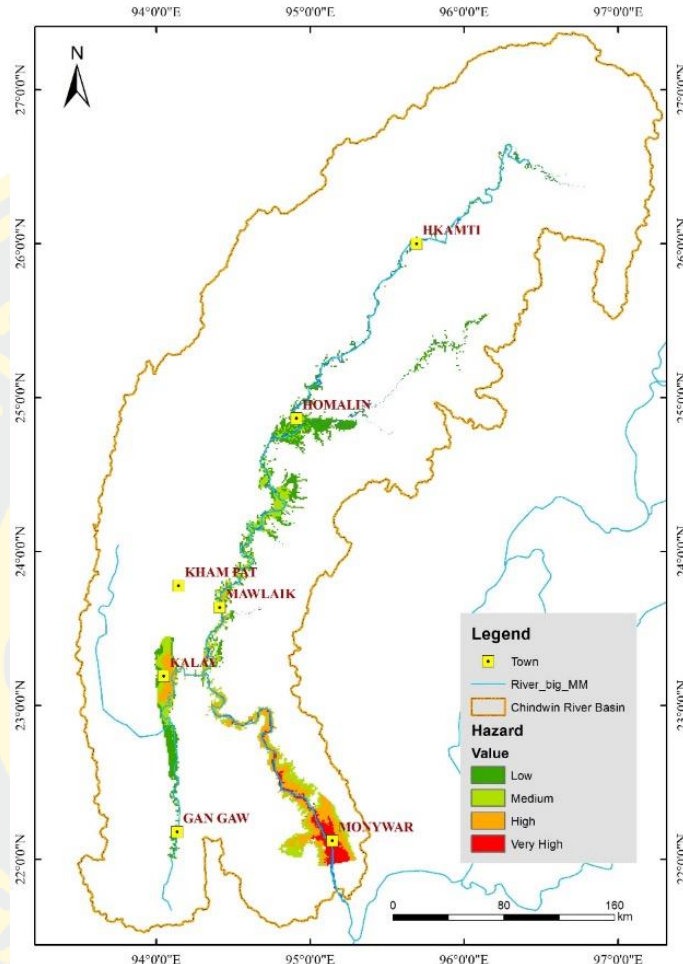


Figure 52 Flood hazard map of Chindwin river basin

Based on the various factors of population, crop, school location, hospital location, and road network, which are potential to be exposures in the Chindwin river basin, the flood exposure map was calculated as shown in Figure 53. The higher flood exposures were occurred in the downstream region of the catchment and flat land terrain of Kalay tributary due to the desnse population density and cultivated area, especially in the locations of Monywa and Kalay Townships.

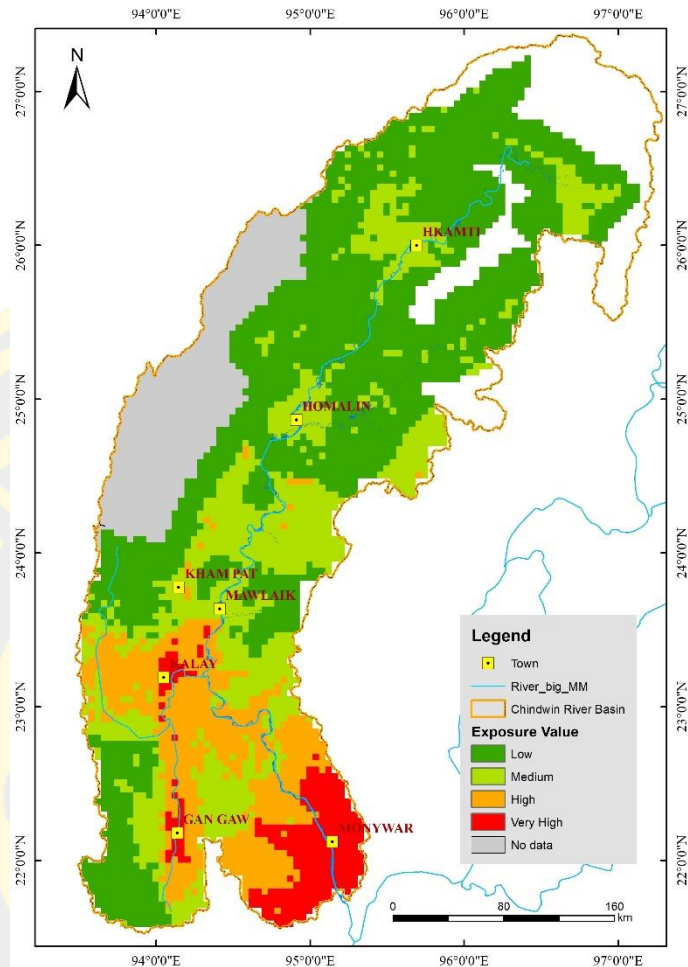


Figure 53 Flood exposure map of Chindwin river basin

Moreover, the flood vulnerability is also critical to consider the flood risk area. In this study, the four factors of the potential flood vulnerabilities are deemed to be, such as the age composition of old and child people (more than 65 years and less than 14 years old), literacy, and urban area. In the result of flood vulnerability analysis, the high flood vulnerabilities areas were found in Homalin, Kalay, and Monywa Townships. In contrast, north of the watershed area was studied as low as shown in Figure 54.

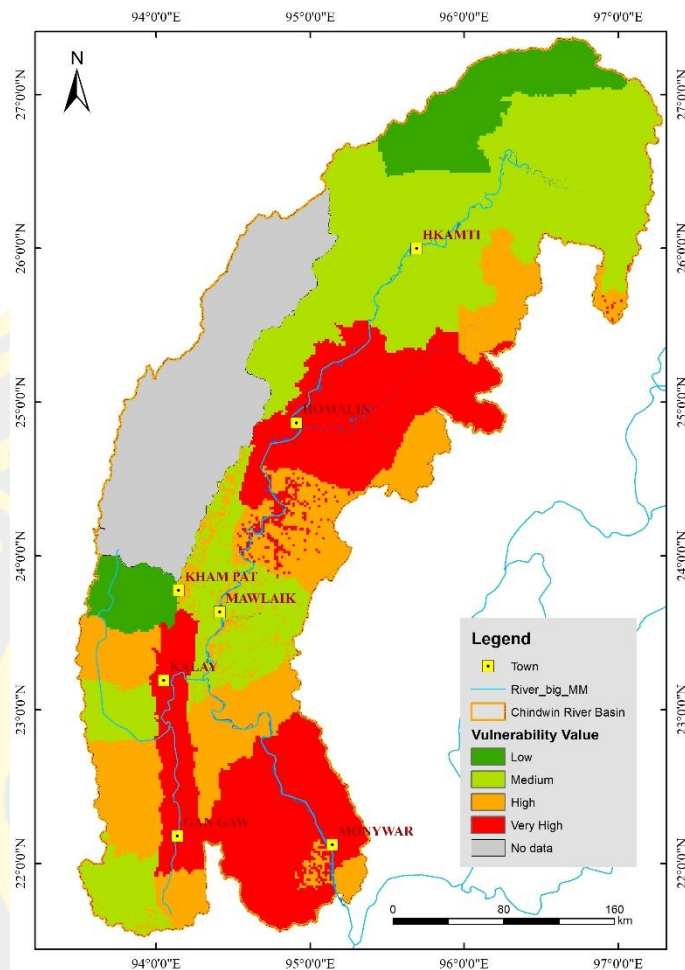


Figure 54 Flood vulnerability map of Chindwin river basin

Finally, the flood risk assessment was calculated by accounting the three main factors of the flood hazard, flood exposure, and flood vulnerability, which was separately calculated in previous sections. Below, Figure 55 is the overall flow chart of risk assessment.

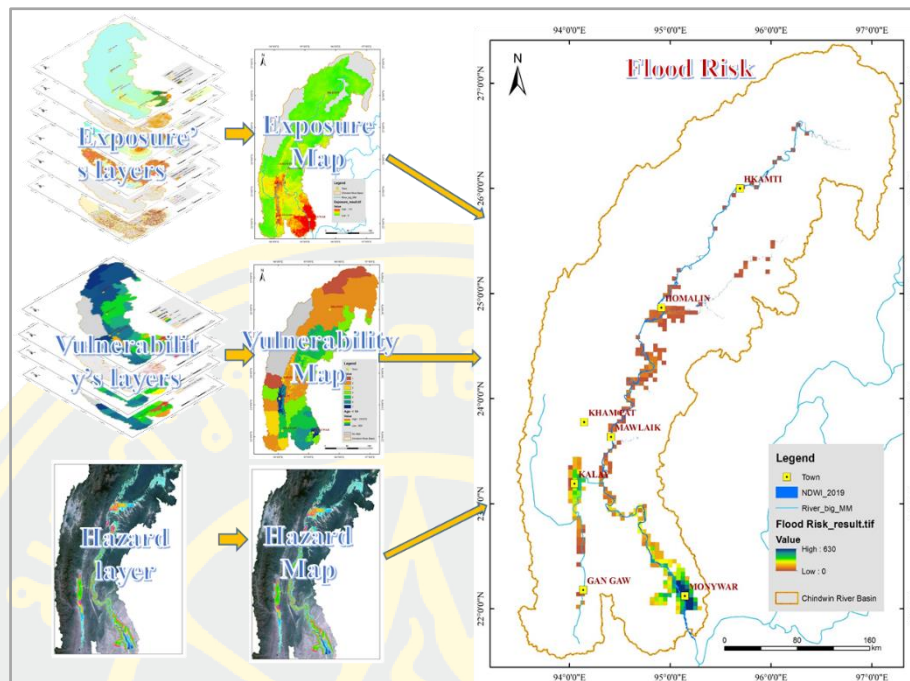


Figure 55 The overall process of flood risk assessment

As the topography controls the study area, the flat land terrain followed by the agriculture area was found in the downstream part and Kalay tributary. So, the potential flood risk areas have also resulted in those areas. Notably, the townships of Kalay and Monwya are standing as higher flood risk than other regions.

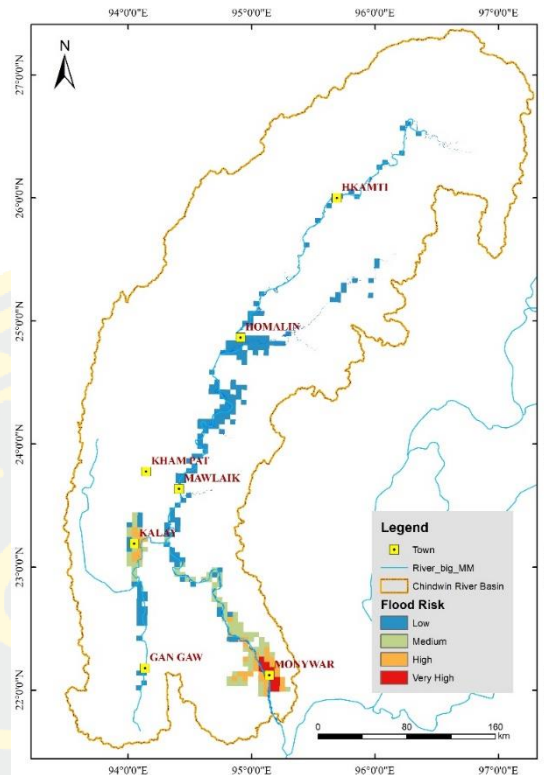


Figure 56 The result of flood risk assessment for Chindwin river basin

4.5 Discussion

In the hydrologic modelling (Figure 40 and 41), the selected flood events were validated and calibrated using the HEC-HMS model, the results of R , R^2 , and ENS for each event are closely the same and presented in a good correlation between the simulated and observed flows. Moreover, the different return period floods were also computed and resulted in a good relationship between the simulated and observed flows.

These computed data were utilized in further flood inundation mapping as certain water levels in the HEC-RAS model. The flood extent and inundation area for 2015 and 2017 storm events were calibrated and validated with the observed water level from rain-gauge stations and river bed flow observation data from the Department of Meteorology and Hydrology (DMH), and flood area mapping computed from the Sentinel 1 with remotely sensed techniques. Figure 51 shows the comparison of flood inundation area between the simulated flood extent and flood area from the remote sensing technique. Even though the study area is too big for simulation, the over-lap flooded area of the Chindwin river basin is about 71.5 % and 72.1% for 2015 and 2017

flood events, respectively and these results are generally acceptable and reasonable between simulation and observed flood extent from remotely sensed technique for validation.

In Table 10 of the flood inundated depth for the selected return period flood events, the seven classes of flood depth area are categorized as the flood hazard depths. Among these classes, the thickness between 4.1 m to 6.0 m is observed as the most flooded area than another flooded extent, while the depth (more than 12 m) was found as the lowest depth in each return period flood. Generally, each return period in the flood depth and area is increasing as the river flow is high.

Table 10 Data of the peak discharge and storm inundation area for the selected return periods

Return Period (year)	Peak Discharge (m ³ /sec)	Total Storm Inundation area (km ²)
2	14,500.8	4,133.9
5	22,199.2	4,151.3
10	28,365.9	4,231.3
20	34,586.9	5,131.8
50	42,973.1	6,157.1
100	49,354.9	7,214.6

Table 10 describes the estimated values of peak discharge from the hydrologic model and the storm inundated area for each selected return period simulated by the hydraulic model. According to the results, the peak discharge and the storm inundation area are consequently increasing in each return period.

In the indication of flood risk assessment level, there are a total of 1341 village tracts except for the part of India in the Chindwin River Basin, as shown in Figure 53. According to the overlay analysis, 23.64 % of total village tracks are flood risk area in scale, and the low, medium, high, and very high magnitude of flood risk are 11.3%, 3.9%, 5.1%, and 3.3% in village tract level respectively. The high flood risk areas have mainly occurred in Homalin, where are the junction of upstream Chindwin river and U Yu tributary, Kalay flat land terrain at Kalay tributary, and downstream area, Monywa city. Detailed village tracks affected by flood risk in scale were described in Appendix VI.

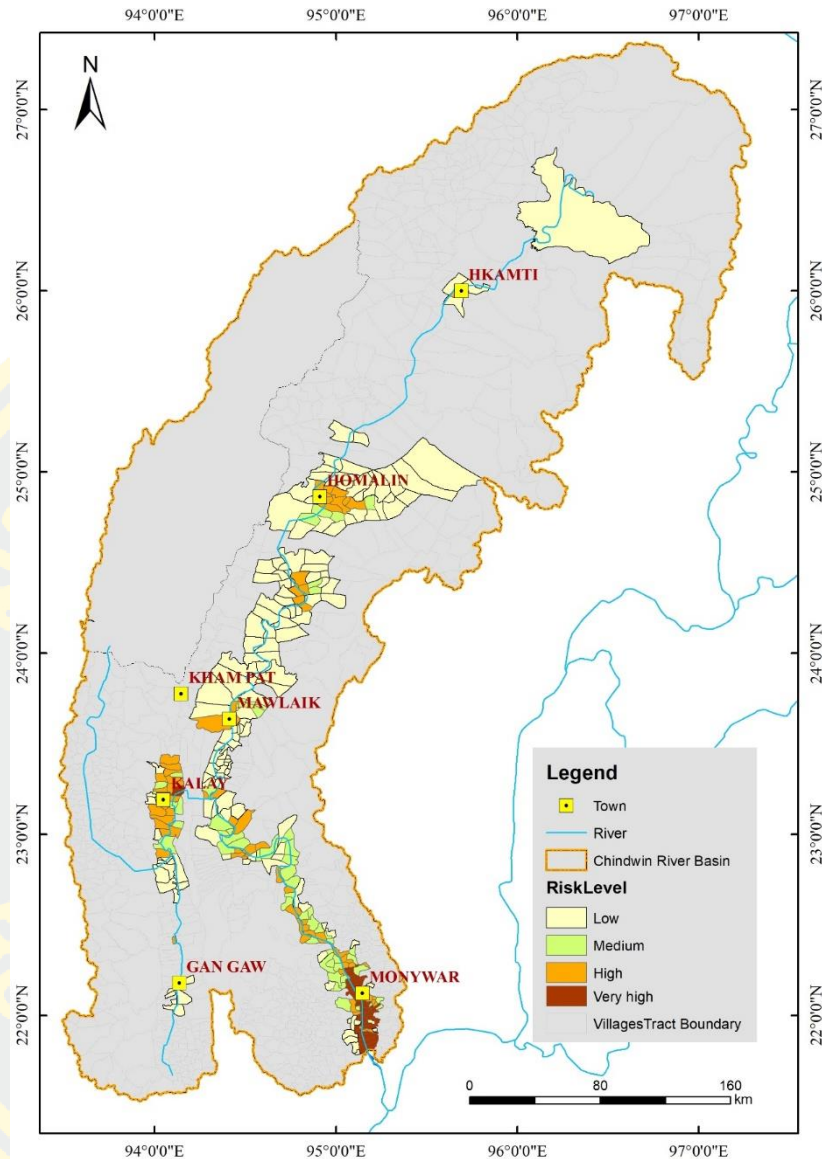


Figure 57 Flood risk assessment in village tract level for Chindwin river basin

CHAPTER 5

CONCLUSION, RECOMMENDATIONS AND FUTURE WORKS

5.1 Conclusion

The primary source of flooding in the Chindwin River basin is a result of riverine flood due to the primary heavy rainfall intensity and the other conditioning factors such as LULC, soil type, permeability, discharge rate, topographic condition, and geomorphological controls and so on.

This research provides the integration of GIS-based hydrologic and hydraulic systems using the HEC-HMS and HEC-RAS models. The selected flood events were validated and calibrated using the hydrologic model, which is to determine the design flow hydrograph between the simulated and computed flow data, and the results of model performance are relatively reasonable in statistical criteria. Moreover, the simulation of design flood hydrography for 2, 5, 10, 20, 50, and 100 year return periods was carried out for the hydrologic model as input data.

The 13859 km length of all streams for 968.2 km length of Main River (Chindwin River) and 4177.7 km length of two tributaries (U Yu tributary with 253.5 km and Kalewa tributary with 164.2 km) were studied. The observed water level data were utilized to compute the flow condition of the different return periods of the river that were analyzed in the HEC-RAS model. The flood area in the river basin was validated with the satellite data of Sentinel 1 for the years of 2015 and 2017, respectively. The overlapped regions between the maps simulated by the hydraulic model and remote sensing data are about 71.5 % and 72.1% for 2015 and 2017 flood events. These can be remarked as a proper validation. The flood depths were also validated with the field observation data and river bed cross-section data of the Department of Meteorology and Hydrology (DMH).

To validate the flood extent, which was derived from the hydraulic model, the Sentinel-1 satellite images for 2015 and 2017 were computed for the flood areas in the cloud-based system of google earth engine (GEE). The overlapped results between simulated map and flood areas from Sentinel-1 were 71.5% and 72.1% for 2015 and

2017 flood events, respectively. The results can be said as somewhat acceptable validation in this study. On the other hand, the validated check for the flood depth between the simulated depth and the observed depth was also applied, and it also strictly results and a good correlation.

Flood risk assessment is very important for flood risk management. However, so many datasets are required due to the consideration of flood hazard areas, flood exposures, and flood vulnerabilities. In this study, the 50 year return period flood modeled by HEC-RAS was utilized as a flood hazard map. For flood exposures, the population density, cropland, school, and hospital locations, and road network were used and converted into raster datasets to calculate the flood exposure map. And flood vulnerabilities map were computed from the datasets of urban area and age composition.

According to the overlay analysis using the flood hazard map of 50 year return period, the high flood risk has occurred about 8.4% of the total village tracts in the Chindwin River Basin, especially in the Homalin, Kalay, and Monywa townships.

5.2 Recommendations

Based on the knowledge of this research, I would like to recommend some as below.

- (1) Digital elevation model (DEM) is fundamental to delineate the river and sub-basins for hydrologic model and geometric data such as cross-sections, which are also required accurately for flood hazard maps. In this study, DEM (12.5 m) was used and needed to validate for better accuracy and exceptional resolution grid of the raster file.
- (2) Due to the limitation of five rainfall gauge stations in the whole river basin, the more rainfall data from stations are needed. Or there is a way to retrieve the meteorological datasets from satellite imageries to cover the entire catchment area.
- (3) In the hydraulic model, geometric data is crucial, especially the cross-section line should be covered the flooded area, and these can be checked by the historic flood area and considered with the topographic levelling on both start and endpoints of every single cross-section line.

- (4) Flood studies should be considered with the different time series analysis from remote sensing data and estimated for the future flood.
- (5) In flood risk assessment, the population density data for flood exposure should be the data grid with the village track/ward level for better risk assessment.

5.3 Future Works

- (1) Detail CN grid value, which is needed to calculate from land cover and soil type, will be applied for better rainfall-runoff simulation.
- (2) As the largest tributary of Main River, Ayeyarwaddy River, the different sub-basin of Main River will be conducted for comparative studies.
- (3) 2D hydrodynamic models will be recommended for higher accuracy and better presentation in the flood analysis of the entire river basin.

REFERENCES



- [1] Bich, T. H., Quang, L. N., Ha, L. T. T., Hanh, T. T. D., & Guha-Sapir, D. (2011). Impacts of flood on health: epidemiologic evidence from Hanoi, Vietnam. *Global Health Action*, 4, 6356. <https://doi.org/10.3402/gha.v4i0.6356>
- [2] Myanmar Engineering Society. (2011). Multi Hazard Risk Assessment In the Rankhine State of Myanmar (p. 268).
- [3] Roy, N., & Kaur, S. (2000). Climatology of monsoon rains of Myanmar (Burma). *International Journal of Climatology*, 20, 913-928. [https://doi.org/10.1002/1097-0088\(20000630\)20:8<913::AID-JOC485>3.0.CO;2-U](https://doi.org/10.1002/1097-0088(20000630)20:8<913::AID-JOC485>3.0.CO;2-U)
- [4] JICA. (2015). Natural Disaster Risk Assessment and Area Business COntinuity Plan Formulation for Industrial Agglomerated Areas in the ASEAN Region (p. 67). Retrieved from <https://openjicareport.jica.go.jp/pdf/1000023399.pdf>
- [5] Latt, Z. Z., & Wittenberg, H. (2015). Hydrology and flood probability of the monsoondominated chindwin river in northern Myanmar. *Journal of Water and Climate Change*, 6(1), 144–160. <https://doi.org/10.2166/wcc.2014.075>
- [6] Yin, H., & Li, C. (2001). Human impact on floods and flood disasters on the Yangtze River. *Geomorphology*, 41(2), 105–109. [https://doi.org/10.1016/S0169-555X\(01\)00108-8](https://doi.org/10.1016/S0169-555X(01)00108-8)
- [7] Analysis, R. (2020). Social Vulnerability Assessment for Flood. <https://doi.org/10.3390/w12020558>
- [8] Tockner, K., Bunn, S. E., Gordon, C., Naiman, R. J., Quinn, G. P., & Stanford, J. A. (2008). Flood plains: Critically threatened ecosystems. In *Aquatic Ecosystems: Trends and Global Prospects* (pp. 45–62). Cambridge University Press. <https://doi.org/10.1017/CBO9780511751790.006>
- [9] Zimmermann, E. D. (2003). *Journal of environmental hydrology* 2003, 11(March), 1–14. Available online at: <http://www.hydro.com>
- [10] Engeland, K., Hisdal, H., & Frigessi, A. (2004). Practical extreme value modelling of hydrological floods and droughts: A case study. *Extremes*, 7(1), 5–30. <https://doi.org/10.1007/s10687-004-4727-5>
- [11] Arnall, A., Thomas, D. S. G., Twyman, C., & Liverman, D. (2013). Flooding, resettlement, and change in livelihoods: Evidence from rural Mozambique. *Disasters*, 37(3), 468–488. <https://doi.org/10.1111/disa.12003>
- [12] Smith, K., & Ward, R. (1998). *Floods: Physical Processes and Human Impacts*. Book (p. 394). Retrieved from <http://eu.wiley.com/WileyCDA/WileyTitle/productCd-0471952486.html>
- [13] Du, J., Xie, S., Xu, Y., Xu, C. yu, & Singh, V. P. (2007). Development and testing of a simple physically-based distributed rainfall-runoff model for storm runoff simulation in humid forested basins. *Journal of Hydrology*, 336(3–4), 334–346. <https://doi.org/10.1016/j.jhydrol.2007.01.015>

- [14] Olayinka, D. N., Iriyobogbe, H. E., Limited, H., & State, L. (2017). FLOOD MODELLING AND RISK ASSESSMENT OF LAGOS ISLAND AND PART OF ETI-OSA LOCAL, 15(1).
- [15] Zin, W. W., Kawasaki, A., & Win, S. (2015). River flood inundation mapping in the Bago River Basin, Myanmar. *Hydrological Research Letters*, 9(4), 97–102. <https://doi.org/10.3178/hrl.9.97>
- [16] Rockwood, D. M. (1968). Application of Streamflow Synthesis and Reservoir Regulation-" SSARR"-Program to the Lower Mekong River. US Army Corps of Engineers.
- [17] Camporese, M., Paniconi, C., Putti, M., & Orlandini, S. (2010). Surface-subsurface flow modeling with path-based runoff routing, boundary condition-based coupling, and assimilation of multisource observation data. *Water Resources Research*, 46(2). <https://doi.org/10.1029/2008WR007536>
- [18] Phuong, H. T., Tien, N. X., Chikamori, H., & Okubo, K. (2018). A hydrological tank model assessing historical runoff variation in the Hieu River Basin. *Asian Journal of Water, Environment and Pollution*, 15(1), 75–86. <https://doi.org/10.3233/AJW-180008>
- [19] NYADAWA, M. O., KOBATAKE, S., & EZAKI, K. (1996). A Modified Tank Model and Applications in Some River Basins in Kenya. *Journal of Japan Society of Hydrology and Water Resources*, 9(6), 498–512. <https://doi.org/10.3178/jjshwr.9.498>
- [20] Duong, V. N., & Gourbesville, P. (2016). Model Uncertainty in Flood Modelling. Case Study at Vu Gia Thu Bon Catchment - Vietnam. In *Procedia Engineering* (Vol. 154, pp. 450–458). Elsevier Ltd. <https://doi.org/10.1016/j.proeng.2016.07.537>
- [21] Ilias, A., Hatzispiroglou, J., Baltas, E., & Anastasiadou-Partheniou, E. (2006). Application of the NAM model to the Ali-Efenti basin. *WIT Transactions on Ecology and the Environment*, 91, 279–289. <https://doi.org/10.2495/RISK060271>
- [22] MIKE. (2017). MIKE 11 River and Channel Modelling: Short Introduction. Retrieved from <https://stop-ttip.org/what-is-the-problem-ttip-ceta/>
- [23] Neitsch, S. L., Arnold, J. G., Kiniry, J. R., Srinivasan, R., & Williams, J. R. (2002). *Soil and Water Assessment Tool—User's Manual 2002*. TWRI Report TR-192 (p. 412). Retrieved from <http://swat.tamu.edu/media/1294/swatuserman.pdf>
- [24] Arnold, J. G., Srinivasan, R., Muttiah, R. S., & Williams, J. R. (1998). Large area hydrologic modeling and assessment part I: Model development. *Journal of the American Water Resources Association*, 34(1), 73–89. <https://doi.org/10.1111/j.1752-1688.1998.tb05961.x>

- [25] Mein, R. G., & Larson, C. L. (1973). Modeling infiltration during a steady rain. *Water Resources Research*, 9(2), 384–394. <https://doi.org/10.1029/WR009i002p00384>
- [26] Devia, G. K., Ganasri, B. P., & Dwarakish, G. S. (2015). A Review on Hydrological Models. *Aquatic Procedia*, 4, 1001–1007. <https://doi.org/10.1016/j.aqpro.2015.02.126>
- [27] Beven, K. J., & Kirkby, M. J. (1979). A physically based, variable contributing area model of basin hydrology. *Hydrological Sciences Bulletin*, 24(1), 43–69. <https://doi.org/10.1080/02626667909491834>
- [28] Brasington, J., & Richards, K. (1998). Interactions between model predictions, parameters and DTM scales for TOPMODEL. *Computers and Geosciences*, 24(4), 299–314. [https://doi.org/10.1016/S0098-3004\(97\)00081-2](https://doi.org/10.1016/S0098-3004(97)00081-2)
- [29] Jung, Y., Kim, D., Kim, D., Kim, M., & Lee, S. O. (2014). Simplified flood inundation mapping based on flood elevation-discharge rating curves using satellite images in gauged watersheds. *Water (Switzerland)*, 6(5), 1280–1299. <https://doi.org/10.3390/w6051280>
- [30] Feldman, A. (2000). Hydrologic Modeling System HEC-HMS. *Hydrologic Modeling System HEC-HMS Technical Reference Manual* (p. 148).
- [31] Gilles, D., & Moore, M. (2010). Review of Hydraulic Flood Modeling Software used in Belgium , The Netherlands , and The United Kingdom. *International Perspectives in Water Resource Management* (p. 15). Retrieved from http://www.iihr.uiowa.edu/education1/international/UK/projects_files/ipwrsm_paper_gilles_moore_Dan_editted.pdf
- [32] US Army Corps of Engineers. (2016). HEC-HMS User's Manual. Hydrologic Engineering Center (HEC). Version 4.2. Available online at: <http://www.hec.usace.army.mil/software/hec-hms/>
- [33] Ngo, L. L., Madsen, H., Rosbjerg, D., & Pedersen, C. B. (2008). Implementation and comparison of reservoir operation strategies for the Hoa Binh reservoir, Vietnam using the Mike 11 model. *Water Resources Management*, 22(4), 457–472. <https://doi.org/10.1007/s11269-007-9172-1>
- [34] Kimberley M. Davis. (2000). Object-Oriented Modeling of Rivers and Watersheds in Geographic Information Systems. Thesis of M.Eng. The University of Texa, Austin.
- [35] Zin, W. W., Kawasaki, A., & Win, S. (2015). River flood inundation mapping in the Bago River Basin, Myanmar. *Hydrological Research Letters*, 9(4), 97–102. <https://doi.org/10.3178/hrl.9.97>
- [36] Horritt, M. S., & Bates, P. D. (2002). Evaluation of 1D and 2D numerical models for predicting river flood inundation. *Journal of Hydrology*, 268(1–4), 87–99. [https://doi.org/10.1016/S0022-1694\(02\)00121-X](https://doi.org/10.1016/S0022-1694(02)00121-X)

- [37] Cook, A., & Merwade, V. (2009). Effect of topographic data, geometric configuration and modeling approach on flood inundation mapping. *Journal of Hydrology*, 377(1–2), 131–142. <https://doi.org/10.1016/j.jhydrol.2009.08.01>
- [38] Manandhar, B. (2010). Flood plain analysis and risk assessment of Lothar Khola, 77. <https://doi.org/10.13140/2.1.1664.1289>
- [39] US Army Corps of Engineers. (2016). HEC-RAS River Analysis System Hydraulic Reference Manual Version 5.0. Hydrologic Engineering Center, (February), 547.
- [40] Brunner, G. W. (2016). HEC-RAS River Analysis System, 2D Modeling User's Manual Version 5.0, (CPD-68A), 1–171. Retrieved from www.hec.usace.army.mil
- [41] Gül, G. O., Harmancioğlu, N., & Gül, A. (2010). A combined hydrologic and hydraulic modeling approach for testing efficiency of structural flood control measures. *Natural Hazards*, 54(2), 245–260. <https://doi.org/10.1007/s11069-009-9464-2>
- [42] Santillan, J. R., Paringit, E. C., Ramos, R. V., Mendoza, J. R. T., Española, N. C., & Alconis, J. (2012). Development of a HEC RAS Model for Near-Real Time Flood Extent Monitoring in Marikina River, Philippines. *Philippine Geomatics: Practice, Applications and Accomplishments*, (November).
- [43] Hnin, T., Student, A., & Engineering, C. (2017). Development of Flood Inundation Map for Bago River Basin, 1–6.
- [44] Oumaima, B., Yves, T., El Mehdi, S. M., Simon, G., & Frederic, L. (2019). Flood Hazard Mapping Using Two Digital Elevation Models: Application in a Semi-Arid Environment of Morocco. *European Scientific Journal ESJ*, 15(33). <https://doi.org/10.19044/esj.2019.v15n33p338>
- [45] Fowze, J. S. M., Nandalal, H. K., Welideniya, D. P., Samarasinge, S. M. J. S., Seneviratne, A., Bormudoi, A., ... Samarkoon, L. (2010). Flood inundation modeling in the lower reach of the Kalu River, Sri Lanka. In *31st Asian Conference on Remote Sensing 2010, ACRS 2010* (Vol. 2, pp. 1440–1445).
- [46] Phongsapan, K., Chishtie, F., Poortinga, A., Bhandari, B., Meechaiya, C., Kunlamai, T., Towashiraporn, P. (2019). Operational Flood Risk Index Mapping for Disaster Risk Reduction Using Earth Observations and Cloud Computing Technologies: A Case Study on Myanmar. *Frontiers in Environmental Science*, 7. <https://doi.org/10.3389/fenvs.2019.00191>
- [47] Latt, Z. Z., Wittenberg, H., & Urban, B. (2014). Clustering Hydrological Homogeneous Regions and Neural Network Based Index Flood Estimation for Ungauged Catchments: an Example of the Chindwin River in Myanmar. *Water Resources Management*, 29(3), 913–928. <https://doi.org/10.1007/s11269-014-0851-4>

- [48] FLOOD FORECASTING USING FGM MODEL IN CHINDWIN RIVER BASIN. (2009), 21(2). <https://doi.org/10.11113/mjce.v21n2.233>
- [49] Piman, T. (2017). Impacts of changing landscapes on water quality in Chindwin River, Ayeyarwady River Basin , Myanmar, (April), 1–13.
- [50] Shibuo, Y. (n.d.). Flood Inundation Analysis by Using RRI Model For Chindwin River Basin, Myanmar.
- [51] Edy Susanto, M. (2019). Development of Flood Inundation Map for Upper Chindwin River Basin By Using HEC-HMS and HEC-RAS. *Journal of Chemical Information and Modeling*, 53(9), 1689–1699. <https://doi.org/10.1017/CBO9781107415324.004>
- [52] Than, H. H. (2005). FLOOD PLAIN MAPPING USING CIS III LOWER PART OF CHINDWIN RIVER IN MYANMAR. Dissertation, Master of Technology in Hydrology, Department of Hydrology, Indian Institute of Technology Roorkee.
- [53] Mimikou, M. A. (2016). Hydrology and Water Resource Systems Analysis. Hydrology and Water Resource Systems Analysis. CRC Press. <https://doi.org/10.1201/9781315374246>
- [54] Alaghmand, S. (2009). River Modelling for Flood Risk Map Prediction: A Case Study of Kayu Ara River Basin, Malaysia. *International Institute of Engineers*. <https://doi.org/10.15242/iae.iae1214510>
- [55] Ye, X., Zhang, Q., Bai, L., & Hu, Q. (2011). A modeling study of catchment discharge to Poyang Lake under future climate in China. *Quaternary International*, 244(2), 221–229. <https://doi.org/10.1016/j.quaint.2010.07.004>
- [56] Eckhardt, K. (2008). A comparison of baseflow indices, which were calculated with seven different baseflow separation methods. *Journal of Hydrology*, 352(1–2), 168–173. <https://doi.org/10.1016/j.jhydrol.2008.01.005>
- [57] Feldman, A. (2000). Hydrologic Modeling System HEC-HMS. *Hydrologic Modeling System HEC-HMS Technical Reference Manual* (p. 148). <https://www.hec.usace.army.mil/software/hec-hms/>
- [58] US Army Corps of Engineers. (2016). Hydrologic Modeling System HEC-HMS User's Manual CPD-74A. Retrieved from http://www.hec.usace.army.mil/software/hec-hms/documentation/HEC-HMS_Users_Manual_4.0.pdf
- [59] Area, S. S. (2020). water Application of Different Separation Methods to Investigate the Baseflow Characteristics of a, 1–22. <https://doi.org/10.3390/w12020434>
- [60] Lee, J., Kim, J., Jang, W. S., Lim, K. J., & Engel, B. A. (2018). Assessment of baseflow estimates considering recession characteristics in SWAT. *Water (Switzerland)*, 10(4). <https://doi.org/10.3390/w10040371>

- [61] Engineers U S Army Corps. (2013). Hydrologic modeling system (HEC-HMS) application guide: version 4.0. 0. Institute for Water Resources, Davis, (December).
- [62] Ramírez, J. A. (2010). Prediction and Modeling of Flood Hydrology and Hydraulics. In *Inland Flood Hazards* (pp. 293–333). Cambridge University Press. <https://doi.org/10.1017/cbo9780511529412.012>
- [63] López, F., & Garcia, M. H. (2001). Mean flow and turbulence structure of open-channel flow through non-emergent vegetation. *Journal of Hydraulic Engineering*, 127(5), 392–402. [https://doi.org/10.1061/\(ASCE\)0733-9429\(2001\)127:5\(392\)](https://doi.org/10.1061/(ASCE)0733-9429(2001)127:5(392))
- [64] James, C. S., & James, C. S. (2020). Basic Hydraulic Concepts. In *Hydraulic Structures* (pp. 1–59). Springer International Publishing. https://doi.org/10.1007/978-3-030-34086-5_1
- [65] Schneider, G. E., & Raw, M. J. (1987). Control volume finite-element method for heat transfer and fluid flow using colocated variables- 1. computational procedure. *Numerical Heat Transfer*, 11(4), 363–390. <https://doi.org/10.1080/10407788708913560>
- [66] Brunner, G. W., & CEIWR-HEC. (2016). HEC-RAS River Analysis System User's Manual. US Army Corps of Engineers–Hydrologic Engineering Center, (January), 1–790. Retrieved from [https://www.hec.usace.army.mil/software/hec-ras/documentation/HEC-RAS 5.0 Users Manual.pdf](https://www.hec.usace.army.mil/software/hec-ras/documentation/HEC-RAS%205.0%20Users%20Manual.pdf)
- [67] Yoganathan, A. P., Cape, E. G., Sung, H. W., Williams, F. P., & Jimoh, A. (1988). Review of hydrodynamic principles for the cardiologist: Applications to the study of blood flow and jets by imaging techniques. *Journal of the American College of Cardiology*. [https://doi.org/10.1016/0735-1097\(88\)92620-4](https://doi.org/10.1016/0735-1097(88)92620-4)
- [68] USACE, H.-G. G. H. M. E. V. 4. 2. (2009). HEC-GeoHMS Geopatial Hydrologic Modeling Extention Version 4.2, (May), 197.
- [69] Smemoe, C., Nelson, J., Zundel, A., & Miller, W. (2006). Floodplain risk analysis using annual exceedance probability maps. *Hydrological Science and Technology*, 22(1), 185–196.
- [70] Mailapalli, D. R., Raghuwanshi, N. S., Singh, R., Schmitz, G. H., & Lennartz, F. (2008). Spatial and temporal variation of manning's roughness coefficient in furrow irrigation. *Journal of Irrigation and Drainage Engineering*, 134(2), 185–192. [https://doi.org/10.1061/\(ASCE\)0733-9437\(2008\)134:2\(185\)](https://doi.org/10.1061/(ASCE)0733-9437(2008)134:2(185))
- [71] Jarrett, R. D. (1985). Determination of roughness coefficients for streams in Colorado. Technical Report, Geological Survey Water-Supply, United States Government Printing Office, Washington, U.S.A, 54. <https://doi.org/10.1017/S0003161500015145>

- [72] R. Bonner, V., & W. Brunner, G. (1996). Bridge Hydraulic Analysis with HEC-RAS. *Water Resources*, (April), 1–26.
- [73] Correia, F. N., Rego, F. C., Saraiva, M. D. G., & Ramos, I. (1998). Coupling GIS with hydrologic and hydraulic flood modelling. *Water Resources Management*, 12(3), 229–249. <https://doi.org/10.1023/A:1008068426567>
- [74] Correia, F. N., Da Graça Saraiva, M., Da Silva, F. N., & Ramos, I. (1999). Floodplain management in urban developing areas. Part I. Urban Growth Scenarios and land-use controls. *Water Resources Management*, 13(1), 1–21. <https://doi.org/10.1023/A:1008097403587>
- [75] Singh, P., Gupta, A., & Singh, M. (2014). Hydrological inferences from watershed analysis for water resource management using remote sensing and GIS techniques. *Egyptian Journal of Remote Sensing and Space Science*, 17(2), 111–121. <https://doi.org/10.1016/j.ejrs.2014.09.003>
- [76] US Army Corps of Engineers, I. for W. R. H. E. (2010). HEC-GeoHMS Extension, (October). Available online at: <https://www.hec.usace.army.mil/software/hec-geohms/downloads.aspx>
- [77] Awal, R. (2003). Application of Steady and Unsteady Flow Model and GIS for Floodplain Analysis and Risk Mapping: A Case Study of Lakhandei River. Master of Engineering. Theiss. Trishuvan University, Nepal.
- [78] Yang, L. (2014). Climate Change , Water Risks and Urban Responses in the Pearl River Delta , China. PhD Thesis, Universitat Hamburg, Hamburg. Available online at: <http://hdl.handle.net/11858/00-001M-0000-0024-04DF-A>
- [79] G., Britain. (1995). A guide to Risk Assessment and Risk Management for Environmental Protection. Department of Environment, United of Kingdom.
- [80] Manandhar, B. (2010). Flood plain analysis and risk assessment of Lothar Khola, 77. 1289 Degree of Master of Science in Watershed Management, Tribhuvan University, Institute of Forestry, Pokhara, Nepal. <https://doi.org/10.13140/2.1.1664>.
- [81] D. Rijkswaterstaat. (2005). Historische analyse van de gevolgen van overstromingen in Nederland: een globale schatting van de situatie rond 1950, 1975 en 2005. Q4005.
- [82] Jongman, B., Koks, E. E., Husby, T. G., & Ward, P. J. (2014). Increasing flood exposure in the Netherlands: Implications for risk financing. *Natural Hazards and Earth System Sciences*, 14(5), 1245–1255. <https://doi.org/10.5194/nhess-14-1245-2014>
- [83] Van Liere, W. J. (1980). Traditional water management in the lower Mekong Basin. *World Archaeology*, 11(3), 265–280. <https://doi.org/10.1080/00438243.1980.9979766>

- [84] Chakraborty, O., Ghosh, S. K., & Mitra, P. (2019). Multi-facilities-based road network analysis for flood hazard management. *Journal of Spatial Science. Mapping Sciences Institute Australia*.
<https://doi.org/10.1080/14498596.2018.1561338>
- [85] Levy, K., Woster, A. P., Goldstein, R. S., & Carlton, E. J. (2016, May 17). Untangling the Impacts of Climate Change on Waterborne Diseases: A Systematic Review of Relationships between Diarrheal Diseases and Temperature, Rainfall, Flooding, and Drought. *Environmental Science and Technology. American Chemical Society*.
<https://doi.org/10.1021/acs.est.5b06186>
- [86] Karmakar, S., Simonovic, S. P., Peck, A., & Black, J. (2010). An Information System for Risk-Vulnerability Assessment to Flood. *Journal of Geographic Information System*, 02(03), 129–146. <https://doi.org/10.4236/jgis.2010.23020>
- [87] Lugeri, N., Kundzewicz, Z. W., Genovese, E., Hochrainer, S., & Radziejewski, M. (2010). River flood risk and adaptation in Europe-assessment of the present status. *Mitigation and Adaptation Strategies for Global Change*, 15(7), 621–639. <https://doi.org/10.1007/s11027-009-9211-8>
- [88] Cannon, T. (2008). Vulnerability, “innocent” disasters and the imperative of cultural understanding. *Disaster Prevention and Management: An International Journal*, 17(3), 350–357. <https://doi.org/10.1108/09653560810887275>
- [89] United Nations Development Programme. (2004). ‘Development at risk’, Reducing disaster: A challenge for development. New York: United Nations. <http://archive-ouverte.unige.ch/unige:77685>
- [90] Borden, K. A., Schmidlein, M. C., Emrich, C. T., Piegorsch, W. W., & Cutter, S. L. (2007). Vulnerability of U.S. cities to environmental hazards. *Journal of Homeland Security and Emergency Management*, 4(2). <https://doi.org/10.2202/1547-7355.1279>
- [91] UN. (1992). Internationally Agreed Glossary of Basic Terms Related to Disaster Management. United Nations Department of Humanitarian Affairs, Geneva. Department of Humanitarian Affairs, United Nation.
- [92] Merz, B., Hall, J., Disse, M., & Schumann, A. (2010). Fluvial flood risk management in a changing world. *Natural Hazards and Earth System Science*, 10(3), 509–527. <https://doi.org/10.5194/nhess-10-509-2010>
- [93] USGS. (2009). Land Cover Type Yearly L3 Global 1km SIN Grid. Retrieved from https://lpdaac.usgs.gov/lpdaac/products/modis_products_table/land_cover/yearly_l3_global_1km2/mod12q1
- [94] FAO. (2007). The digital soil map of the world. Rome, Italy: FAO. Retrieved from <http://www.fao.org/geonetwork/srv/en/metadata.show>

- [95] AlHassoun, S. A. (2011). Developing an empirical formulae to estimate rainfall intensity in Riyadh region. *Journal of King Saud University - Engineering Sciences*, 23(2), 81–88. <https://doi.org/10.1016/j.jksues.2011.03.003>
- [96] Lillesand, T. M., & Kiefer, R. W. (1979). Remote sensing and image interpretation. *Remote Sensing and Image Interpretation*. <https://doi.org/10.2307/634969>
- [97] Hartl, P. (1989). Fundamentals of remote sensing. *Applications of Remote Sensing to Agrometeorology*. Proc. Ispra-Course, Ispra, 1987, 1–18. <https://doi.org/10.5860/choice.42sup-0284>
- [98] Jensen, J. R. (2015). “Introductory Digital Image Processing: A Remote Sensing Perspective”. Fourth edition. United States of America, Pearson Education.
- [99] Gorelick, N., Hancher, M., Dixon, M., Ilyushchenko, S., Thau, D., & Moore, R. (2017). Google Earth Engine: Planetary-scale geospatial analysis for everyone. *Remote Sensing of Environment*, 202, 18–27. <https://doi.org/10.1016/j.rse.2017.06.031>
- [100] Midekisa, A., Holl, F., Savory, D. J., Andrade-Pacheco, R., Gething, P. W., Bennett, A., & Sturrock, H. J. W. (2017). Mapping land cover change over continental Africa using Landsat and Google Earth Engine cloud computing. *PLoS ONE*, 12(9). <https://doi.org/10.1371/journal.pone.0184926>
- [101] Hird, J. N., DeLancey, E. R., McDermid, G. J., & Kariyeva, J. (2017). Google earth engine, open-access satellite data, and machine learning in support of large-area probabilistic wetland mapping. *Remote Sensing*, 9(12). <https://doi.org/10.3390/rs9121315>
- [102] Moreira, A. (1992). Real-Time Synthetic Aperture Radar (SAR) Processing with a New Subaperture Approach. *IEEE Transactions on Geoscience and Remote Sensing*, 30(4), 714–722. <https://doi.org/10.1109/36.158865>
- [103] Wright, D. B., Risk, D., Consultant, M., Ramirez-cort, F., Ishizawa, O. A., Disaster, S. (2016). *Methods in Flood Hazard and Risk Assessment*. The World Bank. 1–20. www.worldbank.org
- [104] Myanmar Information Management Unit (MIMU). Formal Sector School Location Upper Myanmar (2019) by the Ministry of Education (MoE) and compiled by MIMU. Available online at: <http://geonode.themimu.info/>
- [105] OpenStreetMap Contributors, 2017. Planet Dump. Data retrieved from: <https://planet.openstreetmap.org/>
- [106] Department of Population, Ministry of Labor, Immigration and Population, the republic of the Union of Myanmar, 2014. Demographic Data statically retrieved from: <http://www.dop.gov.mm/en>



BIOGRAPHY

NAME	chit Myo Lwin
DATE OF BIRTH	19 September 1988
PLACE OF BIRTH	Taikkyi
PRESENT ADDRESS	No.746 (202), Kyaung Street, 5 Quarter, Kamayut Township, Yangon
EDUCATION	B.Sc. in Geology, West Yangon University, Yangon Region
AWARDS OR GRANTS	M.Sc. in Geoinformatic (SCGI Master Program), Burapha Univesity

